THESIS

AN OBSERVATIONAL STUDY OF TWO UPPER-LEVEL INVERTED TROUGHS DURING THE 2004 NORTH AMERICAN MONSOON EXPERIMENT

Submitted by

Zachary Owen Finch

Department of Atmospheric Science

In partial fulfillment of the requirements

For the Degree of Master of Science

Colorado State University

Fort Collins, Colorado

Fall 2009

COLORADO STATE UNIVERSITY

October 30, 2009

WE HEREBY RECOMMEND THAT THE THESIS PREPARED UNDER OUR SUPERVISION BY ZACHARY OWEN FINCH ENTITLED AN OBSERVATIONAL STUDY OF TWO UPPER-LEVEL INVERTED TROUGHS DURING THE 2004 NORTH AMERICAN MONSOON EXPERIMENT BE ACCEPTED AS FULFILLING IN PART REQUIREMENTS FOR THE DEGREE OF MASTER OF SCIENCE.

Committee on Graduate Work

_____

Pierre Y. Julien

_____

Wayne H. Schubert

_____

Advisor Richard H. Johnson

_____

Department Head Richard H. Johnson

ABSTRACT OF THESIS

AN OBSERVATIONAL STUDY OF TWO UPPER-LEVEL INVERTED TROUGHS DURING THE 2004 NORTH AMERICAN MONSOON EXPERIMENT

An upper-level inverted trough is a subtropical upper-tropospheric low that progresses westward over the North American Monsoon (NAM) region. These systems are important contributors to the variability of rainfall and convection within the NAM system. While past studies have detailed the characteristics of subtropical upper-level lows, these studies have been confined to regions in the North Pacific and North Atlantic. In the present study, high temporal and spatial observations taken during the 2004 North American Monsoon Experiment (NAME) are utilized to analyze two upper-level inverted troughs that passed over northwestern Mexico during the field campaign. The Colorado State University gridded dataset is the primary source of data used in the study. Thermodynamic and kinematic characteristics of both inverted troughs are documented through the fields of temperature, vorticity, quasi-geostrophically (QG) forced vertical motion, and midlevel winds and vertical wind shear.

The vertical temperature structure of the both upper-level inverted troughs is characterized by a warm anomaly around 100 hPa and a cold anomaly that extends from 200 hPa to the surface. The strongest circulation of the systems is in the upper-levels

around 200 hPa. QG vertical motion indicates that the inverted troughs force weak subsidence (rising motion) to the west (east) of the upper-level low center. The pattern of temperature, vorticity, and vertical motion for the NAME inverted troughs agrees with past studies of subtropical upper-level lows. However, the vertical motion forced by the inverted troughs is seemingly in contradiction to observations that indicate an increase in convective organization on their western (leading) flank.

Although vorticity is maximized in the upper-levels with these systems, there is an associated midlevel cyclonic circulation. The general midlevel wind pattern in the vicinity of the inverted troughs is characterized by northeasterly (southeasterly) midlevel flow to the west (east) of the low. Analysis of individual synoptic times reveals that significant mesoscale convective system (MCS) activity along the Sierra Madre Occidental (SMO) foothills is collocated with regions of anomalous northeasterly midlevel flow and increased northeasterly shear on the leading flank of the inverted trough. It is proposed that the inverted trough creates an environment on its leading flank that is favorable for convective storms to grow upscale as they move off the high terrain of the SMO.

Zachary Owen Finch
Department of Atmospheric Science
Colorado State University
Fort Collins, CO 80523
Fall 2009

ACKNOWLEDGEMENTS

This research was supported by National Science Foundation (NSF)/North American Monsoon Experiment (NAME) grant ATM-0639461. First of all, I would like to thank Dr. Wayne Schubert from the Department of Atmospheric Science and Dr. Pierre Julien from the Department of Civil Engineering for serving as members on my graduate thesis committee. Their comments and suggestions on this paper are much appreciated. I would also like to thank my academic advisor, Dr. Richard Johnson, for his guidance and support on this project. I also thank him for the opportunity of participating in the 2008 TIMREX field experiment in Taiwan. The meetings with Dr. Johnson have proved invaluable over my graduate studies at Colorado State University. It was during these meetings that countless research ideas were proposed.

Several thanks go out to members of the Johnson Mesoscale Research Group. To Paul Ciesielski for his effort in quality control of the 2004 NAME data and generating the NAME gridded dataset; to Rick Taft for helping me with computer-related issues; to Brian McNoldy for his assistance in generating and reviewing several of the figures in this paper; to Dan Lindsey for providing the satellite data; to Andy Newman for his help in coding and his ideas on improving the research; and to Gail Cordova for her continuous support during my graduate studies. The suggestions by all other members of the Johnson Research Group during group meetings are appreciated.

Finally, I would like to thank my parents, Keith and Toni, and my brother, Daniel, for their loving support during all my educational endeavors. Their constant encouragement has made my educational experience a success. Thanks go out to all my friends in Fort Collins who have truly made my graduate years memorable at CSU.

CONTENTS

FIGURES

CHAPTER 1

INTRODUCTION AND MOTIVATION

The North American Monsoon (NAM) is an important and complex atmospheric circulation over the continent. It is experienced as a pronounced increase in rainfall from a dry June to a rainy July over the southwestern United States and northwestern Mexico (Adams and Comrie 1997). Results from Douglas et al. (1993) indicate that western Mexico receive 60% to 70% of annual precipitation during the three-month period from July to September. The dramatic increase in rainfall is accompanied by a northward shift in the subtropical ridge at the end of June (Bryson and Lowry 1955, Douglas et al. 1993). This causes midlevel winds over the NAM region to shift from southwesterly during June to southeasterly in July. It was argued by Bryson and Lowry (1955) that the southeasterly flow provided moisture advection from the Gulf of Mexico and accounted for the increase in rainfall. However, later studies (Rasmusson 1967, Hales 1972, Douglas et al. 1993) suggest that the Gulf of California (GOC) and eastern tropical Pacific, not the Gulf of Mexico, contribute to increases in low level moisture to the west of the Sierra Madre Occidental (SMO). Gulf surges are detectable at surface stations along the GOC as a strong shift to south-southeast winds accompanied by lower temperatures and higher dewpoints. Gulf surges, and more generally the lower atmosphere over the GOC, have received considerable attention in the NAM literature (Hales 1972, Douglas 1995, Adams

and Comrie 1997, Rogers and Johnson 2007).

Variability in the summertime convective activity over the NAM region results from complex interactions between synoptic and mesoscale processes (Adams and Comrie 1997). Local topographic effects are critical to the spatial and temporal variability in convection. The SMO is a prominent northwest-southeast oriented mountain range in western Mexico. Convective initiation during the afternoon occurs over the SMO or other high terrain areas in the core NAM region (Douglas et al. 1993, Lang et al. 2007, Bieda et al. 2009). The coastal lowlands of northwestern Mexico and low deserts of southern Arizona experience a nighttime convective maximum (Adams and Comrie 1997) as convection propagates westward off the high terrain. Although the SMO triggers the initial convection almost every afternoon during the NAM, not all days are characterized by precipitating features reaching the coastal lowlands. During undisturbed regimes, Lang et al. (2007) showed that SMO convection does not survive the trip to the GOC. Disturbed regimes, on the other hand, are characterized by a tendency for precipitating systems to grow upscale and organize into mesoscale convective systems (MCSs). Hence, these organized precipitating systems are larger in areal extent and longer-lived. Furthermore, MCSs have been shown to contribute significantly to the total rainfall along the SMO foothills and coastal lowlands (Lang et al. 2007, Periera 2008). Past studies indicate that increases in midlevel easterlies and vertical wind shear can promote MCS development over the NAM region (Smith and Gall 1989, Farfán and Zehnder 1994, Lang et al. 2007, Periera 2008).

While studies of the gulf surge are plentiful over the NAM region, studies of upper-tropospheric phenomena are less numerous. One of the most important upper-tropospheric

systems to traverse the NAM region is the upper-level inverted trough (Pytlak et al. 2005, Douglas and Englehart 2007, Bieda et al. 2009). An upper-level inverted trough (IV, using the nomenclature of forecasters in the Southwest US) is a subtropical upper-tropospheric low that progresses westward over the NAM region on the south side of the subtropical ridge. Past studies of subtropical upper-tropospheric lows have been confined to the data sparse areas of the North Pacific and North Atlantic (Erickson 1971, Kelley and Mock 1982). One of the common genesis areas for upper-level lows in the Gulf of Mexico and Atlantic is the tropical upper-tropospheric trough (TUTT). It is important to note that not every upper-tropospheric low that traverses across the NAM region develops in the TUTT. For this reason, an upper-tropospheric low over the NAM region is referred to an upper-level inverted trough in this paper rather than TUTT low.

The TUTT was first documented by Sadler (1967) as a climatological mean summer circulation with an elongated shear axis in the upper troposphere that stretches from the North Atlantic to the Gulf of Mexico. Using operational analyses, Whitfield and Lyons (1992) investigated a TUTT low that remained over Texas for several days. Previous studies of subtropical upper-tropospheric lows have shown that the circulation is maximized in the upper-levels, around 200 hPa (Erickson 1971, Kelley and Mock 1982, Whitfield and Lyons 1992). Furthermore, there is a cold temperature anomaly that extends from approximately 250 hPa to the surface. The vertical motion pattern is dominated by rising motion on the eastern flank of the low and subsidence on the western flank.

Studies of upper-level inverted troughs over the NAM region are limited, and often involve only cursory examinations of the rainfall and convection in proximity of the inverted trough. Pytlak et al. (2005) argued that upper-level divergence on the

northwestern flank of the inverted trough promotes an increased likelihood for organized convection. Douglas and Englehart (2007) documented rainfall in the proximity of countless inverted troughs and found that rainfall was maximized to the west of the upper-level low. A very recent study by Bieda et al. (2009) indicated that lightning counts increase over the low deserts of southern Arizona and Sonora when an inverted trough is located within their study domain. While these studies suggest that inverted troughs are important contributors to the variability in rainfall and convection across the NAM region, there are many unanswered questions. The method by which an inverted trough modifies the convective environment in its proximity is left unresolved. Moreover, the observation that convection tends to increase on the western flank of the low is seemingly in contradiction to the vertical motion pattern computed around subtropical upper-level lows in previous studies (Erickson 1971, Kelley and Mock 1982, and Whitfield and Lyons 1992) and deserves further study.

While past studies of subtropical upper-tropospheric lows have provided insight into their flow characteristics, there have been no detailed studies of these systems over the NAM region. Previously, the lack of observational data over northwestern Mexico has prevented a detailed analysis of upper-level inverted troughs over the NAM region. However, the 2004 North American Monsoon Experiment (NAME) field campaign (1 June – 30 September 2004) provided an unprecedented observational sounding network over the NAM region. Two prominent inverted troughs passed across northwestern Mexico on 10-13 July 2004 (IV4) and 21-24 July 2004 (IV6). These two inverted troughs are chosen for detailed analysis in the present study. The Colorado State University (CSU) gridded dataset from the 2004 NAME field campaign is the primary data source for this research. The

results provide an unprecedented understanding of the thermodynamic and kinematic characteristics of upper-level inverted troughs over the NAM region, and can be compared to previous studies of upper-level lows over the subtropical North Pacific and North Atlantic.

The remainder of this paper is organized in the following way. Chapter 2 describes past studies of subtropical upper-level lows along with recent NAME studies that are relevant to the present research. Chapter 3 will discuss the observational network of the NAME field campaign. Furthermore, the data analysis procedures (methods) are included in this chapter. Chapter 4 presents plots at 200 and 600 hPa along with water vapor imagery to diagnose the synoptic setup in which both inverted troughs were embedded. Chapter 5 is the first results chapter in the paper and details the temperature and vorticity structure of both inverted troughs. Chapter 6 analyzes the quasi-geostrophic (QG) vertical motion that is forced by the inverted troughs. Chapter 7 details the midlevel winds and vertical wind shear associated with both inverted troughs. Finally, Chapter 8 summarizes the most significant results from the present study.

CHAPTER 2

BACKGROUND AND LITERATURE REVIEW

2.1 Mean Tropospheric Conditions over the NAM Region

Figure 1 highlights some of the important and complex topographic features that relate to the NAM. The region is bounded to the west by the Pacific Ocean and the GOC and to the east by the Gulf of Mexico. The SMO is a northwest-southeast aligned mountain range located in western Mexico that often focuses convective initiation during the NAM (Adams and Comrie 1997, Lang et al. 2007). The SMO rises to elevations above 2500 m and provides a steep topographic gradient with the GOC coastal plain immediately to the west. The coastal lowlands of Sonora and Sinaloa lie between the GOC and the western foothills of the SMO. In southern California and Baja California, the peninsular ranges and northwesterly trades of the eastern Pacific limit the penetration of high dewpoints from the interior monsoon region onto the Pacific coastal plain. The lower Colorado River Basin in southeastern California and southwest Arizona plays a critical role in the formation of a thermal low there during the summer monsoon (Adams and Comrie 1997). Northern parts of the NAM domain are dominated by the elevated terrain areas of the Colorado Plateau, Rocky Mountains, and Arizona's Mogollon Rim. The extremely varied topography has important implications for mesoscale circulation features and spatial variability in precipitation (Adams and Comrie 1997, Rogers et al. 2007, Lang et al. 2007).

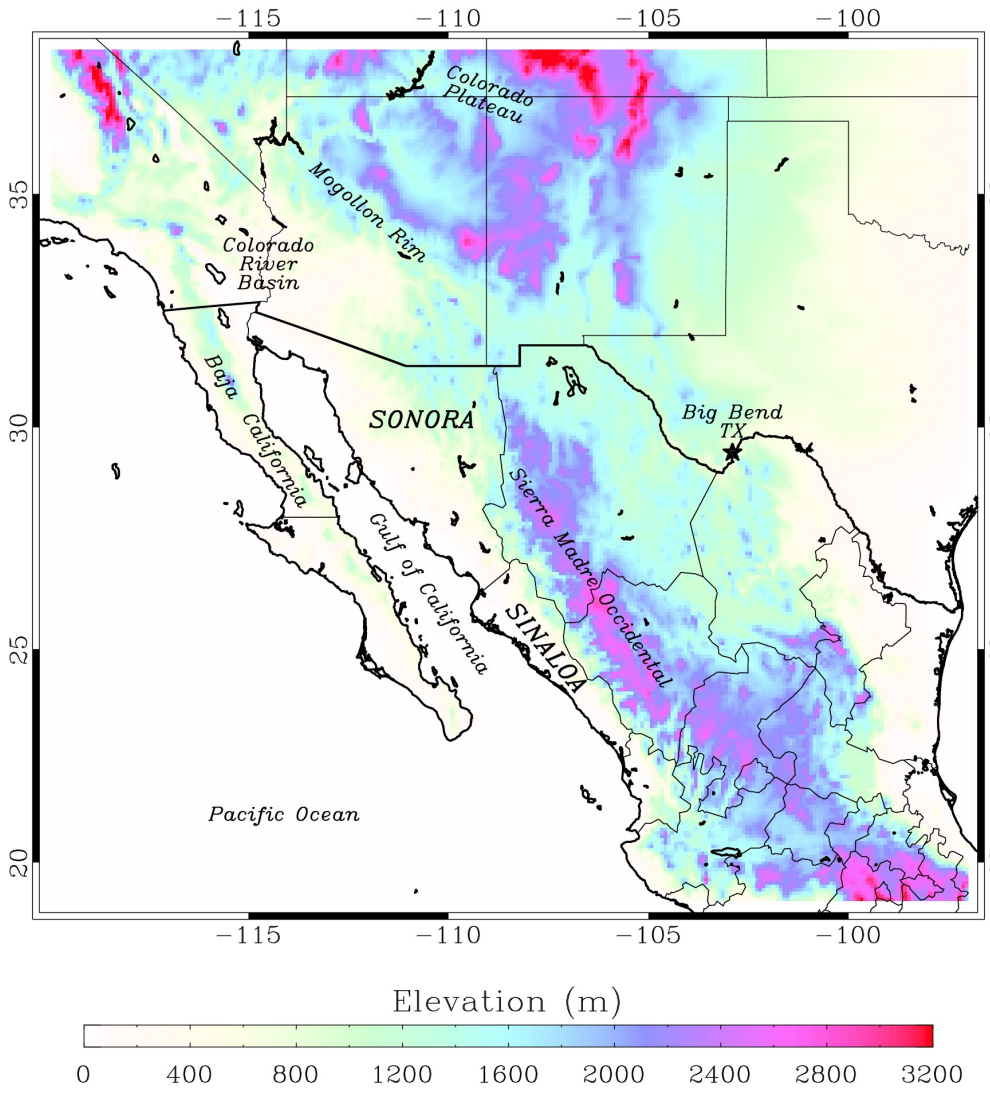

Figure 1: Important topographic features in the NAM geographical domain. Colored contours represent altitude above sea level (m). The Mexican states of Sonora and Sinaloa, along with Big Bend, TX are mentioned numerous times in this study.

Douglas et al. (1993) provided a general description of the NAM using analyses of monthly rainfall, geostationary satellite imagery, and rawinsonde data. The authors computed the ratio (expressed in percent) of rain falling during the three-month summer period (July-September) to the annual mean precipitation. The results show that areas in western Mexico receive 60% to 70% of their annual precipitation during the three-month

period (Figure 2). To emphasize the onset of the monsoonal rains in July, the authors then compared the rainfall between June and July. The most dramatic increase of rainfall occurs along the western slopes and foothills of the SMO, with some stations having a 200 mm increase from June to July. Hence, there is a pronounced increase of rainfall from an extremely dry June to a rainy July over northwestern Mexico and the monsoonal rains are a very important contribution to the annual precipitation in this region. The substantial amounts of rainfall along the western foothills of the SMO in July are corroborated by GOES infrared (IR) imagery. Frequencies of occurrence of cloud top temperatures colder than -38ºC show that the first full month with deep convection over northwestern Mexico is July, in excellent agreement with rainfall data (Douglas et al. 1993). Arizona and Sonora also have a higher frequency of cold clouds in July, implying a northward shift in deep convection into these regions associated with the NAM.

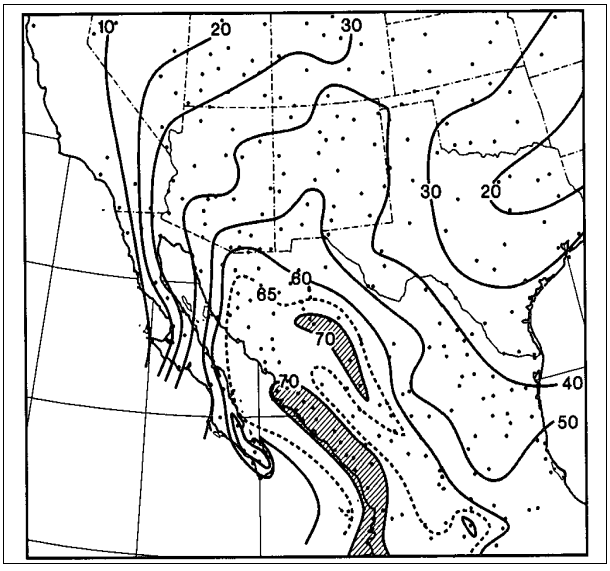

Figure 2: Contribution of the precipitation during the summer monsoonal months (July, August, September) to the annual total, expressed as a percent.

To examine the mean upper-air conditions over Mexico during the summer months, Douglas et al. (1993) constructed monthly mean wind and moisture plots based on rawinsonde observations from the eleven-year period (1979-1989) over northwestern Mexico. Composite 500-hPa plots for June (Fig. 3) and July (Fig. 4) depict a northward shift in the 500-hPa subtropical ridge axis from central Mexico in June to New Mexico in July. The movement of the ridge axis produces a shift from westerly midtropospheric flow in June to easterly and southeasterly flow during July. Bryson and Lowry (1955) were among the first authors to link the onset of summer rains with a northward shift in the subtropical ridge. They argued that westward advection of higher moisture content air from the Gulf of Mexico resulted in the onset of July rainfall in northwestern Mexico. However, as can be seen from Fig. 4, the winds that blow from across Mexico from the Gulf of Mexico actually advect drier air from the east. The dewpoint over the Gulf of Mexico is 4-8ºC less than along the SMO axis, where moister air resides. Douglas et al. (1993) argue that vertical transport of low-level moisture by SMO convection results in the midtropospheric maximum in moisture along the SMO axis.

After the Southwest Area Monsoon Project (SWAMP) 1990 field campaign, Douglas (1995) used data from pilot balloon sites in Mexico and one in Yuma, AZ to analyze the diurnal cycle of lower-tropospheric flow along the GOC. At 1200 UTC (0600 LST) lower-tropospheric flow (450 m AGL) is dominated by south-southeasterly winds along the GOC axis with a wind speed maximum over northern GOC (not shown). At 0000 UTC (1800 LST) there is still south-southeasterly flow immediately over the GOC, but the flow is upslope (southwesterly) along the lowlands and foothills of Sonora and Sinaloa due to strong daytime heating along the steeply sloped terrain of the SMO foothills.

An occasional intensification of the low-level southerly flow along the GOC axis, accompanied by lower temperatures and higher dewpoints, is known in the literature as a "gulf surge." Although the majority of this paper focuses on mid and upper-tropospheric conditions associated with inverted troughs, I will follow with a brief overview of the gulf surge phenomenon.

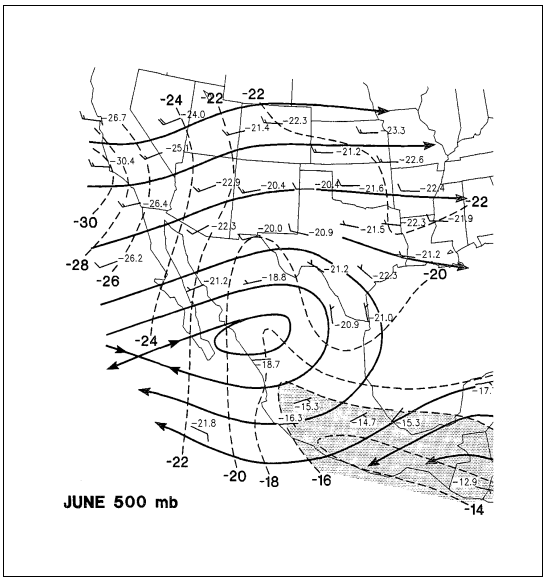

Figure 3: Mean winds, streamlines, and dewpoint at 500 hPa for the month of June.

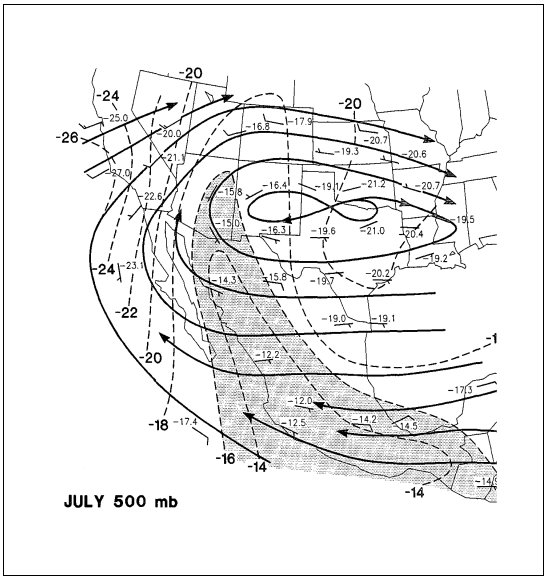

Figure 4: Same as Fig. 3, except for the month of July

The gulf surge has received much attention in the NAM literature. One of the earlier studies by Hales (1972) argued that a surge of moist tropical Pacific air is channeled up the GOC as a result of a low-level pressure gradient. By studying satellite photographs, Hales discovered a positive relationship between large cloud masses over the central/southern GOC and subsequent surges of moisture. The author proposed an intensification of the along-gulf pressure gradient as the thermal heat low over the lower Colorado River Basin coincides with higher surface pressure over the central/southern

GOC caused by convective activity or evaporational cooling from precipitation. The increased north-south pressure gradient could then result in a surge of moist air northward into the southwest United States. A fourteen-year period of data was examined by Fuller and Stensrud (2000) to determine whether or not gulf surges develop in association with passing tropical easterly waves. Easterly waves are best defined using wind data at 700 hPa and typically move to the south of the core NAM region. Fuller and Stensrud (2000) produced Hovmöller diagrams of the 850-hPa meridional wind speed for the latitudes between 10ºN and 22.5ºN to track the tropical easterly waves. Results from the study show that a tropical easterly wave trough often crossed western Mexico (110ºW) 1-3 days prior to surge onset at Yuma, AZ. However, the data also show that surges can occur without the passage of an easterly wave, indicating that other mechanisms are involved in gulf surge initiation. Gulf surges are important within the NAM domain because the northward transport of low-level moisture into the lowlands of the Sonoran Desert increases convective potential.

2.2 Previous Subtropical Upper-Level Low Studies

The primary area of formation of subtropical upper-level cold lows in the summertime is in the TUTT. The TUTT is a mean summer circulation feature that was first detailed by Sadler (1967). Using radiosonde, aircraft, and satellite wind observations, Sadler (1975) showed that TUTTs are a permanent summer feature of the North Pacific, South Pacific, North Atlantic, and South Atlantic. For example, in the North Atlantic region, the mean TUTT axis tilts west-southwestward from the central North Atlantic into

the Gulf of Mexico (Fig. 5). The TUTT is characterized by a narrow, cyclonic shear zone that typically displays large horizontal tilt. When the midlatitude westerlies retreat anomalously far northward, the TUTT axis can shift northward and lie near 25-30°N. Once the trough axis has shifted northward, individual lows that develop in the cyclonic shear zone often migrate westward into the southern and southwestern United States (Whitfield and Lyons 1992).

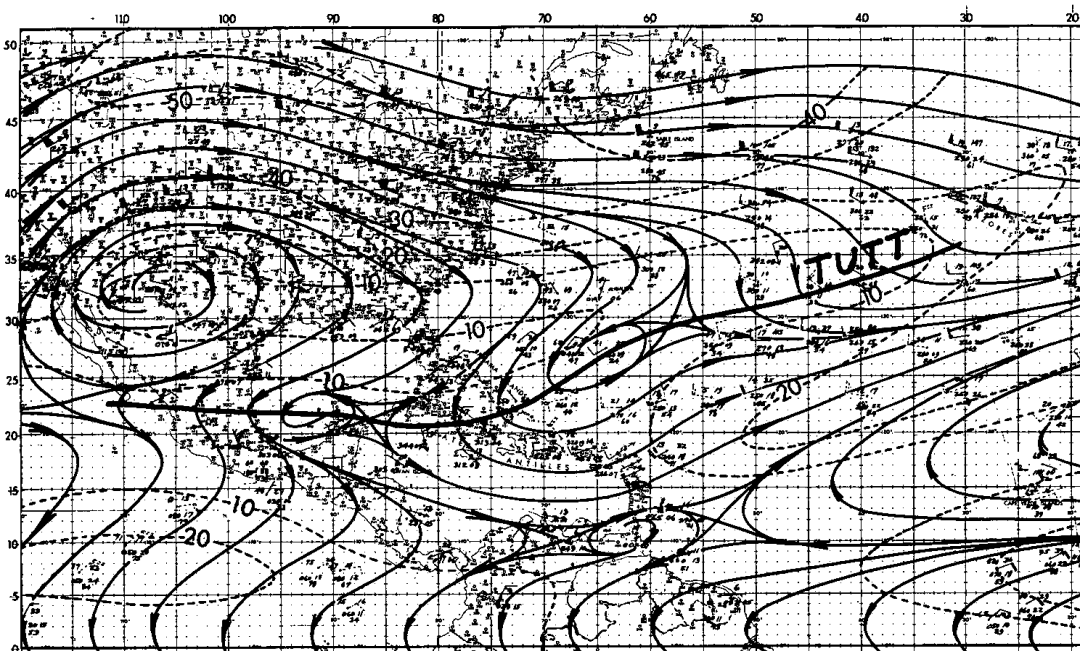

Figure 5: Long-term mean 200-hPa streamlines over the Gulf of Mexico, Caribbean, and Atlantic Ocean during July. The TUTT axis is shown by the heavy black line.

Erickson (1971) was one of the earliest studies to investigate the temperature anomalies and vertical motion pattern associated with a westward moving upper-level cold low. The upper-level low moved over the Bahamas region and produced significant cloudiness on its eastern flank. A large area of negative temperature anomaly extended from 250 hPa to the surface with warm anomalies in the 150-100 hPa layer. The upper-

level system achieved a maximum circulation near 200 hPa. Erickson used a diagnostic numerical model to show that the Laplacian of temperature advection was the most important forcing function in determining the total vertical motion pattern around the low. While the calculated omega values were rather small (by midlatitude standards), there was a tendency for upward motion east and southeast of the 200-hPa low and downward motion to the west and northwest.

The purpose of an early study by Kelley and Mock (1982) was to quantitatively determine the mean characteristics of subtropical upper-tropospheric cold lows found in the summertime mid-Pacific TUTT. Four summers (1967,1969-1971) of rawinsonde data from four western North Pacific island stations were used to calculate a composite of 117 lows. The authors then examined vertical cross sections through the composite low of the following fields: zonal and meridional winds, temperature and height anomalies, relative vorticity, divergence, vertical motion, and relative humidity fields. They found that the cold anomaly was largest near 300 hPa and extended weakly to the surface while there was a warm anomaly maximum near 125 hPa directly over the low center (Fig. 6). With regard to relative vorticity, the low circulation was primarily confined to the layer between 700 and 100 hPa (tilting northeast with height) with a vorticity maximum around 200 hPa (Fig. 7). The northwestern quadrant of the low was characterized by subsidence and relatively little cloudiness while the southeastern quadrant of the low was characterized by ascent and more cloudiness (not shown).

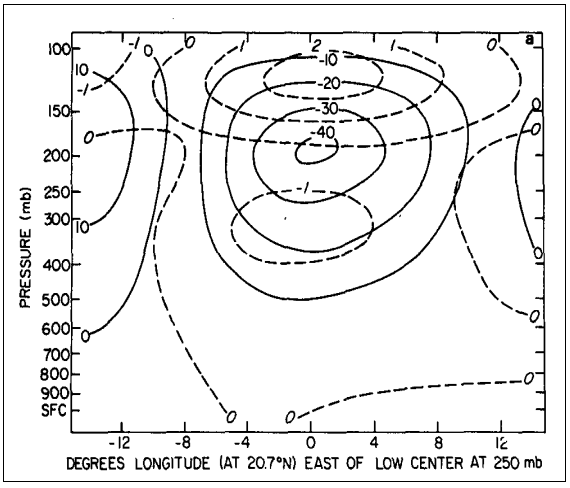

Figure 6: Composite height anomalies (m) (solid) and temperature anomalies (ºC) (dashed) in a west-east cross section through the 250-hPa low center.

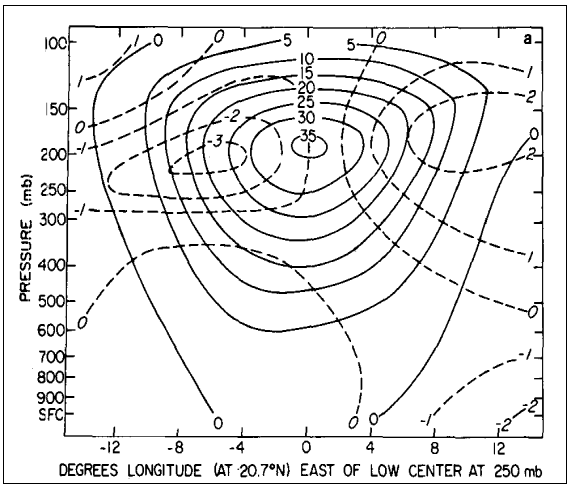

Figure 7: Composite relative vorticity (solid) and divergence (dashed) in units of $10^{-6}s^{-1}$in a in a west-east cross section through the 250-hPa low center.

While the Kelley and Mock (1982) analyses were conducted over the oceanic region of the North Pacific, a later study by Whitfield and Lyons (1992) examined a TUTT cold low that remained quasi-stationary over Texas in 1988. The authors used National Meteorological Center global gridded analyses from the National Center for Atmospheric Research (NCAR) along with daily rainfall data from a network of 660 rain gages in Texas to document their case. Horizontal and vertical cross sections of wind, temperature, vorticity and relative humidity were created. The results from this study were very similar to the findings from Kelley and Mock (1982). In particular, the strongest cold anomaly was found near 300 hPa within the TUTT low and the cold anomaly weakens downward to 700 hPa (Fig. 8). The TUTT low circulation is strongest, or has the largest relative vorticity, at 200 hPa (Fig. 8). Moreover, anomalous subsidence (with respect to the area average) was found near the center and along with the western flank of the low while weak anomalous rising motion was found along the eastern flank. The precipitation statistics are

in general agreement with the vertical motion fields. Rainfall stations in the southeastern quadrant of the TUTT low reported more rainfall than stations in the northwestern quadrant. The authors suggest that southward-directed positive vorticity advection from midlatitudes, conservation of absolute vorticity, and local vorticity convergence within the TUTT axis supplied the initial vorticity for the developing low.

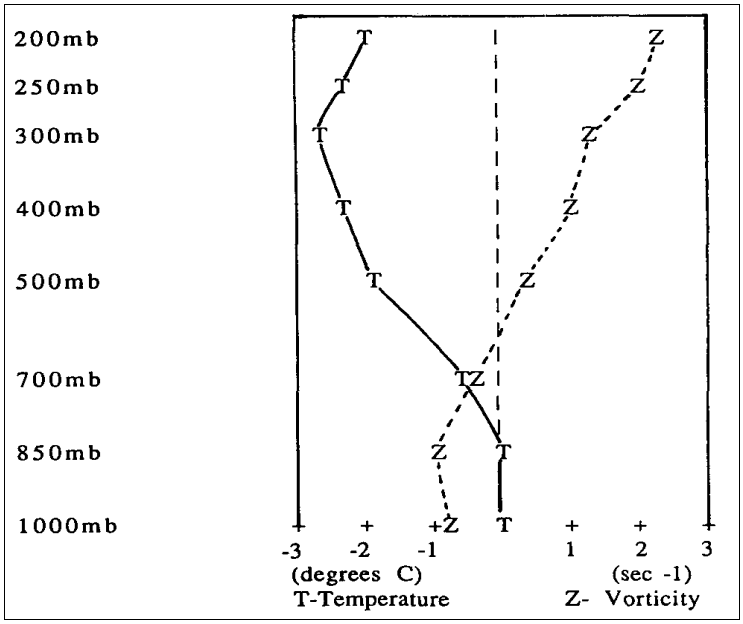

Figure 8: Vertical profiles of temperature anomalies (ºC) and vorticity ($10^{-5}s^{-1}$) averaged over the grid points encompassing the TUTT low center over Texas. Values are averaged over the period 27 July 2008 through 5 August 2008.

A preliminary examination of eleven TUTT lows from the 2004 NAME was performed by Pytlak et al. (2005). During NAME, the forecasters at the Forecast Operations Center (FOC) realized that numerous upper-level lows frequently passed the NAM region and also played a significant role in modulating the development of MCSs. In particular, the authors recognized that both leading and trailing portions of these upper

level systems can play a critical role in initiating and organizing convection into MCSs. The authors proposed a conceptual model (Fig. 9) whereby an upper-level closed circulation could approach the southwest edge of the monsoon ridge and create an area of upper-level divergence on the northwest flank of the low. Such upper-level divergence could enhance rising motion on the leading (west) flank of the low, seemingly in contrast to the previous studies of Kelley and Mock (1982) and Whitfield and Lyons (1992) which showed subsidence in that same area. Pytlak et al. (2005) also noted that some upper-level lows originated from short wave troughs that dropped into the southeastern United States, wrapped underneath the subtropical ridge, and then became steered into the NAM region by the subtropical easterlies.

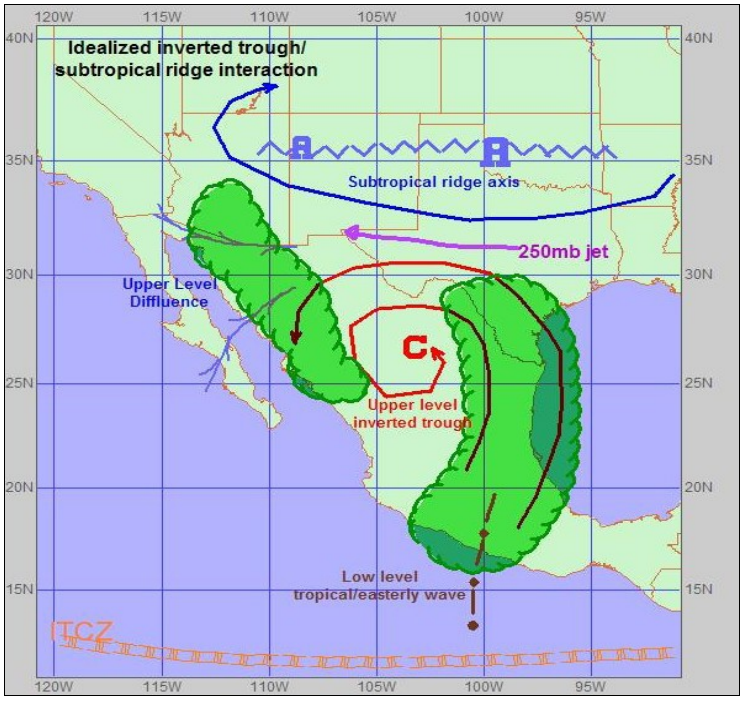

Figure 9: Conceptual model of an upper tropospheric circulation (inverted trough) approaching the western edge of the subtropical ridge and the associated flow.

A very recent study by Bieda et al. (2009) highlights the important role that inverted troughs play in modulating convection and precipitation over the NAM region. Utilizing cloud-to-ground lightning data, the authors compared flash counts on inverted trough days to non-inverted trough days. Times that had an inverted trough pass within the domain bounded by 23.5°N, 40°N, 100°W, and 120°W were considered inverted trough days. On inverted trough days, there is an enhancement of lightning counts as convection initiates over the climatologically favored high terrain of the Mogollon Rim and SMO by 1100 LST. As convection propagates westward away from the high terrain, the positive anomaly in lightning counts becomes more significant over the low deserts of northwest Mexico and southwest Arizona. When precipitation is accumulated using North American Regional Reanalysis (NARR) data, enhancement on inverted trough days can add up to 6 mm over a 24-h period over the low deserts. Thus, the study suggests that convective activity is increased over the NAM region, especially over the lower deserts, on inverted trough days compared to the background non-inverted trough days.

In a different study, Thorncroft et al. (1993) used a baroclinic spectral model to examine two contrasting types of upper-air trough behavior. The first type, characterized by a thinning trough, supports TUTT low initiation. The authors found that southwest-to-northeast tilting troughs that develop on the anticyclonic side of the jet will tend to thin as the trough moves equatorward. A small-scale cut-off cyclone can then develop as the trough wraps up anticyclonically in an equatorward wave-breaking event. From an examination of analyses done at the European Centre for Medium-range Weather Forecasts (ECMWF), the authors noticed that troughs moving over the eastern United States sometimes would thin, leaving a cut-off over the southern United States. Such a process

can lead to TUTT low initiation and the subsequent westward movement of the TUTT low on the southern flank of the subtropical monsoon high.

2.3 NAME Studies

Johnson et al. (2007) used multiple sources of NAME data in order to understand the mean upper-tropospheric and lower-tropospheric flow characteristics during NAME. The onset of the 2004 NAM (defined as a shift in the 300 hPa wind from westerly to easterly) occurred around 10 July, which was about ten days later than the 25-year NCEP Reanalysis mean. During the post-onset phase of the monsoon, there is a dominance of westward propagating disturbances across the NAME domain. The 300 hPa meridional wind fluctuated between northerly and southerly in association with the passage of inverted troughs. The authors note that a prominent upper-level trough passed through the Enhanced Budget Array (EBA) around 13 and 23 July. Both of these troughs were associated with gulf surges, with the 13 July surge documented in Rogers et al. (2007). The 300 hPa mean flow, 300 hPa height anomalies, and potential vorticity (PV) variance during the experiment was also computed (Fig. 10). The 300 hPa height anomalies clearly indicate that the subtropical anticyclone was shifted south of its normal position in 2004. Also, the maxima in PV variance downstream of the trough axis over Texas was attributed to frequent occurrence of TUTT-like lows in that area.

Douglas and Englehart (2007) recently developed a long-term (1967-2001) summer climatology of transient synoptic systems that move across northern Mexico. The synoptic features investigated in the study include inverted troughs, cutoff lows, cold fronts, and

open troughs (westerly short waves). The principal data source for the project was images from the NOAA "Daily Weather Map" series. After developing the long-term climatology, the authors found that inverted trough days in the NAM region exceeded all other synoptic features by about a factor of two. All westward-moving waves at 500 hPa were referred to as inverted troughs. It should be noted that 500 hPa is low enough in the atmosphere to sample easterly waves. However, since the geographic domain used in the study is north of 23°N, and easterly waves often propagate south of this latitude, the majority of detected 500-hPa troughs are likely midlevel manifestations of upper-level inverted troughs.

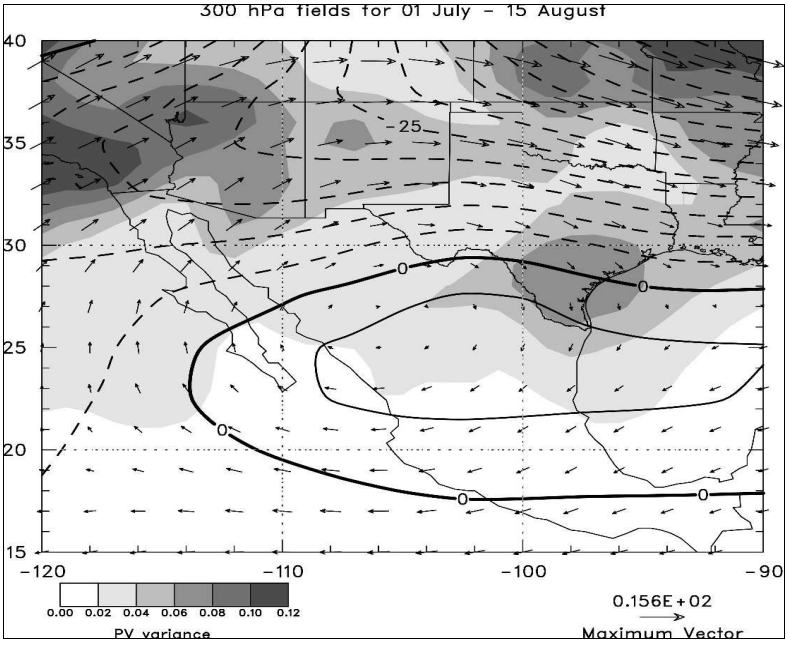

Figure 10: Mean 300-hPa flow, height anomalies from the 25-yr mean (1980-2004), and potential vorticity variance (PVU^2) for the 2004 NAME EOP.

Since inverted troughs were the most prevalent feature in the climatology, Douglas and Englehart (2007) evaluated the impact of inverted troughs on daily rainfall totals in northern Mexico. Several climate divisions (Fig. 11) were identified in order to calculate

average daily rainfall. The position of the inverted trough and its relationship with subsequent 24-hour precipitation for climate division two (central Sonora) is shown in Fig. 12. Interestingly, average daily rainfall in Sonora is higher when the trough is located to the east of the division. This finding is in general agreement with observations from forecasters during NAME and Pytlak et al. (2005) that enhanced rainfall tends to occur on the west (leading) flank of the upper-level low. Inverted troughs are an important contributor to rainfall in the NAM region, as the authors found that western sections of the SMO receive up to twenty percent of the summer rainfall from these synoptic systems.

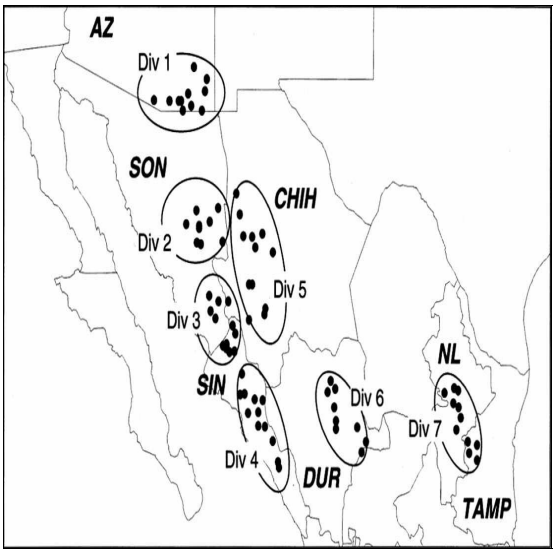

Figure 11: Location of synoptic climate divisions in northern Mexico. For each division, average daily rainfall (mm) was calculated.

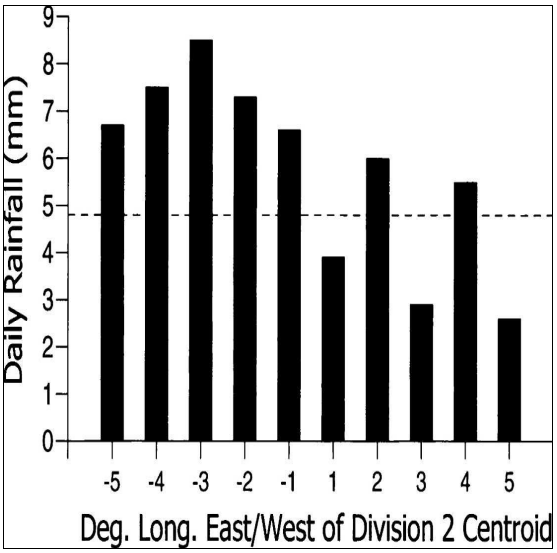

Figure 12: For rainfall division two, the relationship between inverted trough position and daily rainfall reported in the 24 hour period following this position. Positions are east (-) and west (+) of the region and the dashed line represents mean daily rainfall of all positions.

By developing a long-term summer climatology of transient systems crossing northern Mexico, Douglas and Englehart (2007) were able to compare synoptic feature

frequencies during 2004 NAME to the long-term mean. In 2004 the summer monsoon season was greatly shortened due to a poorly developed subtropical high. This meant that the number of inverted trough days across northern Mexico was about seventy percent of the long-term mean. However, despite the shortened monsoon season across the NAME domain, rainfall in central Sonora (climate division two) was actually near normal due to very heavy rainfall associated with inverted troughs. The peaks in average daily rainfall that occurred in Sonora around July 14 and 23, 2004 (Fig. 13) correspond to times when an inverted trough was located to the east of the division.

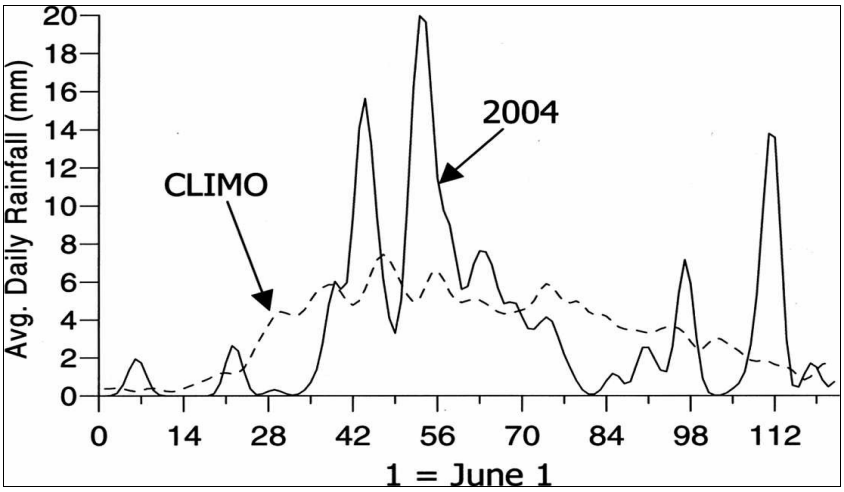

Figure 13: Daily rainfall in Sonora (division 2, Fig. 11) for the 2004 monsoon season as compared to the long-term climatology.

Another recent study by Lang et al. (2007) analyzed NAME precipitating features over the Sinaloa region using a multi-radar network. The network consisted of three radars: the NCAR S-Pol radar north of Mazatlán and two Servício Meteorológico Nacional Doppler radars (one at Guasave, north of S-pol on the coastal plain, and one at Cabo San Lucas). Looking at the diurnal cycle of convection, the authors discovered that convective

triggering occurs over the SMO almost every afternoon. During "undisturbed" periods, the initial convective cells do not organize, and hence convection does not reach the gulf after sunset. However, during "disturbed" periods, the precipitation features grow upscale and are longer-lived. The authors characterized three disturbed regimes to account for the movement of larger-scale precipitating features. Regime A is characterized by a coherent progression of enhanced rainfall in a coast-normal sense from the SMO to the GOC (Fig. 14). On non-regime A days, the precipitation largely remains over the SMO foothills and peaks. Regime A days, on the other hand, exhibit a much higher frequency of rainfall during the evening and overnight (1800-0600 LT) along the lower foothills and coastal lowlands. Regime B is defined by a progression of precipitation nearly parallel to the coast. Finally, regime AB refers to instances where the precipitation moves both cross-coast and along-coast (the intersection of regime A and regime B).

In order to ascertain the environmental influences (thermodynamic and shear profiles) associated with the different regimes, Lang et al. (2007) collected sounding data at Los Mochis, Sinaloa and Mazatlán, Sinaloa (for locations see Fig. 15). There is very little difference in the CAPE and CIN values between regime and non-regime days at Los Mochis. All regime-averaged soundings contain at least 1500 J kg^{-1} of CAPE, with slightly higher CAPE during non-regime days. However, during disturbed periods the 0-4 km shear is noticeably increased, especially at Mazatlán where low-level shear is nearly a factor of two larger during disturbed periods. The authors also discovered that cross-coast 700-hPa winds and along-coast 700-hPa winds are greater at Mazatlán during regime days than non-regime days. Hence, the results of this study suggest that increases in midlevel wind speeds correspond to increases in the environmental low-level wind shear, which

promotes organization and longer-lived systems in regime periods. The authors concluded the study by compositing 700-hPa heights and winds from NARR data. During regime AB the radar domain is located in close proximity to a 700-hPa trough, with the trough axis located to the southeast of the domain. The trough axis is absent from the non-regime NARR composite.

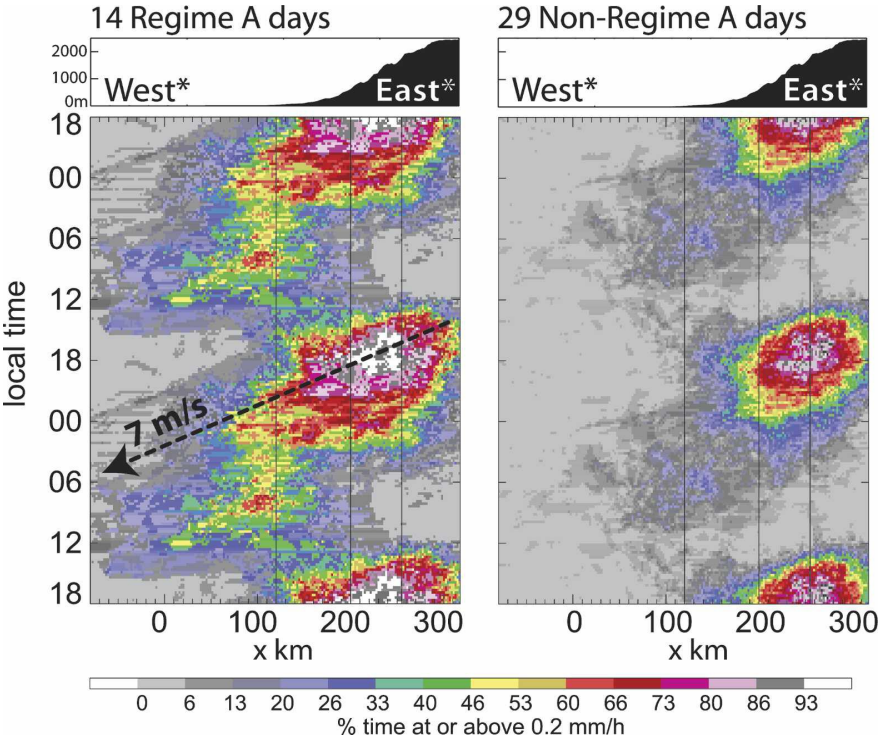

Figure 14: Percentage of time that the rainfall rate meets or exceeds 0.2 mm h^{-1} as a function of local time: (left) regime A days and (right) non-regime A days. Mean surface elevation in the cross-coast dimension is profiled at top.

2.4 Summary

Previous studies by Erickson (1971), Kelley and Mock (1982), and Whitfield and Lyons (1992) have detailed the temperature and vorticity structure of subtropical upper-level cold lows. These authors discovered a cold anomaly that extended from 300 hPa to

the surface and a vorticity maximum near 200 hPa. The circulation of the lows is largely confined to the mid and upper-levels of the atmosphere. The studies revealed anomalous rising motion on the eastern side of the upper-level low while there was general subsidence to the west. Recent studies focusing on the NAME region suggest that the spatial patterns of vertical motion surrounding upper-level inverted troughs that move across northern Mexico may be different from the studies above. Based on forecasting experience, Pytlak et al. (2005) proposed a conceptual model whereby increased upper-level divergence on the western flank of the inverted trough can promote enhanced rising motion. In agreement with Pytlak et al. (2005), Douglas and Englehart (2007) discovered an increase in Sonoran rainfall when the inverted trough was located to the east of the division.

The present study will use gridded analyses data from the 2004 NAME to examine two upper-level inverted troughs that moved across northern Mexico. The temperature and vorticity structure of the two lows can be compared to the findings of previous studies. In addition, satellite imagery is used to visualize where deep convection occurs in relation to the upper-low. Since previous NAME studies, in particular Lang et al. (2007), have documented an increase in convective organization with increasing vertical wind shear, the midlevel winds and vertical wind shear associated with the two upper-level inverted troughs will be examined.

CHAPTER 3

DATA AND METHODS

3.1 NAME Tiered Structure

From June through September 2004 the NAME field campaign was conducted over northwest Mexico and the southwest United States to study the NAM. More specifically, the experiment's primary objective was to determine the "sources and limits of predictability of warm season precipitation over North America, with an emphasis on time scales ranging from seasonal-to-interannual" (Higgins et al. 2006). The following are just some of the complex aspects of the NAM that were to be examined: GOC low-level jet, gulf surges, easterly waves, upper-level inverted troughs, MCSs, and the diurnal cycle of convection. In order to accomplish these multifaceted goals, a tiered (nested) structure was developed for the 2004 field campaign with three nested domains (Figure 15).

The three nested domains (in increasing spatial dimensions) are the Enhanced Budget Array (EBA), Tier I Array (T1A), and the Tier II Array (T2A). In the EBA, a dense network of soundings was provided to examine heat and moisture budgets in proximity to the rain gauge and radar networks (Johnson et al. 2007). The T1A domain (20°-35°N, 105°-115°W) covers the core NAME region where the primary objective is to resolve the wind, temperature, and moisture fields around the GOC. Finally, the T2A domain (15°-

40°N, 90°-120°W) covered most of Mexico and the southwestern United States. The primary objective of T2A was to understand phenomena associated with the intraseasonal variability of the NAM. Many of the results and plots from this study utilize data within the T2A domain since the tracks of the upper-level inverted troughs often included locations inside the T2A domain, but not necessarily in the T1A domain.

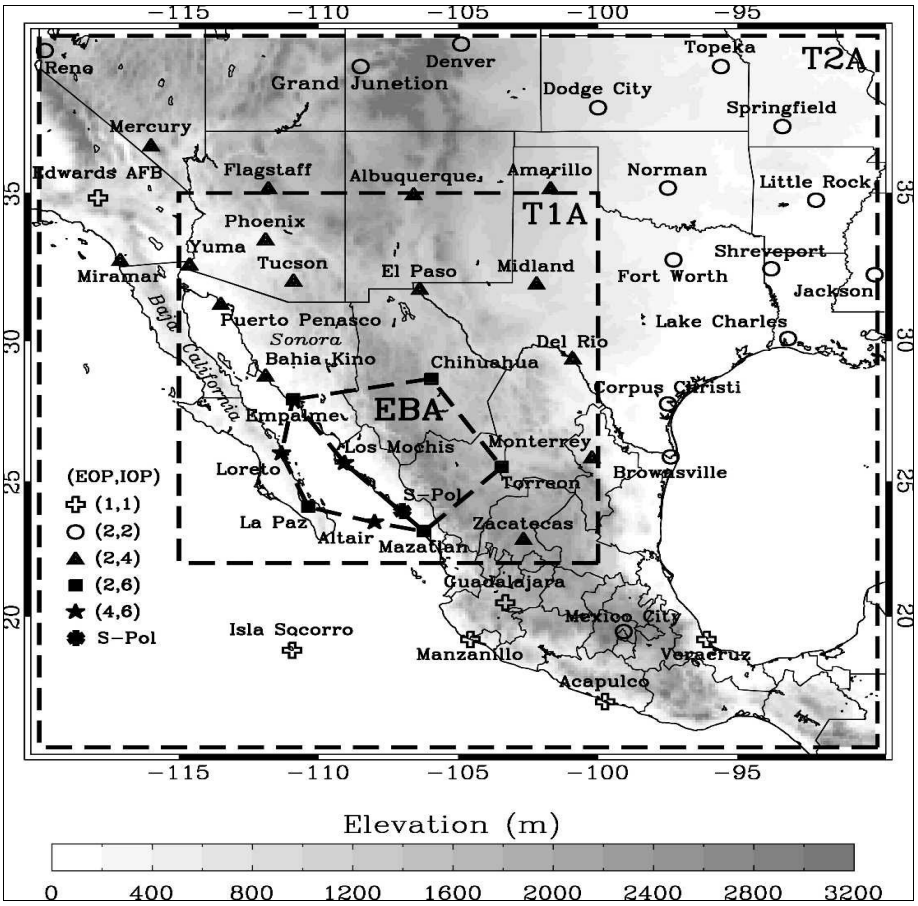

Figure 15: NAME sounding network and three grids (EBA, T1A, T2A) used for sounding analysis. The symbols indicate frequency of sounding launches per day during the EOP (left number) and frequency of increased sounding launches (right number) during IOPs.

3.2 Rawinsonde Data

The T2A domain consists of operational National Weather Service (NWS) sounding sites in the United States and the Mexico Weather Service (Servicio Meteorológico Nacional or SMN). The extended observing period (EOP) of the NAME field campaign ran from 1 June – 30 September 2004, although many of the instrumentation platforms were only in operation from 1 July – 15 August. Many of the sounding sites within the T2A domain increased their launch frequency during the nine intensive observing periods (IOPs) (Fig. 15). Of the 23 NWS supported sites, 10 sites launched four rawinsondes per day during IOPs. The SMN supported 13 sites, 5 (2) of which launched six (four) rawinsondes per day during IOPs. In addition to the NWS and SMN sounding sites, there were five additional sounding sites established along the GOC at Puerto Peñasco, Bahia Kino, Los Mochis, Loreto, and the Mexican Navy vessel *R/V Altair*. The Department of Defense (DOD) provided launch sites at Edwards Air Force Base in California and Yuma, AZ.

In addition to the rawinsonde sites within the T2A domain, there were three NCAR Integrated Sounding Systems (ISSs) which operated at Puerto Peñasco, Bahia Kino, and Los Mochis. The ISSs consisted of Vaisala GPS sounding systems, 915-MHz wind profilers, radio acoustic sounding systems (RASSs), and an enhanced surface observing station. The 915-MHz wind profiler provided high time resolution wind profiles in the lowest 2-3km of the atmosphere. The RASS provided a vertical profile of potential temperature in the lowest 1.25 km. The NOAA P-3 aircraft conducted ten missions along the GOC with the primary objective to study the low-level jet and gulf surges. A final

source of data was obtained from the National Aeronautics and Space Administration's Quick Scatterometer (QuickSCAT), which provided surface wind estimates over the GOC and the Eastern Pacific.

Quality control procedures modeled after those used in TOGA COARE (Loehrer et al. 1996) were performed on the raw NAME sounding data. The procedure includes automated internal consistency checks and the assignment of quality flags. After the assignment of quality flags, detailed quality control checks were conducted by the Colorado State University (CSU) Mesoscale Dynamics group. This included visually inspecting thermodynamic variables and vertical profiles for the u and v-wind components using skew-T plots (Johnson et al. 2007). The quality control procedure in its entirety can be found at *http://tornado.atmos.colostate.edu/name/*.

3.3 NAME Gridded Dataset

The quality controlled sounding data was objectively analyzed using the multiquadric interpolation scheme of Nuss and Titley (1994). In Version 3.0 of the CSU-NAME gridded dataset, fields of horizontal wind components, temperature, specific humidity, and geopotential height were computed using the interpolation scheme at 1º horizontal resolution and 25 hPa (from 1000 to 50 hPa) vertical intervals. The gridded analyses over the T2A domain were produced at 0000 UTC and 1200 UTC for the period 1 July to 15 August. Gridded analyses over the T1A domain were produced at 0000 UTC, 0600 UTC, 1200 UTC, and 1800 UTC during the time of intensive observations from 7 July – 15 August. Profiler data from the ISS sites and pibal soundings were merged into

the gridded datasets at times when rawinsonde winds were unavailable. Moreover, observations from METAR stations over land and QuikSCAT winds over the ocean were incorporated into surface analyses. It should be noted that results from this paper used Version 3.0 of the CSU-NAME gridded analyses. The recently updated Version 3.1 contains humidity corrections to the upper-air data at all the sounding sites in the T1A domain, however no calculations using specific humidity fields were made in this study.

In addition to the gridded basic fields discussed above, a set of gridded "derived" fields was also computed. The derived fields included vertical p-velocity ω, divergence, vorticity, apparent heating Q1, and apparent drying Q2. The gridded omega values were computed through the kinematic method where horizontal divergence is integrated upward starting at the surface (Johnson et al. 2007). In Version 3.0 of the CSU-NAME gridded dataset, surface winds were used to calculate orographically forced vertical motion at the surface (slope flows).

Due to the data-sparse ocean regions in the T2A domain, grid points over the Eastern Pacific and Gulf of Mexico used NCEP Reanalysis data (Kalnay et al. 1996). NCEP Reanalysis data were only applied to the large-scale T2A analyses so that meaningful results could be obtained over the open ocean where no soundings existed. There were a few times, especially at the beginning of their life cycles, when IV4 and IV6 were located in close proximity and/or over the Gulf of Mexico. However, the reanalysis data was not applied to the interior T2A domain over land where observations are more plentiful. Thus, the results of this study are largely independent of model data. Reanalysis data was not applied over the GOC or the interior NAME domains (T1A and EBA).

3.4 Satellite Data

Geostationary Operational Environmental Satellite (GOES)-10 images were obtained from the NAME field catalog website (http://catalog.eol.ucar.edu/name/). There were visible, IR, and water vapor (WV) images available, but IR and WV images were primarily used in this study. Convective features during the NAME generally developed over the SMO in the early afternoon/evening. Sometimes the convective cells organized into an MCS and moved westward to the coastal plain after sunset. Since visible imagery ends near sunset, IR and WV imagery were much more useful in analysis. IR imagery was used to help identify areas of deep convection relative to the inverted trough, especially after sunset. The WV channel gives an indication of water vapor in the mid-to upper-troposphere. Since inverted troughs are largely upper-level features, the WV imagery was very useful in tracking the upper-level circulation. On many occasions, the position of an inverted trough based on WV imagery was compared to upper-level relative vorticity plots from the gridded analyses to discern agreement.

3.5 Tracking the Inverted Troughs

In order to track the inverted trough as it moved across the NAME domain, the position of the inverted trough at a particular time had to be determined in some way. Based on previous studies by Kelley and Mock (1982) and Whitfield and Lyons (1992), the maximum relative vorticity of the upper-level lows in their studies was found around 200 hPa. Thus, I determined the position of the inverted trough every twelve hours (0000 UTC

and 1200 UTC) by noting the location of the maximum 200-hPa relative vorticity in the T2A gridded analyses. The 200-hPa wind field had to be closed at a particular synoptic time to be considered an inverted trough event. There were a few times when the location of the maximum 200-hPa relative vorticity was difficult to determine because there were two vorticity centers in close proximity. These times were omitted from the compositing procedures. During NAME, the forecasters at the FOC numbered the inverted troughs. Smaller (larger) numbers indicated that the inverted trough occurred earlier (later) in the experiment. In this study I kept the same numbering convention when referring to the inverted trough (i.e. if the forecasters called a particular inverted trough IV4, I also called it IV4).

The tracks of five inverted troughs that I chose to analyze are shown in Fig. 16. All the upper-level lows started at the easternmost endpoint and ended at the westernmost endpoint, indicating a general movement to the west. Note that two of the inverted troughs (IV4 and IV6) moved across northern Mexico while the other three (IV3, IV9, and IV10) moved across southern Mexico and into the eastern Pacific. This paper presents a detailed analysis of the two lows that moved across northern Mexico (IV4 and IV6). Both IV4 and IV6 spent the majority of their lifetime over land in northern Mexico where the network of operational and supplemental soundings could be utilized (Fig. 16). Notice that the three "southern" lows passed briefly over southern Mexico but then moved over the data sparse eastern Pacific Ocean for the remainder of their lifetimes. IV4 and IV6 are chosen for detailed analysis since a primary objective of this observational study is to utilize the unprecedented and dense NAME sounding network over northern Mexico. The fact that these lows were located in close proximity to the SMO means that one can study how these

lows modify the environment near the SMO, which has important implications for convection over the SMO and along the adjacent GOC coastal plain. Because the subtropical ridge was displaced anomalously far south during NAME, the number of inverted troughs moving across northern Mexico was limited to primarily IV4 and IV6. The three "southern" lows were used as a comparison (in terms of their thermodynamic and kinematic structure) to IV4 and IV6, but a more detailed analysis of these "southern" lows is not presented herein.

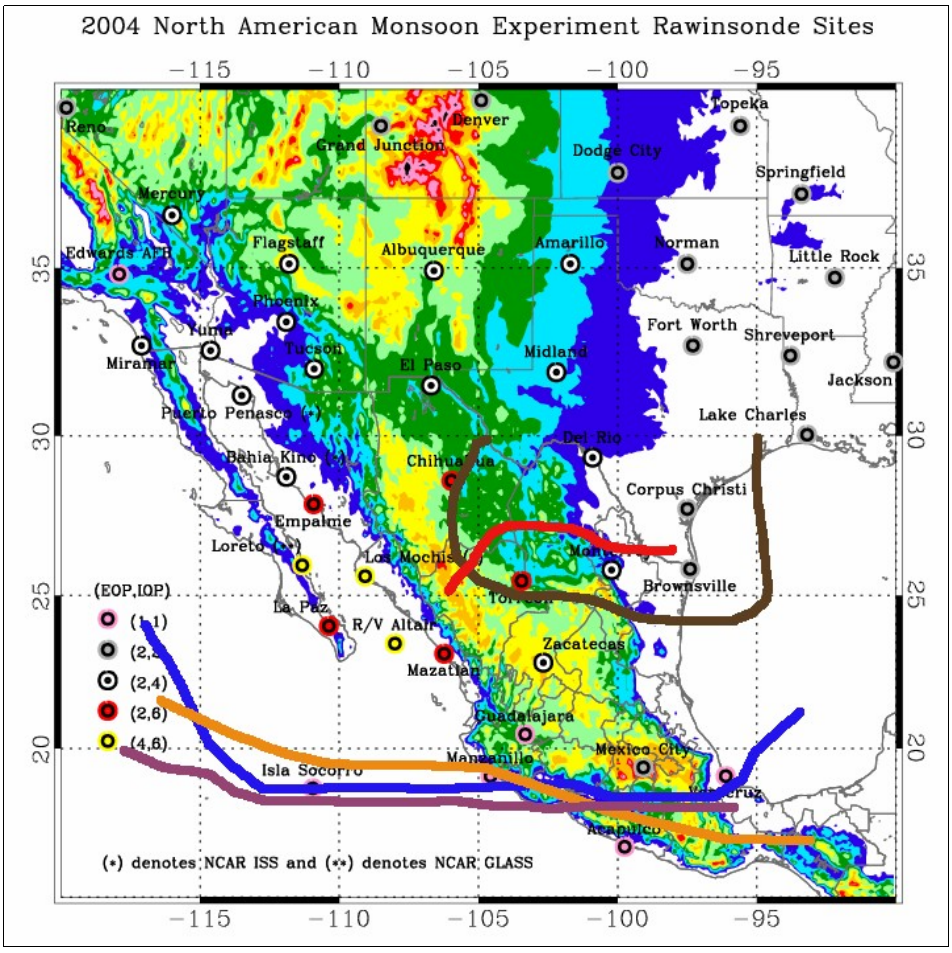

Figure 16: Tracks of five inverted troughs during 2004 NAME over the NAME enhanced sounding network. The two inverted troughs moving across northern Mexico are IV4 (brown) and IV6 (red). The three inverted troughs moving across the southern part of the NAME domain are IV3 (blue), IV9 (magenta), and IV10 (orange).

3.6 Anomaly and Compositing Procedures

Several of the plots in the following chapters will involve anomalies and composites of different fields. The anomalies were computed in one of two ways depending on the field being analyzed. For analysis of temperature, average values were computed at 0000 UTC and 1200 UTC over the period of the T2A gridded dataset (1 July – 15 August). These average values were then subtracted from their corresponding individual times. The purpose of using this method is to remove the diurnal signal from the observations. For analysis of potential vorticity, average values were computed over the 1 July – 15 August period (i.e., means of this field are averaged over the diurnal cycle).

Composites of different fields for the inverted troughs were calculated by averaging over individual synoptic times. The purpose of compositing is to obtain a mean structure of the inverted trough, similar to the methods of Kelley and Mock (1982) and Whitfield and Lyons (1992). The center of the composite plots corresponds to the location of the 200-hPa low center (as discussed earlier) that was used to track the upper-level low. In the case of IV4 (IV6), there were nine (six) individual times in the temperature and vorticity composites. Several of these composite plots are west-east vertical cross sections through the low center that enable a detailed examination of the mean vertical structure of the low. Increased horizontal dimensions were desired in the QG omega and midlevel wind composite plots. Hence, some of the synoptic times where the inverted trough was located near the eastern boundary of the T2A domain had to be removed from these composites. Six (five) synoptic times were included in the QG omega composites for IV4 (IV6). Six synoptic times were included in the midlevel wind composites for both inverted troughs.

3.7 QG Omega Calculations

3.7.1 Traditional Quasi-Geostrophic (QG) Equation

In order to investigate the QG vertical motion that is forced by the upper-level inverted troughs, the traditional QG omega equation is utilized in this study. The traditional QG equation can be written following Bluestein (1992) as:

$$[\nabla_p^2+(f_o^2/\sigma)(\partial^2/\partial p^2)]\omega = -(f_o/\sigma)\partial/\partial p[-\mathbf{v_g}\bullet\nabla_p(\xi_g + f)] - (R/\sigma p)\nabla_p^2[-\mathbf{v_g}\bullet\nabla_p T] \qquad (1)$$

(A) (B) (C)

The static stability parameter σ [$\sigma = -(RT/P\Theta)(\partial\Theta/\partial p)$] is assumed to be a function of pressure only and f_o is the constant Coriolis parameter ($4.9x10^{-5}$ s^{-1}). The first term (B) on the right-hand-side (RHS) of the above equation represents the vertical rate of change of horizontal vorticity advection (differential vorticity advection). The second term (C) on the RHS represents the horizontal Laplacian of temperature advection. We can make the common assumption that term (A) is proportional to $-\omega$. This approximation, which holds most true in the middletroposphere (Bluestein 1992), implies that vertical velocity can be determined from the sign and intensity of the RHS forcing mechanisms. If the forcing function is positive (negative) then upward (downward) motion is forced. For example, synoptic-scale ascent (subsidence) is often associated with vorticity advection increasing (decreasing) with height and a local maximum in warm (cold) advection.

Given the "forcing functions" of (B) and (C) along with the proper boundary conditions on ω, the vertical motion field can be found at any time by inverting the operator

on the left-hand-side (LHS) of (1). However, one cannot diagnose the vertical velocity locally, in isolation from its surroundings. The three-dimensional elliptic operator on the LHS of (1) means that the vertical velocity at a particular point in the atmosphere depends on the omega values at other locations in space.

Since (1) is linear in ω, then the total vertical motion can be written as the sum of the solutions given by the two individual forcing components (Bluestein 1992). Suppose that ω_v and ω_T are contributions from the differential vorticity advection and Laplacian of temperature advection, respectively. If homogeneous boundary conditions are applied (ω set to zero on the lateral and vertical boundaries of the computational domain) then the total vertical velocity can be expressed as $\omega = \omega_v + \omega_T$. Thus, the advantage of using the traditional form of the QG equation is that you can determine the contribution from the individual forcing terms to the total vertical velocity. One can answer the question: what vertical velocity is the vorticity advection term or temperature advection term forcing?

The "forcing" terms and omega values were solved for over the pressure layer between 700 and 100 hPa. The choice of using 700 hPa as the lower boundary ensures that the lower boundary is above the SMO at all times. Also, since upper-level inverted troughs are largely mid-to-upper tropospheric features, we expect the induced forcing to be greatest in this pressure layer.

3.7.2 Finite Differencing and Relaxation Procedure

In order to apply the QG omega equation, horizontal and vertical derivatives must be calculated on the LHS and RHS of (1). The fields of $\mathbf{v_g}$ and ξ_g were expressed in terms

of the instantaneous geopotential height field. Both the horizontal and vertical derivatives on the RHS were approximated by centered finite differencing. The RHS forcing terms were computed at each grid point then summed to obtain the total RHS forcing at each grid point. The LHS quantities were approximated using centered finite differencing in deriving the relaxation equation. Thus, the RHS "forcing" terms were first computed in finite difference form and then used as input into a relaxation-type solution (Pauley and Nieman 1992).

To use a relaxation procedure to solve (1) for omega, the equations must be elliptic. For the case of the QG omega equation, ellipticity is ensured if σ is positive (Bluestein 1992). Since σ is positive for non-superadiabatic lapse rates (i.e. everywhere in the 700-100 hPa layer), then the omega equation is elliptic. Suitable boundary conditions for ω must also be specified before relaxation can be used. The lateral boundary condition is set to zero. The upper and lower boundary values for ω are also set to zero. By using 700 hPa as the lower pressure level in the computations, the lower boundary is far enough removed (in a vertical sense) from the surface pressure level across most of the domain. Hence, vertical motion associated with orographic forcing across the lower boundary is rather negligible. The relaxation was continued until the greatest difference between successive iterations was less than 10^{-3} Pa s^{-1} across the entire domain. This produces a solution that is accurate to a few hundreths of a Pascal per second. For both lows, approximately twenty-five iterations was sufficient to ensure convergence.

The solution obtained from the traditional QG omega equation was checked by solving the QG omega equation a second time using the Q-vector method (Bluestein 1992). The Q-vector representation combines the two terms on the RHS of (1) into one forcing

term. Vertical velocities can be approximated by the divergence of the Q-vector. After solving for QG omega using the two independent methods (traditional and Q-vector approach), there was very good agreement in the plots of total QG omega (not shown). It should be emphasized that the Q-vector method was only used to validate the solution obtained from the traditional method. All QG omega plots in this paper involve solutions using the traditional method, that is solutions to equation (1).

3.7.3 Boundary Condition Sensitivity

Alternative boundary conditions instead of zero were used to test the sensitivity of the vertical motion field to the choice of boundary conditions. To obtain this new set of boundary conditions, the QG omega equation was first solved with homogeneous boundary conditions, which gives estimates for ω at the grid points along the pressure levels adjacent to the vertical boundaries and along the rows and columns adjacent to the lateral boundaries. These values were then assigned to the adjacent boundaries. The omega equation is solved again with the new boundary conditions. It was found that significant changes in ω when compared to the homogeneous boundary conditions only occurred along the grid points immediately adjacent to the boundaries. At the remaining interior grid points, there was little sensitivity to the boundary conditions. The analysis of ω in the interior of the computational domain is most desired and not significantly affected by the choice of boundary conditions. Hence, the QG omega equation was solved by setting ω equal to zero along the lateral and vertical boundaries.

3.8 Kinematic Calculations

3.8.1 Midlevel Flow

To discern the midlevel steering flow in the vicinity of the inverted trough, the winds were averaged in the layer between 700 and 400 hPa. The choice of this pressure layer is somewhat arbitrary, but corresponds to roughly the lower half of the cloud bearing layer. The main purpose of generating steering flow plots is to identify the strength and magnitude of the midlevel flow, which influences not only the direction of storm movement but shear considerations. Composite plots of the midlevel flow were generated for both inverted troughs.

Additionally, the midlevel flow at individual synoptic times over the core NAM region was considered for the two periods encompassing inverted trough passage. The midlevel flow is computed at 0000 UTC since convection is initiating and organizing at this time in the evening along the SMO axis and adjacent foothills. The mean midlevel flow at 0000 UTC is also calculated by averaging over all 0000 UTC analyses during the period from 1 July – 15 August 2004. Thus, by comparing the steering flow vectors at a particular synoptic time to the average steering flow vectors, one can determine how the midlevel flow in the core NAM region deviates from normal monsoon conditions.

3.8.2 Vertical Wind Shear Calculations

There have been many observational and modeling studies that show the

importance of vertical wind shear in controlling the organization and longevity of convective systems (Rotunno et al. 1988, Weisman and Rotunno 2004, Jirak and Cotton 2007). There are several depths over which the vertical shear can be calculated. Weisman and Rotunno (2004) suggest that 0-5 km AGL shear is the most important in controlling MCS strength and longevity. Jirak and Cotton (2007) found shear over a depth of 0-3 km AGL as the best MCS predictor, however 0-6 km AGL shear had similar predictability scores. The present study considers an average shear, due to uncertainties in the shear depth that is most important for MCS organization over the core NAM region.

For each grid point where the shear is being calculated, the shear algorithm uses the surface pressure as the bottom pressure level. The mean zonal and meridional wind components at the lowest three pressure levels (i.e. surface, 25 hPa AGL, and 50 hPa AGL) are used to compute the surface wind conditions. Next, the algorithm determines the pressure levels that correspond to 3 km AGL and 6 km AGL. The variations in surface elevation inherently change the altitude (and pressure level) of 3 and 6 km AGL. The winds are averaged over the pressure levels that encompass the 3-6 km AGL layer to produce the midlevel wind conditions. Hence, at each grid point a surface wind (with components U_{sfc} and V_{sfc}) and a midlevel wind (with components U_{mid} and V_{mid}) is generated. The wind shear vector can then be computed by subtracting the surface wind vector from the midlevel wind vector.

CHAPTER 4

SYNOPTIC AND CONVECTIVE CONDITIONS

In order to diagnose the synoptic and convective conditions surrounding the two upper-level inverted troughs, plots at 200 and 600 hPa along with water vapor (WV) images will be presented in this chapter. The 200 hPa (600 hPa) pressure level was chosen to represent conditions in the upper (middle) troposphere. The plots begin at the synoptic time that is 12 h before upper-low formation and then continue at successive 24-h intervals until the upper-low dissipates. This means that six plots at 1200 UTC (8–13 July) are generated for IV4 while four plots at 0000 UTC (21–24 July) are presented for IV6. Maps at 200 hPa show heights, wind vectors, and the PV anomaly while maps at 600 hPa show heights, wind vectors, and relative vorticity. PV anomalies were plotted at 200 hPa but not 600 hPa since PV anomalies are maximized in the upper troposphere and are significantly weaker in the midtroposphere. By examining successive 24-h plots, one is able to detail the time evolution of important synoptic features associated with the inverted troughs.

WV images are presented to detail the mid and upper-level moisture conditions in the circulation of the upper-low. The advantage of using WV images over IR images stems from the fact that the upper-low circulation can be readily seen in WV and not in IR. Deep convection can also be seen in WV images as very cold brightness temperatures. Thus, the area of deep convection relative to the upper-low location can be analyzed. The WV

images were selected to depict times when the convection appeared to have its greatest extent or intensity. Therefore, the times associated with the WV images do not necessarily match the pressure plot times.

4.1 IV4

4.1.1 200-hPa Analyses

At 1200 UTC 8 July, 12 h before upper-low formation, a kink in the height field develops over the Texas-Louisiana area to the east of the 200-hPa jet on the east side of the subtropical ridge over central Mexico (Fig. 17a). The kink in the height field appears to be associated with an eastward moving shortwave trough in the westerlies. At 1200 UTC 9 July, the 200-hPa circulation becomes better defined with the northwesterly 200-hPa jet on its west side (Fig. 17b). The ridge axis builds northward to the west of the low. The formation of the upper-low agrees somewhat with the general region of cut-off low formation suggested by Thorncroft et al. (1993). However, IV4 develops from a shortwave trough that is different from the longwave NE-SW thinning trough considered in that study. The PV anomaly associated with the developing low begins to pinch off and drift southward with the attendant low. A much weaker TUTT low, originally over the Caribbean, moves westward and on 0000 UTC 10 July appears to merge with the main upper-level circulation that is moving southward (not shown). By 1200 UTC 10 July, the 200-hPa low circulation has become better defined with closed height contours over the western Gulf of Mexico (Fig. 17c).

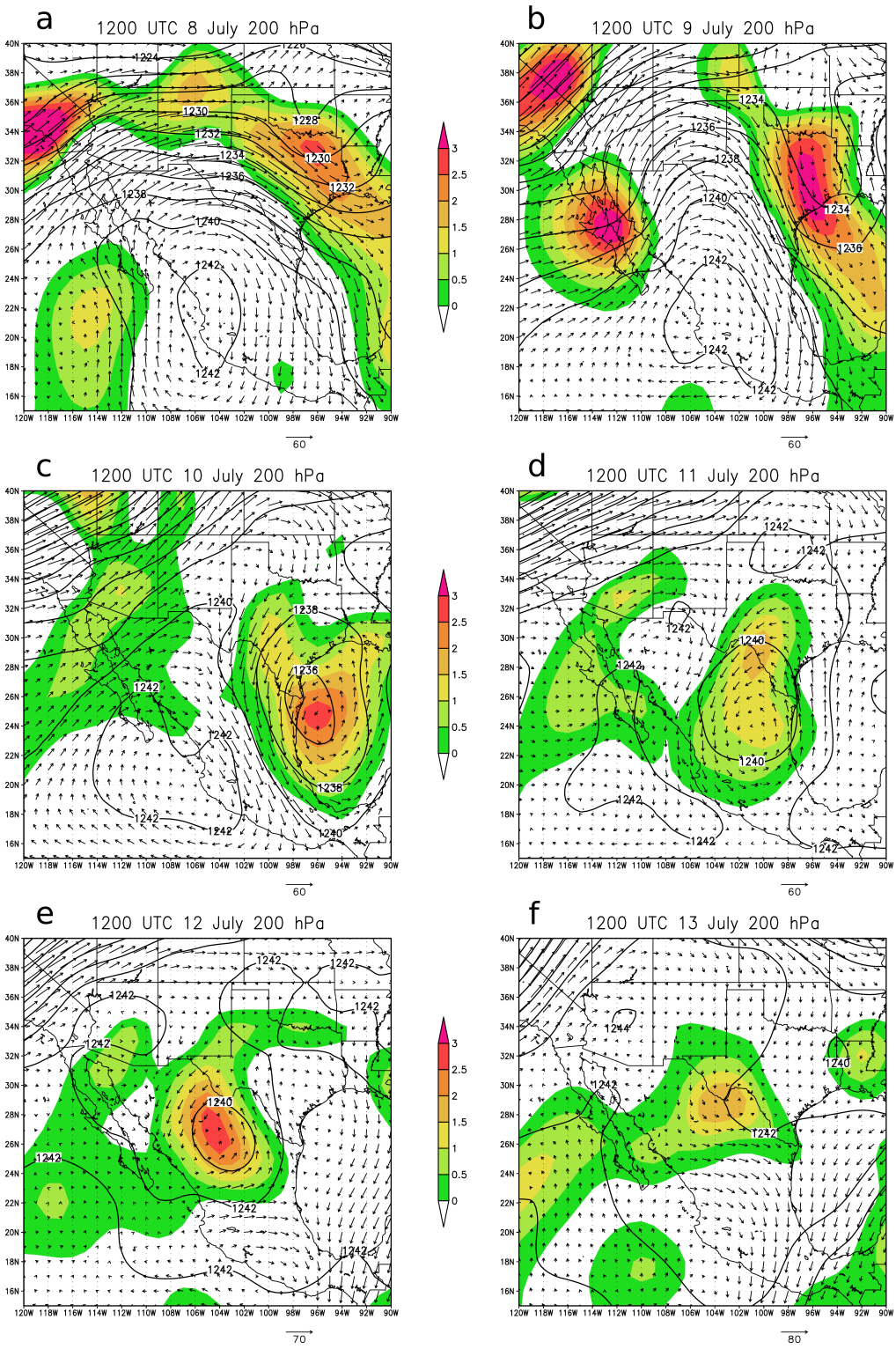

Figure 17: 200-hPa heights (decameters)(contoured), wind vectors (knots), and potential vorticity anomaly (PVU) (shaded) over the T2A domain at 1200 UTC from 8 July to 13 July.

It is at this time that IV4 begins moving westward to a position over central Mexico at 1200 UTC 11 July (Fig. 17d). The upper-low's movement is linked to the northwest propagation of the subtropical ridge to a position near Sonora. The low begins moving to the northwest shortly thereafter and at 1200 UTC 12 July the 200-hPa circulation remains strong along with the closed height contour (Fig. 17e). Heights continue to increase on the northwest flank of IV4 associated with the moving subtropical ridge. The upper-low then moves northward to a position near Big Bend, Texas on 1200 UTC 13 July (Fig. 17f). The diffluent 200-hPa flow to the west of IV4 likely contributed to the large MCS that formed over Sonora at 0600 UTC 13 July (Fig. 19e). Note that the 200-hPa circulation has become ill-defined, the positive PV anomaly has decreased in magnitude, and there are no longer closed height contours. This indicates a significantly weakened system over the Big Bend area and IV4 dissipated shortly thereafter. The average translational speed of IV4 over its lifetime is approximately 7 m s^{-1}. Several smaller-scale embedded circulation centers were identified by WV imagery to rotate within the larger system (Bob Maddox, personal communication). The large-scale circulation associated with IV4 is readily apparent in WV imagery and the T2A gridded dataset, while the small-scale circulations are not evident in the dataset.

4.1.2 600-hPa Analyses

Three important synoptic features of IV4 are identified at midlevels: the IV4 circulation itself, the subtropical ridge, and a tropical easterly wave (Fig. 18). Early in the period (8-9 July) the subtropical ridge is clearly located over the New Mexico-Texas area

(Figs. 18a,b). The midlevel manifestation of IV4 is evident by the 600-hPa relative vorticity maximum over southern Texas. Although the 200-hPa circulation is closed, IV4 is an open trough at 600 hPa. At 1200 UTC 10 July there are two main 600-hPa vorticity maxima across the T2A domain. One is over southern Texas associated with IV4 and the other is in the far southeast part of the domain (near Central America) that is associated with a westward moving tropical easterly wave (Fig. 18c). The easterly wave originated outside the T2A domain and was tracked into the NAM region using NCEP-NCAR reanalyses over a larger region (not shown). On 1200 UTC 11 July, the northernmost midlevel vorticity center associated with IV4 has moved westward and is now located at 27°N,102°W (Fig. 18d).

By 1200 UTC 12 July the midlevel vorticity center of IV4 is located over north-central Mexico with the easterly wave vorticity center located near 18°N,106°W (Fig. 18e). It is clear that the midlevel circulation of IV4 and the tropical easterly wave on the southern border of the plot are separate features identified by two separate vorticity maxima. As IV4 moves westward, the 600-hPa heights increase over the desert Southwest with the 600-hPa ridge center located near the Four Corners area at 1200 UTC 12 July. The tropical wave along the southern part of the domain eventually develops into Tropical Storm Blas on 12 July. The northwestward movement of Blas takes the low and midlevel circulation of Blas to the southwest of the southern tip of Baja California by 1200 UTC 13 July (Fig. 18f). At the same time, the midlevel circulation of IV4 is located to the north of Big Bend, Texas. The location of IV4 and Blas is such that a SW-NE tilted open trough stretches from southwest Texas to the circulation of Blas. The 600-hPa subtropical high has moved quite

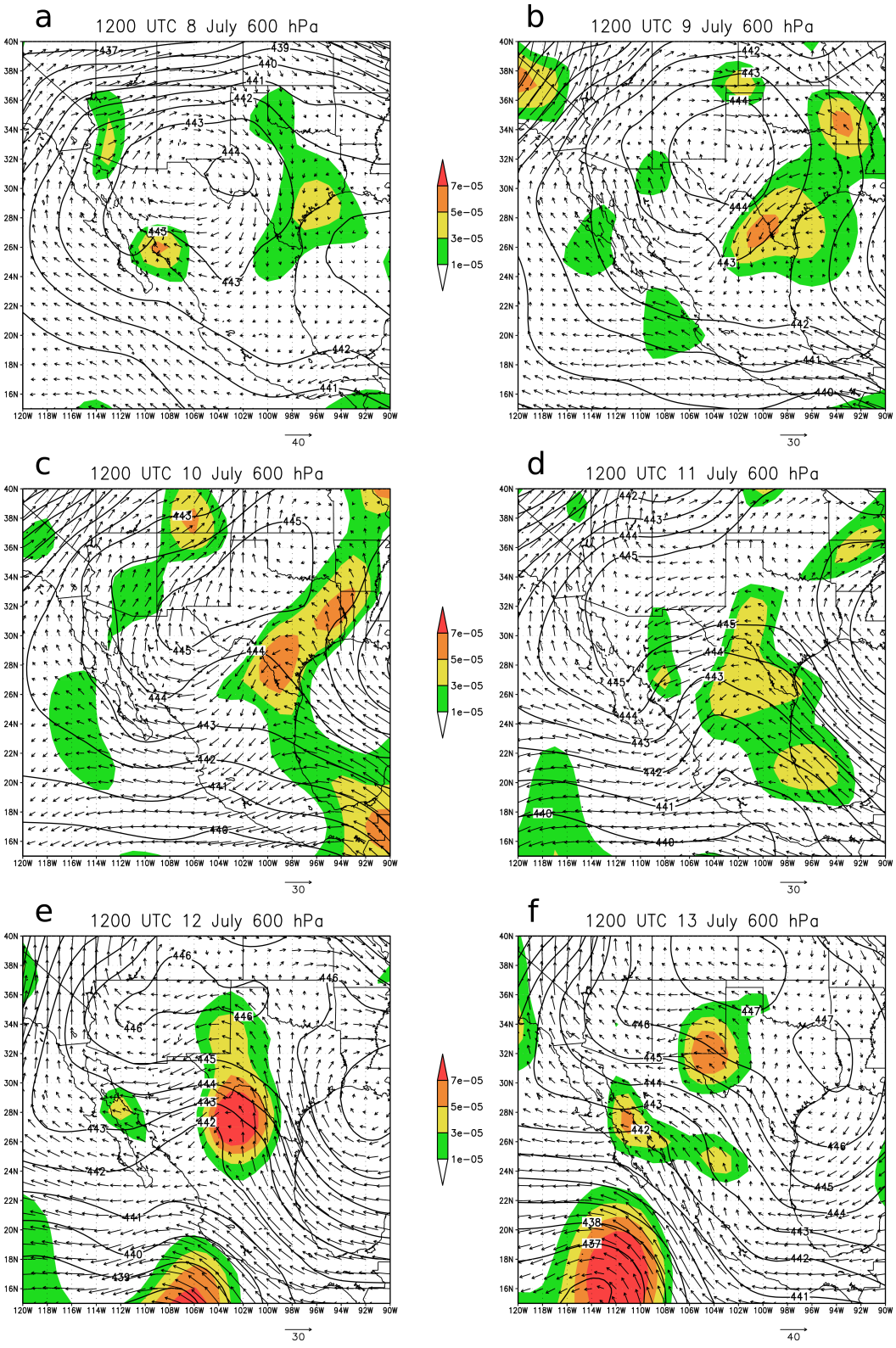

Figure 18: 600-hPa heights (decameters)(contoured), wind vectors (knots), and relative vorticity (s^{-1}) over the T2A domain at 1200 UTC from 8 July to 13 July.

far northward into southeast Colorado. Strong height gradients and very strong 600-hPa southeasterly winds occur over the mouth of the GOC by 1200 UTC 13 July. As a result of these southeasterly winds, moister air is advected northward into areas around the GOC (Rogers and Johnson 2007).

4.1.3 Convective Conditions

The evolution of the convection conditions around IV4 can be seen from the WV images in Fig. 19. During the initial formative stage of the upper low, the center of the low drops southward on 1209 UTC 9 July (Fig. 19a). The low center is characterized by relatively dry conditions in the upper troposphere while there is an MCS to the northeast of IV4 over the coastline of Louisiana. Two days later (1209 UTC 11 July) the low has moved over east-central Mexico. The deepest convection, along with a developing MCS, occurs over the Gulf and along the Mexican Gulf coast to the east of IV4 (Fig. 19b). Extremely dry conditions in the upper troposphere are evident in the western part of the domain (Baja Peninsula and adjacent Eastern Pacific) where strong southwesterly upper-level flow is advecting drier into that region.

As the upper-low moves westward over the time period from 10 July to 12 July, deep convection over western Mexico occurs over progressively lower elevations west of the Continental Divide. By 0308 UTC 12 July convection organizes into a large MCS over the southern GOC coastal plain near Los Mochis (Fig. 19c). The MCS moves westward and dissipates shortly after reaching the GOC. This marks the first time since the formation of IV4 on 9 July that deep convection reaches the GOC as convection had

largely been limited to higher elevations of the SMO before this date. Other important features include the large area of cloudiness and high moisture content to the southwest of IV4, which is associated with the developing tropical depression. It appears that upper-level moisture from the south is being wrapped into the circulation of IV4, as evidenced by the moist conditions along the southern periphery of the low (Fig. 19c). Again, convection appears to be suppressed in the low center with a relative minimum in moisture.

Deep convection on 13 July follows the northwestward progression of IV4. At 0008 UTC 13 July there is a developing MCS in northwest Sonora and increased thunderstorm activity over southern Arizona compared to the previous evening (Fig. 19d). The convective environment over the Sonora region must have become more favorable on this day to support organized convection. There is also a line of thunderstorms initiating along the SMO axis in Sinaloa. Deep convection has clearly decreased to the east of IV4 although upper-level moisture and clouds encircle the low along its periphery. After six hours (0609 UTC 13 July), the initial thunderstorm complex in the Sonoran Desert and the thunderstorms over Sinaloa merge together and development of a significant MCS ensues between Los Mochis and Bahia Kino (Fig. 19e). Profiler data shortly thereafter showed a strong and deep wind surge in Puerto Peñasco. Thus, the initiation of the gulf surge that moved through Yuma at 1200 UTC 13 July was likely tied to the significant convective development along the GOC coastal plain that occurred a few hours before (Rogers and Johnson 2007). The significant convective outbreaks on 12 and 13 July over the GOC coastal plain were classified as Regime AB days in the Lang et al. (2007) study. Convective organization and propagation of these systems was more pronounced on these days than the average monsoonal day. Hence, it is essential to examine how the approach

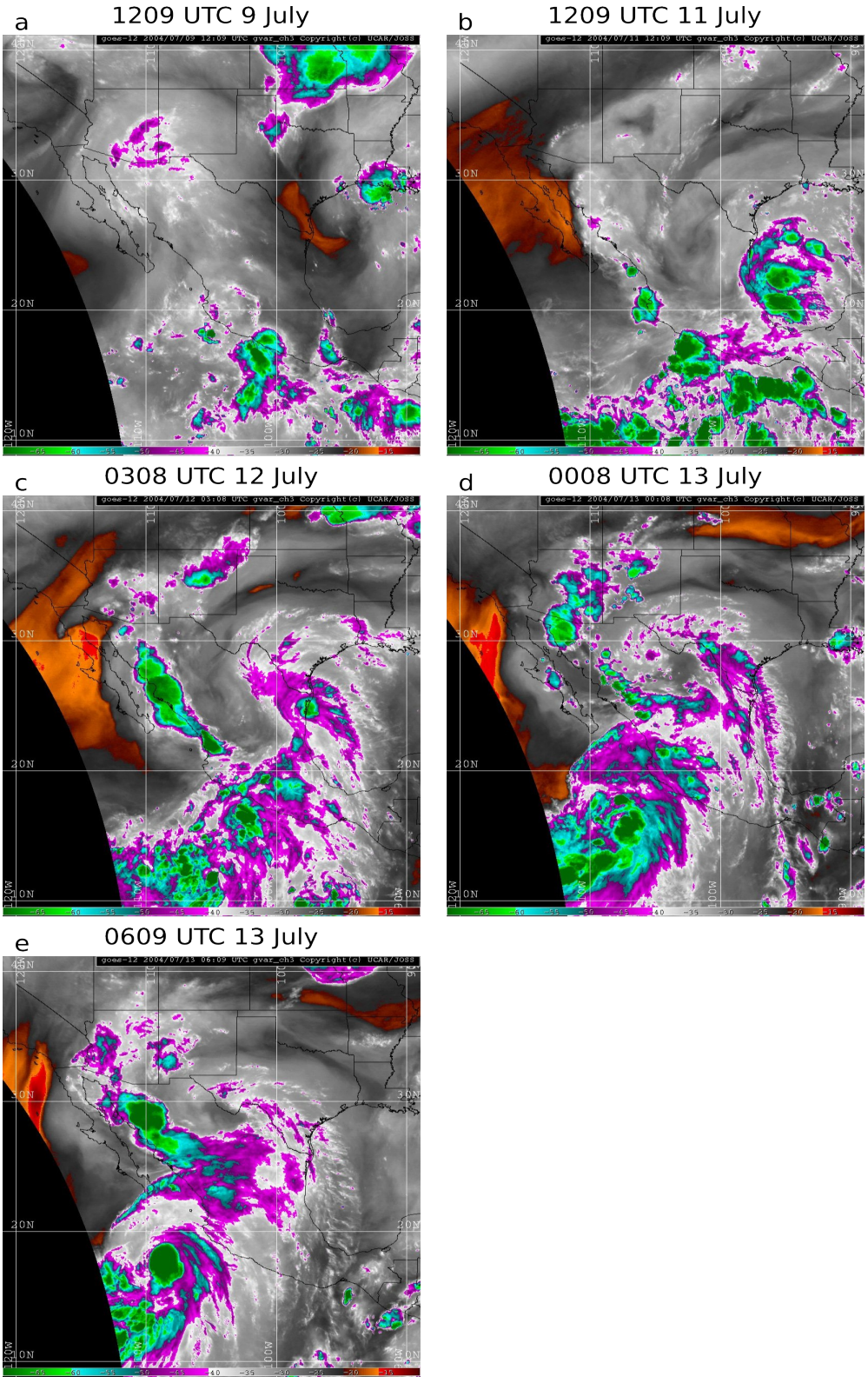

Figure 19: Water vapor GOES-12 satellite imagery at (a), 1209 UTC 9 July (b), 1209 UTC 11 July (c), 0308 UTC 12 July (d), 0008 UTC 13 July, and (e) 0609 UTC 13 July

of IV4 may have modified the large-scale convective environment on these days.

At 0609 UTC 13 July, the intensification of the tropical system to the south of the tip of Baja California is apparent from the increase in deep convection. Developing tropical storm Blas is advecting high moisture content into the circulation of IV4 to the north (Fig. 19e). On the subsequent day (0000 UTC 14 July), it is important to note that a large MCS developed over the low deserts of Arizona (not shown). The gulf surge that penetrated into the Arizona low deserts greatly increased low-level moisture and likely enhanced convective instability and subsequent convective development.

4.2 IV6

4.2.1 200-hPa Analyses

The 200-hPa synoptic setup surrounding IV6 is quite different than IV4, especially with regard to the location of the subtropical high. At 0000 UTC 21 July (12 h before upper-low formation), a NE-SW oriented trough axis is located over the Texas-Louisiana region with an amplified subtropical ridge to the west over New Mexico (Fig 20a). The strong anticyclonic shear associated with the northeasterly 200-hPa jet on the west side of the trough is apparently causing the backward-tilted nature of the trough (Thorncroft et al. 1993). Over the next 24 h the trough thins and a closed circulation forms near Brownsville, Texas by 0000 UTC 22 July. The process by which an upper-low forms from a thinning NE-SW oriented trough is very similar to the method proposed by Thorncroft et al. (1993). Note that the anticyclonic circulation of the 200-hPa high is located over Sonora at this

time. The position of the subtropical high in the upper-levels and midlevels (to be discussed later) is displaced substantially farther south and west compared to the situation for IV4. The combination of the cyclonic circulation of IV6 and the anticyclonic circulation of the subtropical high results in a strong 200-hPa northeasterly jet between western Texas and Sinaloa.

At 0000 UTC 22 July, IV6 begins a slow westward drift to a location just east of Big Bend, Texas on 0000 UTC 23 July (Figs. 20b,c). The subtropical ridge remains

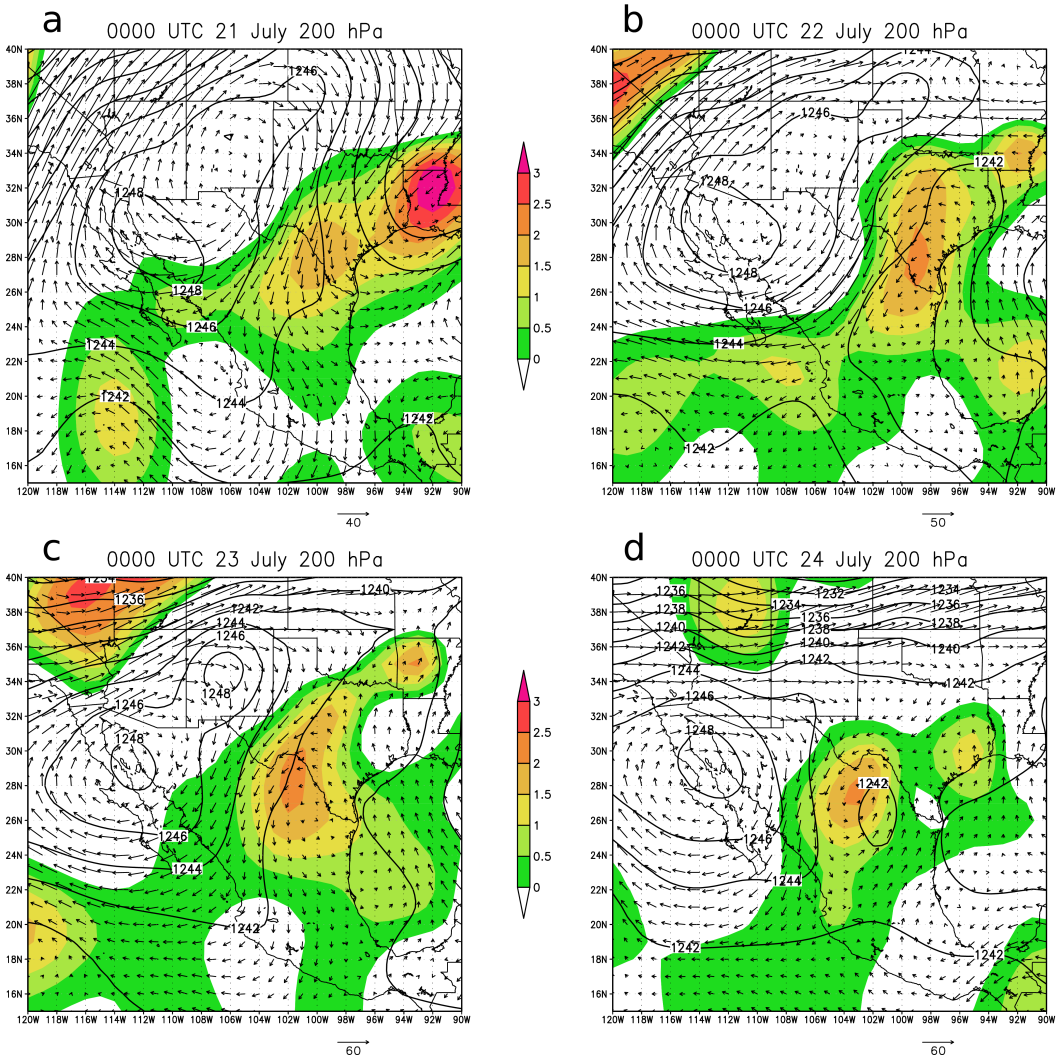

Figure 20: Same as Fig. 17, but at 0000 UTC from 21 July to 24 July

entrenched over the northern GOC. The relative stationary nature of the two main synoptic features over the domain (IV6 and the ridge) produces the persistent northeasterly upper-level jet over the southern GOC region. IV6 continues to move slowly westward and on 0000 UTC 24 July the upper-low is located over central Mexico (Fig. 20d). The subtropical ridge is pushed slightly to the southwest but remains over the northern GOC region. The displacement of the ridge to the south results in upper-level westerlies over the desert Southwest and zonal flow across the northern part of the T2A domain. IV6 moves to the southwest over the next 12 hours and becomes an open trough at 200 hPa near the SMO axis with dissipation shortly thereafter (not shown). The average translational speed of IV6 over its lifetime is 3 m s^{-1}, which is substantially slower than IV4.

4.2.2 600-hPa Analyses

The midlevel synoptic setup is quite similar to the upper-level conditions for IV6. The developing vorticity center over southern Texas on 21 and 22 July (Figs. 21a,b) is the midlevel circulation associated with IV6. There may be a tropical easterly wave along 96°W over the southern part of the domain but this feature is substantially weaker than the tropical wave that produced Blas. At 600 hPa the subtropical ridge is located over northwestern Mexico. It is important to note that the persistent northeasterly jet that was present at 200 hPa is also a feature at midlevels. The juxtaposition of IV6 to the east and the subtropical high to the west causes a tight midlevel height gradient between the two features. On 21 and 22 July the northeasterly midlevel jet stretches from central Mexico to the southern GOC.

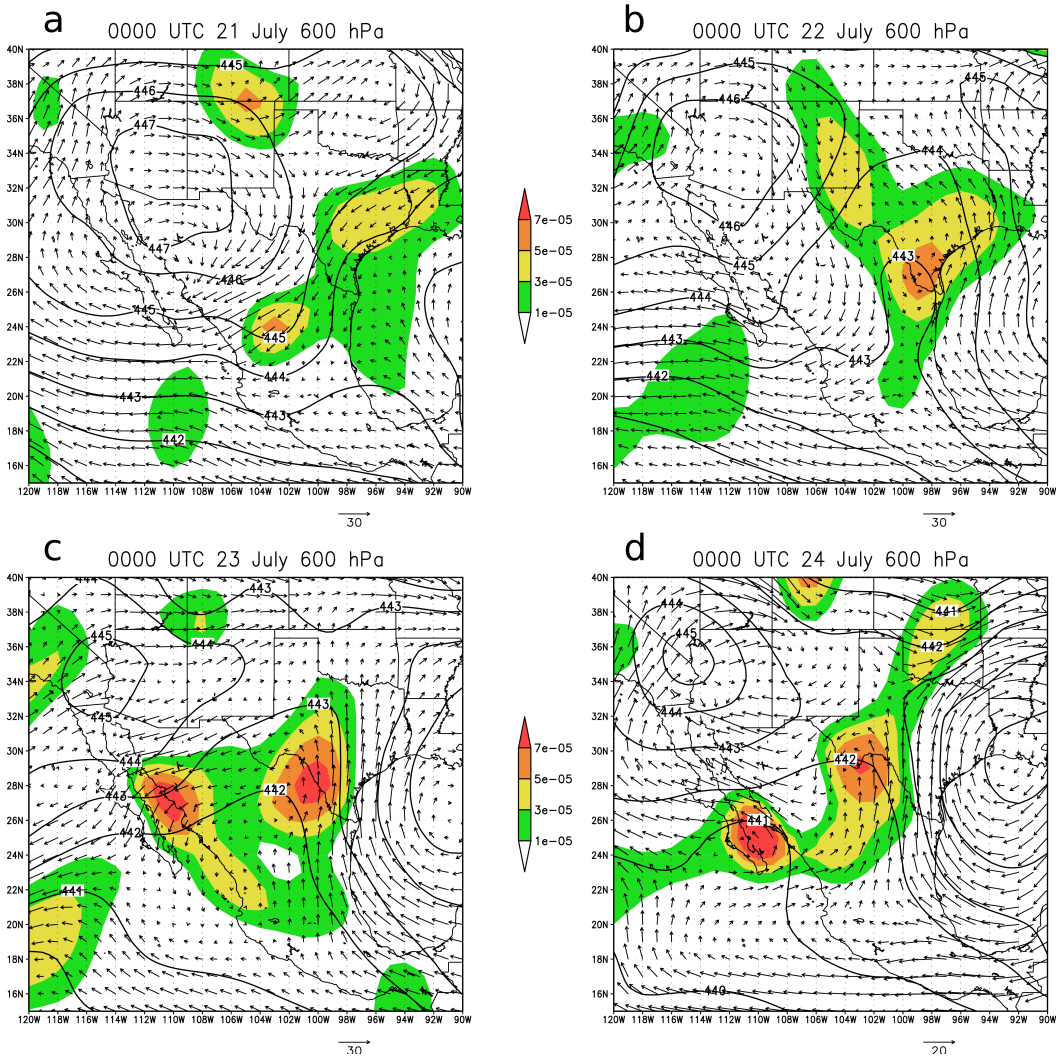

Figure 21: Same as Fig. 18, but at 0000 UTC from 21 July to 24 July

The midlevel vorticity center of IV6 moves westward and is located to the east of Big Bend, TX on 0000 UTC 23 July (Fig. 21c). The westward movement of the 600-hPa trough is in connection to the westward movement of the subtropical ridge to a position over southern California. As a result of the movement of these two features, the midlevel northeasterly jet shifts northwestward with the axis of strong midlevel winds now located over the central/northern GOC region near Sonora. The shift in the axis of strongest 600-hPa winds from Sinaloa on 0000 UTC 22 July to Sonora on 0000 UTC 23 July may have

important implications for organized MCS activity (discussed in Ch. 7). On 0000 UTC 24 July, the 600-hPa trough and associated vorticity center continues a slow progression to the west (Fig. 21d). The subtropical high remains anchored over southern California, but a new anticyclonic circulation emerges to the east of IV6 over Louisiana. Midlevel winds over Sonora shift to easterly but remain strong. In comparison to IV4, the midlevel circulation of IV6 is more collocated with the 200-hPa circulation. The 600-hPa circulation of IV6 is also more closed in streamline plots (not shown) than the open midlevel trough associated with IV4.

4.2.3 Convective Conditions

The evolution of the convective conditions and upper-level moisture pattern for IV6 can be viewed in Fig. 22. One day prior to the formation of IV6 (0309 UTC 20 July), deep convection is mainly confined to the higher terrain of the SMO and the eastern New Mexico area (Fig. 22a). Convection along the GOC coastal plain is largely suppressed. The very dry upper-level axis over the Texas-Louisiana coastline is associated with the thinning trough that develops into IV6. The following day (21 July), an impressive MCC develops over much of the central GOC coastal plain by 0300 UTC (not shown). This organized system likely caused a strong, yet shallow wind surge seen in the profiler data at Puerto Peñasco and Bahia Kino soon after (also not shown).

On 22 July a very similar convective pattern develops over the GOC coastal plain as the day before (Fig. 22b). The WV image from 21 July was omitted from Figure 22 because the MCS location and MCS areal extent was so similar to 22 July. By 1039 UTC

22 July a large MCS has formed over the central GOC coastal plain. The MCS developed as convective cells that initiated over the SMO quickly grew upscale into an organized convective system and subsequently propagated toward the coastal plain. The similarity in the convective pattern between 21 and 22 July was likely due to the rather static large scale pattern over the core NAM region over these two days. The subtropical ridge over Sonora and the upper-level IV6 did not move much from 21 to 22 July. Analogous to IV4, the center of IV6 is dry in the upper-levels and convectively inactive over southern Texas. For almost the entire lifetime of IV6, there is a consistent lack of deep convection to the east of the upper-low.

On 0709 UTC 23 July, yet another large MCS forms over the domain, for the third night in a row (Fig. 22c). However, this MCS is located over the Sonoran Desert, noticeably farther north than previous days. The northward displacement of this MCS relative to previous days may be attributed to the westward movement of IV6. The upper-low at this time is evident to the south of Big Bend in the relatively dry area of the WV image. It appears that the westward progression of IV6 caused a substantial increase in the midlevel easterly winds over Sonora on 23 July (Fig. 21c). The final image on 0309 UTC 24 July (Fig. 22d) shows another MCS over the Sonoran Desert, but not as large in areal extent as previous days. There is an increase in moisture near the low center and even some convection near the center over the Mexican Plateau. Extremely dry air is advecting into southern California with the upper-level westerlies (Fig. 21d). Upper-level conditions are significantly moister over northwest Mexico under upper-level easterly flow. This juxtaposition of two air masses produces a tight moisture gradient over the northern GOC.

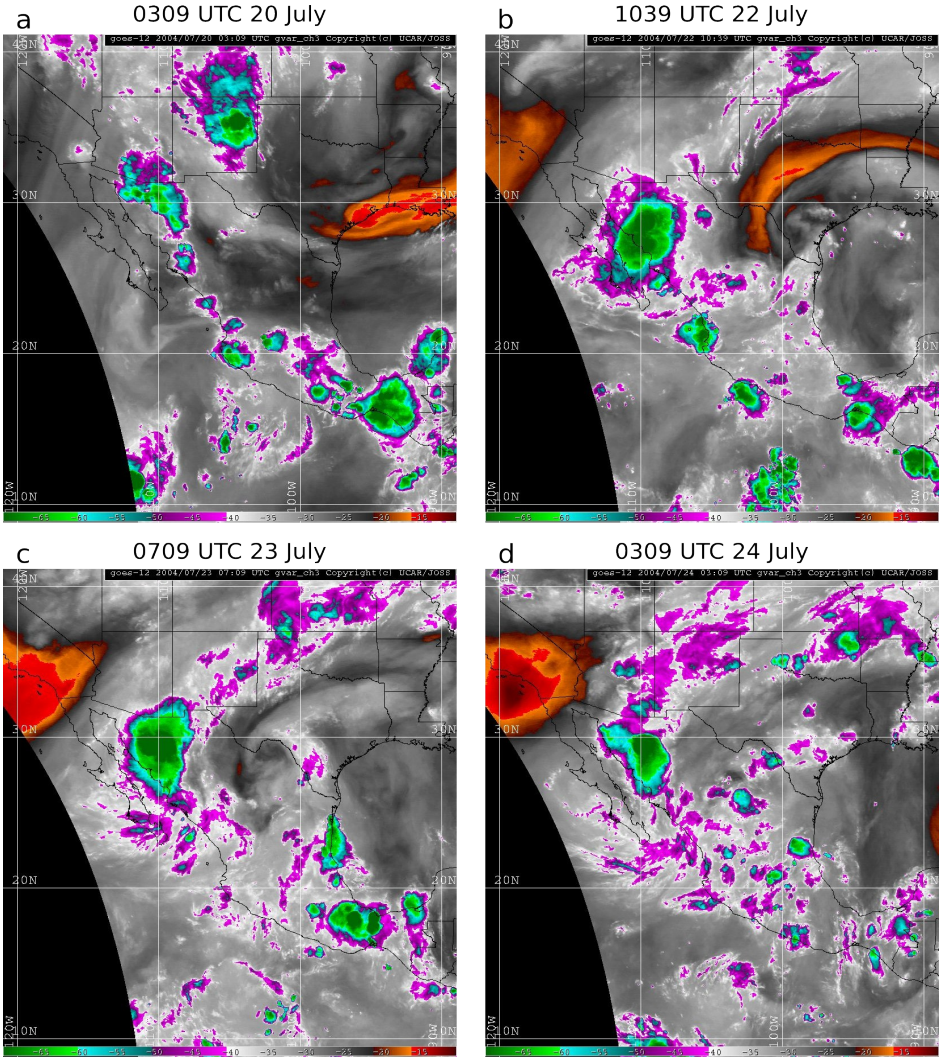

Figure 22: Same as Fig. 19, but for (a), 0309 UTC 20 July (b), 1039 UTC 22 July (c), 0709 UTC 23 July, and (d) 0309 UTC 24 July

Overall, the convective pattern during the period is very repetitive with large MCS development over the central and northern sections of the GOC coastal plain. The period from 0000 UTC 22 July to 0000 UTC 24 July was marked as Regime A by Lang et al. (2007). The episodic MCS development resulted in repeated shallow moisture surges into the desert Southwest (Rogers 2005). However, there was a lack of deep convection over southern Arizona for the entire period. The mid and upper-level anticyclone was centered

over Arizona and the stronger midlevel easterly winds resided across the International Border. Perhaps the subsidence caused by the ridge combined with the lack of significant easterly component to the midlevel flow aided in the suppression of any organized, deep convection despite the influx of low-level moisture.

CHAPTER 5

TEMPERATURE AND VORTICITY STRUCTURE

This chapter examines the vertical temperature and vorticity structure of the two upper-level inverted troughs. The anomaly and compositing procedures are described in Section 3.6. In a manner similar to Kelley and Mock (1982) and Whitfield and Lyons (1992), the mean vertical structure of the inverted trough will be detailed. The evolution of temperature and vorticity for the grid points encompassing the low center is presented. Hence, the question posed as to how the vertical structure of the low changes as it progresses across the NAM domain can be answered. In the time evolution plots, the value of temperature/vorticity at a particular time and pressure level was determined by averaging over a 6º lat. x 6º lon. box, with the 200-hPa low position at the center of this area. Since the gridded analyses for temperature included grid points below ground, results below 750 hPa (in the shaded box) are considered uncertain.

5.1 Temperature Structure

5.1.1 IV4

Figure 23 depicts the temperature anomaly in a west-east cross section through the

composite 200-hPa low center of IV4. There is a warm anomaly, as large as 4ºC, that is maximized near 100 hPa slightly east of the low. The warm anomaly changes to a cold anomaly at approximately 150 hPa. One upper-level cold anomaly maximum is centered near 400 hPa at the composite low center with an additional cold anomaly maximum at 650 hPa peaking 1-3º east of the center. Hence, the cold anomaly associated with the low is not just an upper-level feature, as it extends toward the surface, most strongly to the east of the low center. This result is in agreement with the previous studies of Erickson (1971), Kelley and Mock (1982), and Whitfield and Lyons (1992) (see section 2.2).

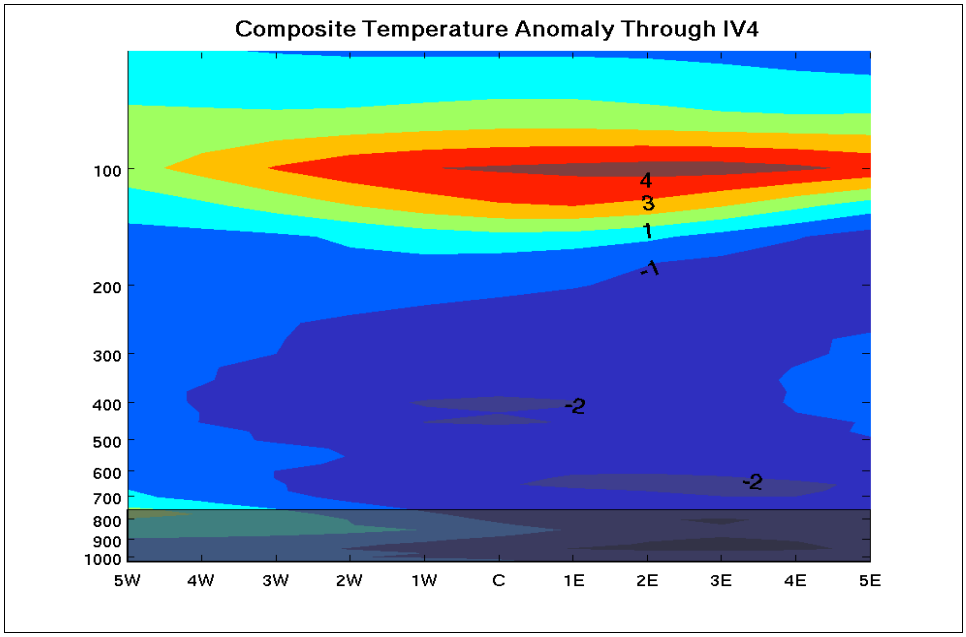

Figure 23: Temperature anomaly (ºC) in west-east vertical cross section through the composite IV4. Latitudinal degrees are west (W) and east (E) of the low center (C).

Although the magnitude of the warm and cold anomaly for IV4 is larger than in Kelley and Mock (1982), the general vertical temperature structure is similar. The maximum cold anomaly for IV4 is located at a slightly higher pressure (400 hPa) than in

the Kelley and Mock (1982) study (300 hPa). Subtle differences in the magnitude and vertical placement of the temperature anomalies are expected considering Kelley and Mock (1982) averaged over 117 lows, whereas the present plot just details one low. Whitfield and Lyons (1992) found a cold anomaly maximum of approximately -2.5ºC centered near 300 hPa. They averaged over the grid points encompassing the low center rather than computing a vertical cross section through the low center. In Whitfield and Lyons (1992), the cold anomaly was largest at 300 hPa, but extended down to 850 hPa. Hence, the vertical temperature structure of IV4 with a warm anomaly overlying a cold anomaly, is in general agreement with previous TUTT low studies.

The time evolution of temperature anomaly for IV4 is shown in Fig. 24. Time increases from left to right across the plot. The procedure of averaging over the grid points encompassing IV4, rather than taking a vertical cross section, is comparable to the methods of Whitfield and Lyons (1992). While the magnitude of the warm anomaly centered near 100 hPa remains relatively constant over the lifetime of IV4, its depth appears to decrease with time. However, the underlying cold anomaly exhibits a very different evolution. The cold anomaly is strongest at the beginning of the period, but weakens considerably with time. At 1200 UTC 10 July the cold anomaly near 400 hPa is -3ºC and extends weakly into the midtroposphere (as shown in Fig. 23). As the low progresses westward across the NAM domain, the cold anomaly decreases steadily, becoming a neutral temperature anomaly by 1200 UTC 13 July. The decrease in the magnitude of the cold anomaly is a feature of the upper and midtroposphere, at all pressure levels between 700 and 200 hPa. The evolution of the cold anomaly associated with this upper-level inverted trough is very different from IV6, as will be shown subsequently. At this point, there is no obvious

explanation for the weakening of the cold anomaly associated with IV4.

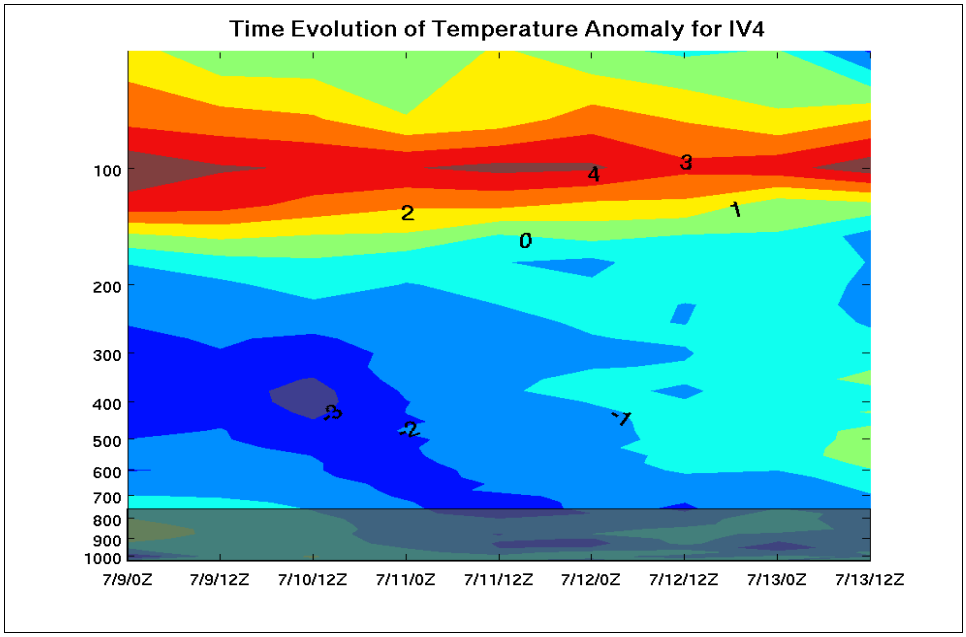

Figure 24: Pressure-time section of temperature anomaly (°C) averaged over the grid points encompassing IV4. Time is represented as *month/day/UTC*.

5.1.2 IV6

Figure 25 depicts the vertical temperature structure of IV6. The general temperature pattern of IV6 is very similar to IV4, however there are subtle differences. The warm anomaly for IV6 is centered near 125 hPa over the low center, with a cold anomaly below 225 hPa. The magnitude of the maximum warm anomaly is 2ºC, which is smaller than IV4, but more in line with the Kelley and Mock (1982) study. Like IV4, the cold anomaly is centered around 400 hPa with a magnitude of -2ºC. The cold anomaly is strongest near 400 hPa, but extends weakly to the surface, which is consistent with previous studies. Also notice that the axis of the cold anomaly tilts to the east with height

as one moves from the midlevels to upper-levels. This result is opposite from the westward tilt with height that was displayed in the temperature anomaly for IV4.

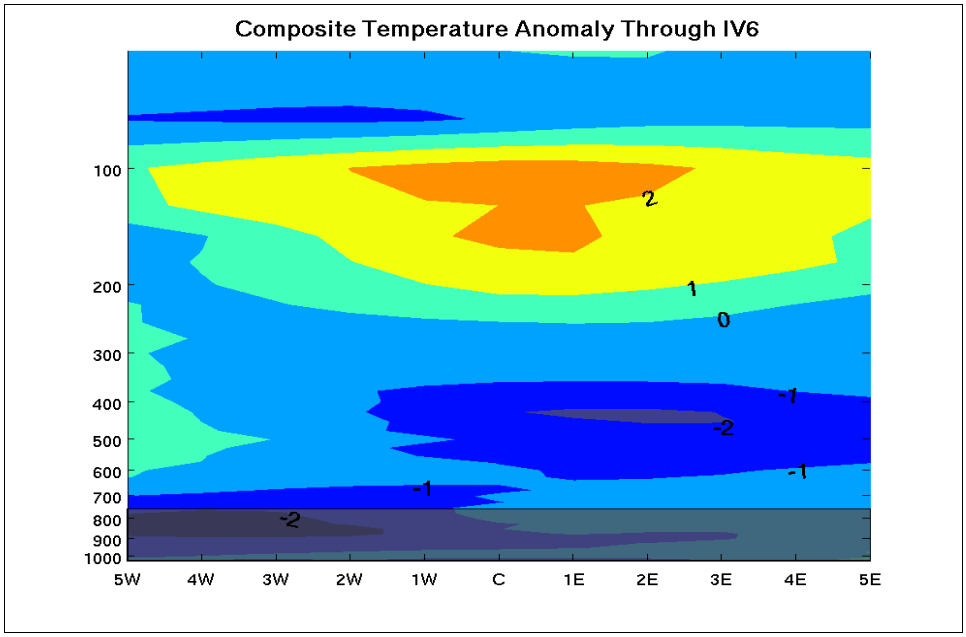

Figure 25: Same as Fig. 23, except for IV6

In order to discern the relatively static nature of IV6's temperature structure, Fig. 26 depicts the time evolution of the temperature anomaly for IV6. The magnitude of the warm anomaly between 200 and 100 hPa remains constant with time. Although the cold anomaly in the upper-levels (500-300 hPa) shows a slight decrease in magnitude with time, the decline is not nearly as pronounced as for IV4. For example, at 400 hPa the cold anomaly remains near -1ºC for the entire time period. The midlevel (750-500 hPa) cold anomaly actually becomes stronger at the later times. At 600 hPa, the temperature anomaly is weak at low formation (1200 UTC 21 July) and becomes a cold anomaly of -1ºC shortly before low dissipation (0000 UTC 24 July). Thus, the evolution of the cold anomaly for the two

inverted troughs is very different. One plot suggests a steadily weakening system (IV4) while the other suggests a static system (IV6).

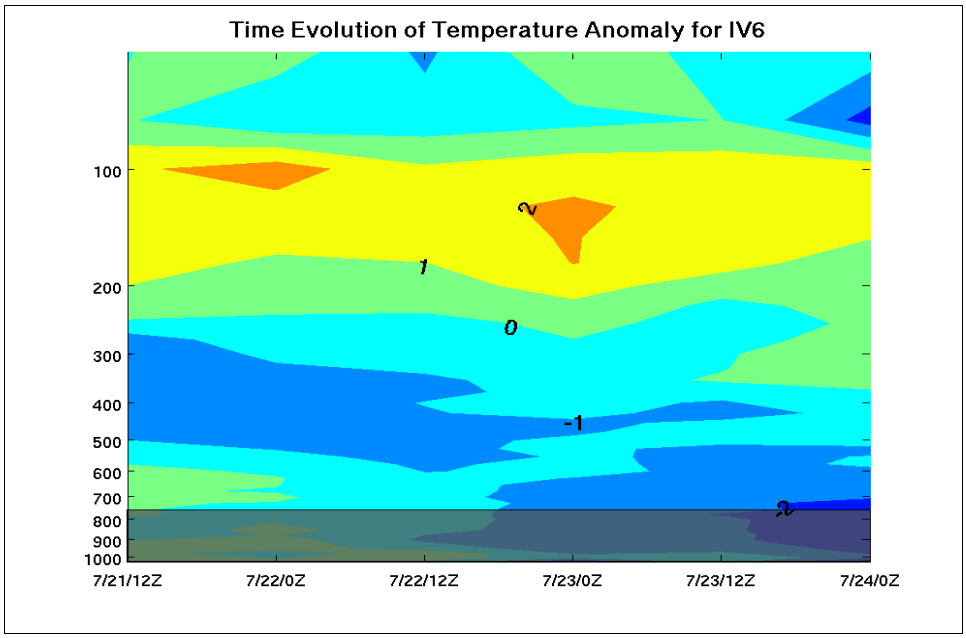

Figure 26: Same as Fig. 24, except for IV6

5.2 Vorticity Structure

5.2.1 IV4

In order to examine the vertical circulation of IV4, the relative vorticity through the composite 200-hPa low center is plotted in Fig. 27. The strongest relative vorticity of 14×10^{-5} s^{-1} is located over the low center at 200 hPa. This circulation maximum around 200 hPa was also found in Kelley and Mock (1982) and Whitfield and Lyons (1992). Kelley and Mock (1982) found a composite relative vorticity of 3.5×10^{-5} s^{-1} at 200 hPa over the low center while Whitfield and Lyons (1992) found a composite relative vorticity of $3 \times 10^{-}$

$^{5}s^{-1}$ at 200 hPa over the grid points encompassing the low center. Hence, the upper-level circulation of this inverted trough appears comparatively stronger than the TUTT low over Texas in Whitfield and Lyons (1992). The increased density of the NAME sounding network and the increased resolution (1º lat x 1º lon) of the NAME gridded dataset over the DMC gridded dataset (2.5º lat x 2.5º lon) could help explain this result. The circulation of IV4 decreases rapidly into the midlevels, with a relative vorticity less than $2x10^{-5}$ s^{-1} below 600 hPa. While there is a midlevel manifestation of IV4, the strongest circulation of the system is largely confined to upper-levels. The plot of composite relative vorticity also suggests a slight eastward tilt in the system with height.

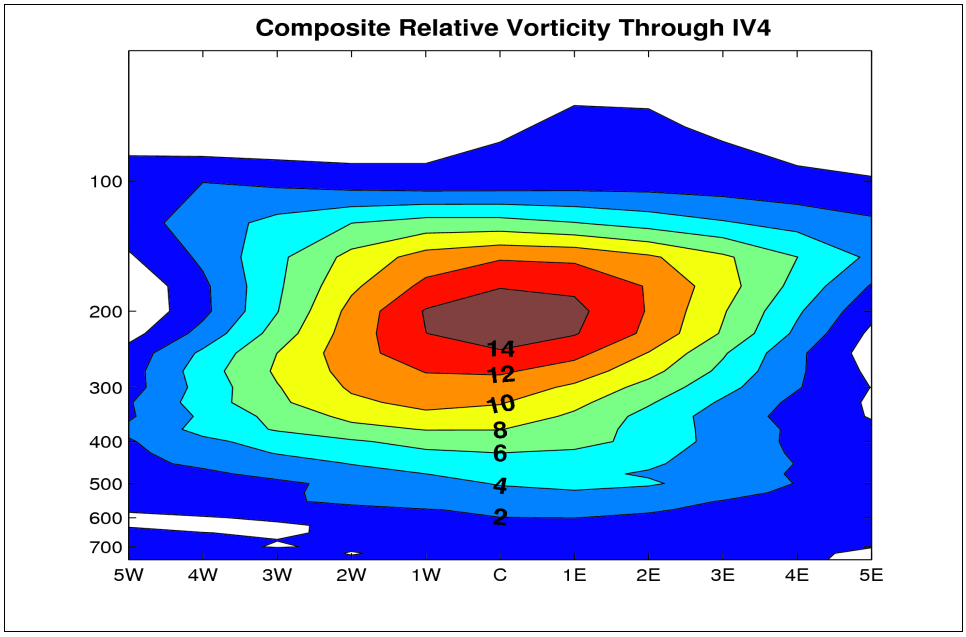

Figure 27: Relative vorticity (units of 10^{-5} s^{-1}) in west-east vertical cross section through the composite IV4. Values less than zero are white.

The time evolution of relative vorticity can also be examined (Fig. 28) for IV4. First, notice that even when an areal average is performed at a particular time, the

maximum in relative vorticity is around 200 hPa. The plot indicates that the inverted trough circulation weakens with time, especially at upper-levels during the last day (13 July). At 1200 UTC 12 July the relative vorticity at 200 hPa is greater than $8x10^{-5}$ s^{-1}, but decreases to $4x10^{-5}$ s^{-1} one day later. It is interesting to note that 0000 UTC 13 July, the time the upper-level circulation associated with IV4 shows a pronounced weakening, corresponds to the time when IV4 reached the SMO axis and began moving northward, suggesting topographic effects may play a role in the weakening. The midlevel relative vorticity remains relatively constant with time. The evolution of relative vorticity and temperature anomaly for IV4 are consistent with each other, indicating that this system became progressively weaker, especially at upper-levels, as it moved across northwestern Mexico.

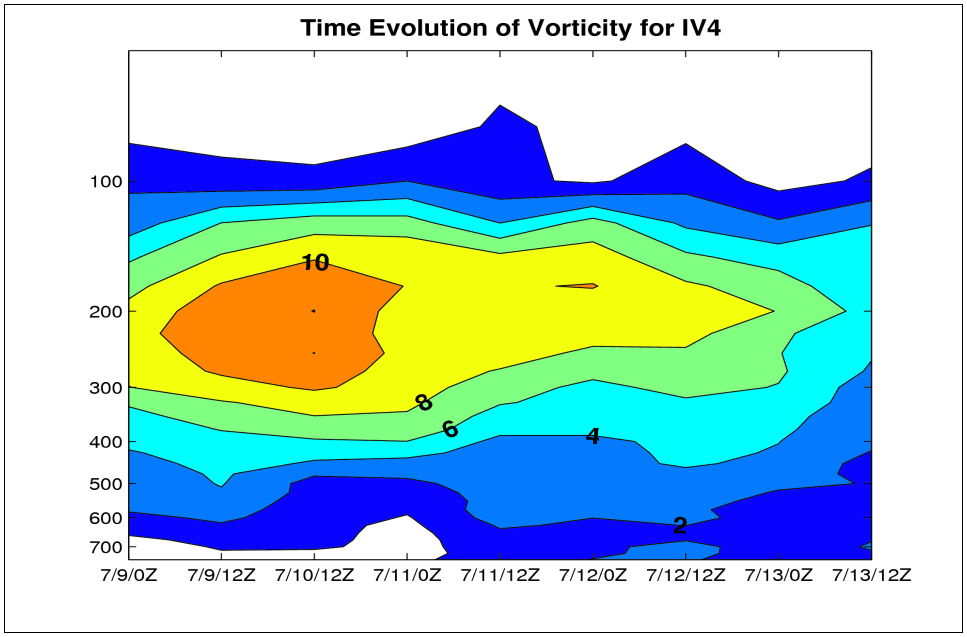

Figure 28: Pressure-time section of relative vorticity (units of 10^{-5} s^{-1}) averaged over the grid points encompassing IV4.

5.2.2 IV6

The circulation pattern for IV6 is shown in the west-east cross section through the low center (Fig. 29). The maximum in relative vorticity is located at 250 hPa over the low center with a magnitude of 12×10^{-5} s^{-1}. Hence, the upper-level circulation of IV6 is of comparable strength to IV4, and stronger than the TUTT low circulation of previous studies (discussed before). A close comparison of Figs. 27 and 29 reveals that the main difference between the circulation pattern for IV6 and IV4 resides in the midlevels (700–500 hPa). It is in this layer that the relative vorticity values for IV6 are larger than IV4. This is partly a function of the strength and location of the midlevel circulation associated with IV6. The 600-hPa wind vector plots reveal a more closed circulation for IV6 (compare Figs. 18 and 21). Moreover, the 600-hPa vorticity center is collocated with the 200-hPa center for IV6 (see Figs. 20 and 21), whereas for IV4 the mid and upper-level circulation centers are more separated (see Figs. 17 and 18). Since the vertical cross sections are made though the 200-hPa low center, then the midlevel relative vorticity in the cross section will be higher for IV6 simply by virtue of the mid and upper-level vorticity centers being spatially collocated. Also evident in Fig. 29 is the westward tilt of IV6's circulation with height, which is opposite from IV4.

The relative vorticity values within the circulation of IV6 are relatively constant with time (Fig. 30). Performing a spatial average on the relative vorticity values does not change the result that the maximum relative vorticity is located near 250 hPa. Comparing Fig. 30 to Fig. 28 further supports the claim that the midlevel (700– 500 hPa) circulation of IV6 is stronger than IV4 over its entire lifetime. From 1200 UTC 21 July to 0000 UTC 24

July, both the upper-levels and midlevels show little change in the relative vorticity values. IV6 largely maintains its circulation strength as it propagates westward across northern Mexico. This is substantially different from IV4, which exhibited a substantial decrease in upper-level circulation strength in the last day of its lifetime. Of course, the tracks of these two inverted troughs are somewhat different, a factor which may need to be considered when comparing the evolution of their intensities. The track of IV6 crossed the SMO axis at 0000 UTC 24 July and shortly thereafter the system began to weaken substantially. Like IV4, this suggests that topography may influence inverted trough intensity in the core NAM region. The unchanging values of relative vorticity for IV6 is consistent with the static nature of the temperature anomaly (Fig. 26).

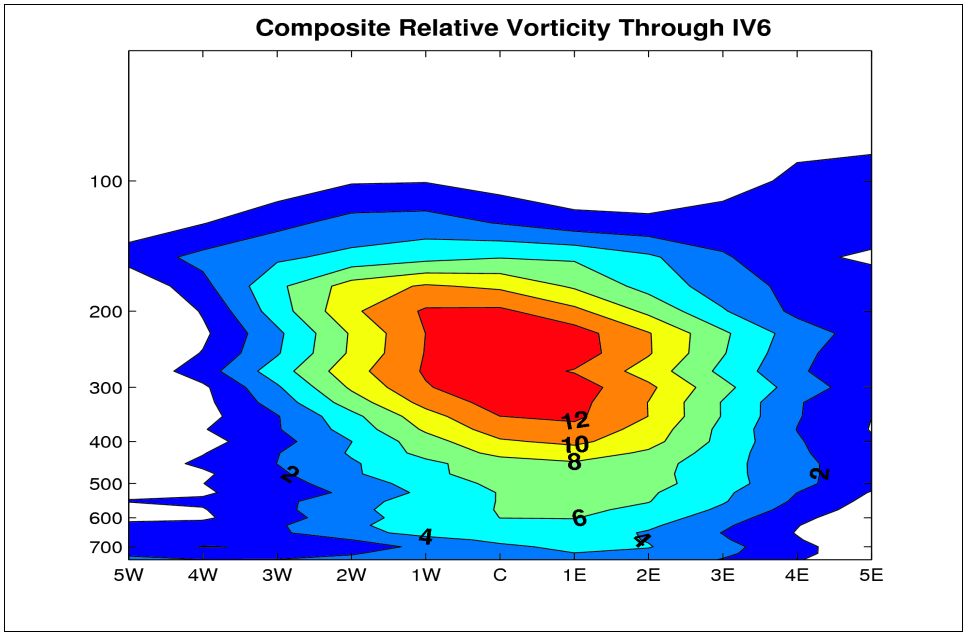

Figure 29: Same as Fig. 27, except for IV6

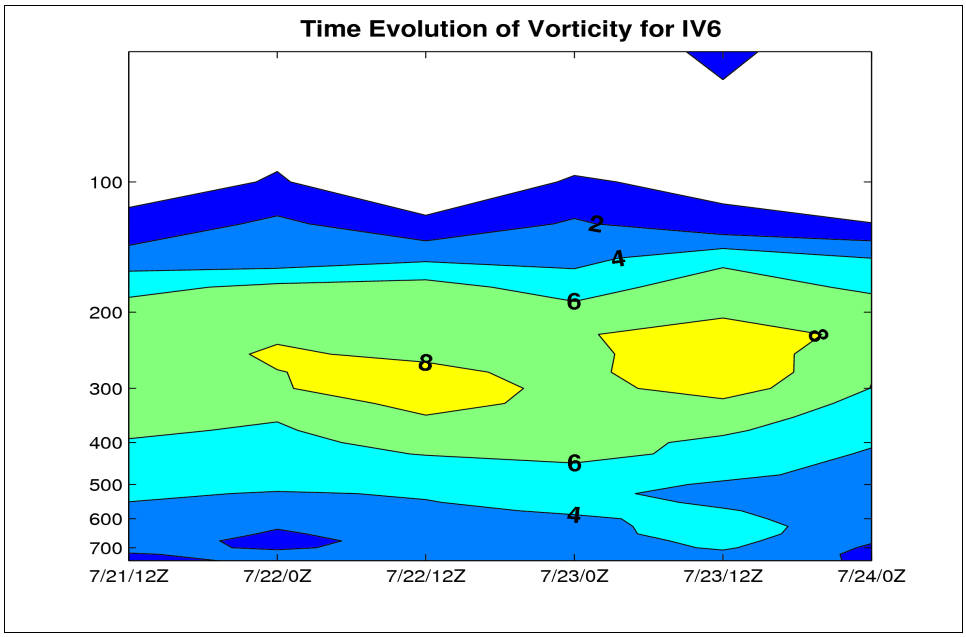

Figure 30: Same as Fig. 28, except for IV6.

CHAPTER 6

QG FORCING OF VERTICAL MOTION BY INVERTED TROUGHS

The following chapter presents an analysis of the composite QG omega in the 700-300 hPa layer associated with the two inverted troughs. Computing a 700-300 hPa layer mean of QG omega incorporates vertical motion over a significant depth of the atmosphere (mid and upper-levels). The objective of the study is to understand the spatial pattern of omega over a deep layer of the atmosphere, not at only one pressure level. Plots of total QG omega along with the omega contribution from the differential vorticity advection (RHS1) and Laplacian of temperature advection terms (RHS2) will be shown. A detailed description of the methodology used to calculate QG omega using the traditional omega equation is presented in Section 3.7.1. A typical Rossby number for the inverted troughs is between 0.1 and 0.2. While the QG approximation is most applicable for Rossby numbers less than 0.1 (Bluestein 1992), the Rossby number of the inverted trough is sufficiently small for the QG omega calculations to still be valid.

6.1 IV4

6.1.1 Total QG Omega

The composite total QG omega for the 700-300 hPa layer associated with IV4 is shown in Fig. 31a. The general spatial pattern of omega indicates weak subsidence (rising motion) to the west (east) of the low center. This spatial pattern is consistent with previous studies (Erickson 1971, Kelley and Mock 1982, Whitfield and Lyons 1992) that showed subsidence (rising motion) to the west (east) of the TUTT low. The subsidence is maximized 4 degrees west of the low while the rising motion maximum is located 2 degrees east of the low. The absolute magnitudes of the omega values in Fig. 31a are small. However, Erickson (1971) found similar magnitudes for vertical motion for an upper-level cold low over the Bahamas. Erickson (1971) conducted a numerical analysis of vertical motion, in a manner very similar to the present study. Calculated omega values were relatively small with maximum values at 300 hPa on the order of 0.1 Pa s^{-1}.

There are reasons for the small absolute magnitudes of QG omega. Averaging over seventeen vertical pressure levels and six synoptic times will naturally reduce the absolute magnitude of the omega values. Maybe more important is the fact that the inverted trough is quite barotropic in the mid and upper-levels (shown in Section 6.1.3). The Sutcliffe-Trenberth form of the QG omega equation says that the RHS forcing for the omega equation is proportional to the advection of geostrophic relative vorticity by the thermal wind (Bluestein 1992). Since the inverted trough is quite barotropic, by definition the thermal wind is small. Advection by the thermal wind will be minimal and the RHS forcing and resulting omega magnitudes will be small. Hence, the small (by midlatitude standards) values of omega in the present study are probably not unrealistic for synoptic scale subtropical disturbances.

6.1.2 Vorticity Advection Contribution to Omega

One of the advantages of using the traditional form of the QG omega equation is that the total omega can be partitioned into the two RHS forcing functions. Figure 31b shows the calculated QG omega associated with the differential vorticity advection term of the omega equation. Very weak rising motion occurs to the west of the low center with very weak subsidence to the east of the low. Note that the absolute magnitudes of omega in Fig. 31b are approximately three times smaller than the total QG omega. The spatial pattern of the omega values associated with the vorticity advection term is to be expected. On the forward (west) flank of the inverted trough there is positive vorticity advection while negative vorticity advection occurs on the trailing (east) flank of the low. However, it is the vertical derivative of vorticity advection that determines RHS1. That is, vorticity advection must change substantially with height for RHS1 to be large. This usually requires the wind speed to increase substantially with height. However, large vertical wind shear does not occur in these inverted troughs (not shown) due to their barotropic nature in the subtropics.

6.1.3 Temperature Advection Contribution to Omega

Figure 31c displays the QG omega associated with the temperature advection term of the traditional omega equation. The spatial pattern of omega in Fig. 31c looks very similar to the total QG omega shown in Fig. 31a. Subsidence is maximized approximately 4 degrees west of the low center while upward motion is maximized 2 degrees southeast of

the low center. We can conclude that thermal advection forcing is the dominant factor in the calculated total QG omega pattern for IV4. In his partitioned analysis of vertical motion, Erickson (1971) also found that the Laplacian of thermal advection was the single most important forcing function in the pattern of omega. In order to emphasize this point in the present study, a vertical profile of omega rms amplitude associated with RHS1 and RHS2 was calculated (not shown). The rms amplitudes were averaged over the six synoptic times considered for IV4. It was found that throughout the 700-300 hPa layer, the omega rms amplitude associated with RHS2 was three to four times larger than the omega rms amplitude from RHS1.

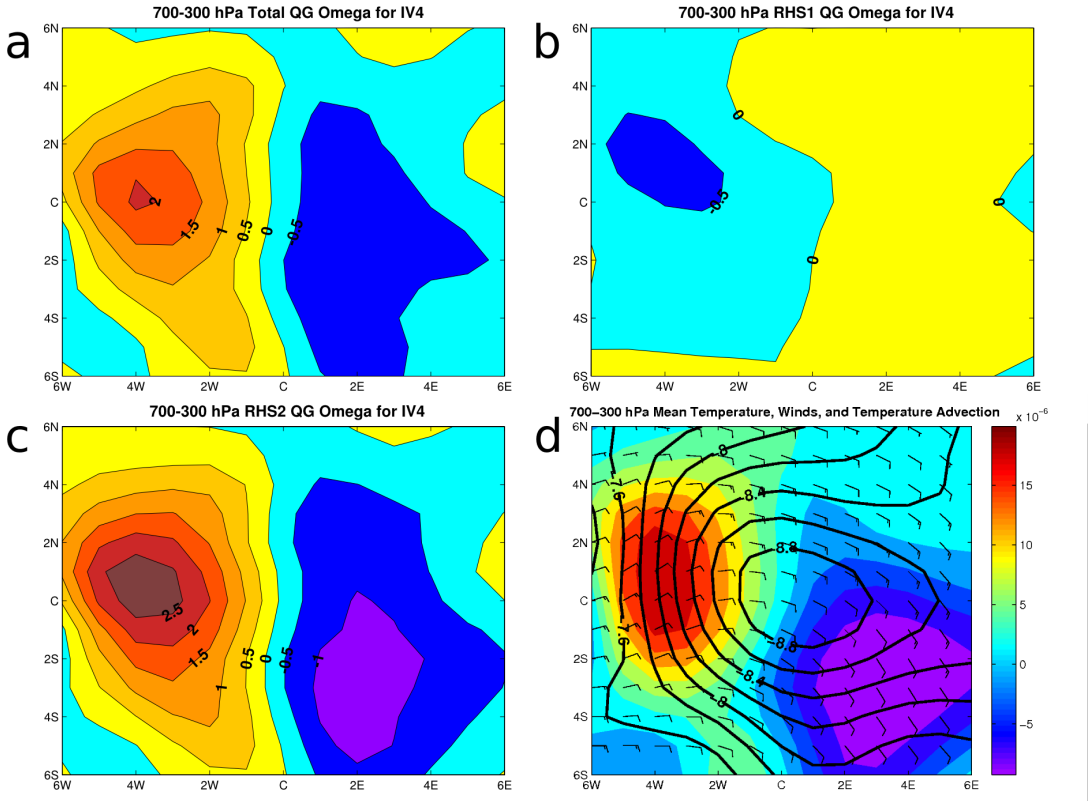

Figure 31: Composited over six synoptic times and over the pressure layer from 700-300 hPa, the QG omega (10^{-2} Pa s^{-1}) fields for IV4 include (a), the total omega (b), the omega contribution from RHS1 (c), the omega contribution from RHS2, and (d) the mean temperature (°C) (contoured), geostrophic winds (m s^{-1}), and geostrophic temperature advection (°C/s) (shaded). Degrees are west (W), east (E), south (S), and north (N) of the 200-hPa low center.

The spatial pattern of QG omega associated with RHS2 implies cold (warm) air advection to the west (east) of the low (Fig. 31d). Cold air advection (CAA) is strongest four degrees west of the low and warm air advection (WAA) is strongest three degrees southeast of the low. The coldest temperatures are located at the low center (-8.8°C). Note also that the temperature gradient is rather weak with slightly over 1°C rise in mean temperature from the low center to the outer fringes of the plot. Hence, unlike baroclinic mid latitude systems, IV4 is a rather barotropic system. The temperature gradient is noticeably larger to the west of the low than the east.

6.2 IV6

6.2.1 Total QG Omega

The total QG omega averaged over the 700-300 hPa layer for IV6 is plotted in Fig. 32a. The spatial pattern of total QG omega indicates general downward motion to the northwest of the low center and rising motion to the south. Strongest subsidence occurs approximately 4 degrees to the northwest of the low. Strongest rising motion actually occurs 2 degrees west-southwest of the low center. This is in contrast to IV4 which provided subsidence directly to the west of its center. While the magnitude of the subsidence maximum for IV6 is about 0.01 Pa s^{-1} smaller than for IV4, the magnitude of the rising motion maximum is of similar magnitude. The general spatial pattern of total QG omega corroborates previous studies, especially Kelley and Mock (1982). Recall that Kelley and Mock (1982) showed anomalous subsidence and minimum cloudiness on the

northwest flank of the composite TUTT low and anomalous rising motion on the southeast flank. Similar to IV4, the absolute magnitude of total QG omega across the entire domain is small for IV6. The proposed reasons for this result are identical to those provided in Section 6.1.1.

6.2.2 Vorticity Advection Contribution to Omega

The contribution to the total QG omega that is generated from RHS1 is shown in Fig. 32b. Rising motion is maximized two degrees to the southwest of the low center. General subsidence, albeit extremely weak, is located primarily to the northeast of the low center. The upward motion maximum to the southwest of the low center is half the magnitude of the total QG omega in the same location. Thus, the upward motion area generated from the positive vorticity advection to the southwest of the low definitely contributes to the rising motion maximum seen in Fig. 32a. Like IV4, the absolute magnitudes of the omega values in Fig. 32b are very small. This means that the vertical derivative of vorticity advection with height is quite small. It will be shown in the next section that, similar to the IV4 system, IV6 exhibits weak temperature gradients and thus little change in wind speed (vorticity advection) with height.

6.2.3 Temperature Advection Contribution to Omega

The plot of QG omega arising from RHS2 is shown in Fig. 32c. There is clear similarity between the QG omega generated from the temperature advection term and the

total QG omega. Hence, RHS2 appears to be the dominating forcing term on the RHS of the traditional omega equation. A vertical profile of omega rms amplitude from the two forcing terms (RHS1 and RHS2) was calculated in an identical manner to IV4. Throughout the 700-300 hPa layer, the rms amplitude of omega from RHS2 is two to three times greater than the omega rms amplitude from RHS1 (not shown). Hence, the temperature advection term dominates the forcing signal for omega, though not quite as strongly as for IV4. Looking at Fig. 32c, the area of subsidence produced from CAA is maximized four degrees northwest of the low center. WAA to the southeast of the low center (Fig. 32d) induces an area of rising motion with a maximum magnitude of -5×10^{-3} Pa s^{-1}. Because the temperature advection is again the dominating forcing term, it is imperative to analyze the advection pattern for IV6.

The 700-300 hPa mean temperature, geostrophic winds, and geostrophic temperature advection are illustrated in Fig. 32d. The major difference in the spatial pattern of temperature between IV4 and IV6 is the location of the cold core. For IV6, the 700-300 hPa cold core is located to the northeast of the 200-hPa low center. Another difference is the more distinct cyclonic circulation in the 700-300 hPa layer compared to IV4. The magnitude of the cold core is identical (-8.8°C) to IV4 and the temperature gradient is stronger to the west of the low center than the east. Fig. 32d reveals that, similar to IV4, IV6 is quite barotropic with weak overall temperature gradients compared to midlatitude troughs. The obvious similarity between the temperature advection pattern and the total QG omega for IV6 once again highlights the importance of the temperature advection forcing term in determining the resulting QG omega field. While RHS1 is important in inducing the upward motion maximum in total QG omega to the southwest of

IV6, the rest of the domain is dominated by RHS2. The difference in the location of the subsidence maximum relative to the 200-hPa low center between IV4 and IV6 results from the different CAA pattern. CAA is maximized to the west (northwest) of IV4 (IV6).

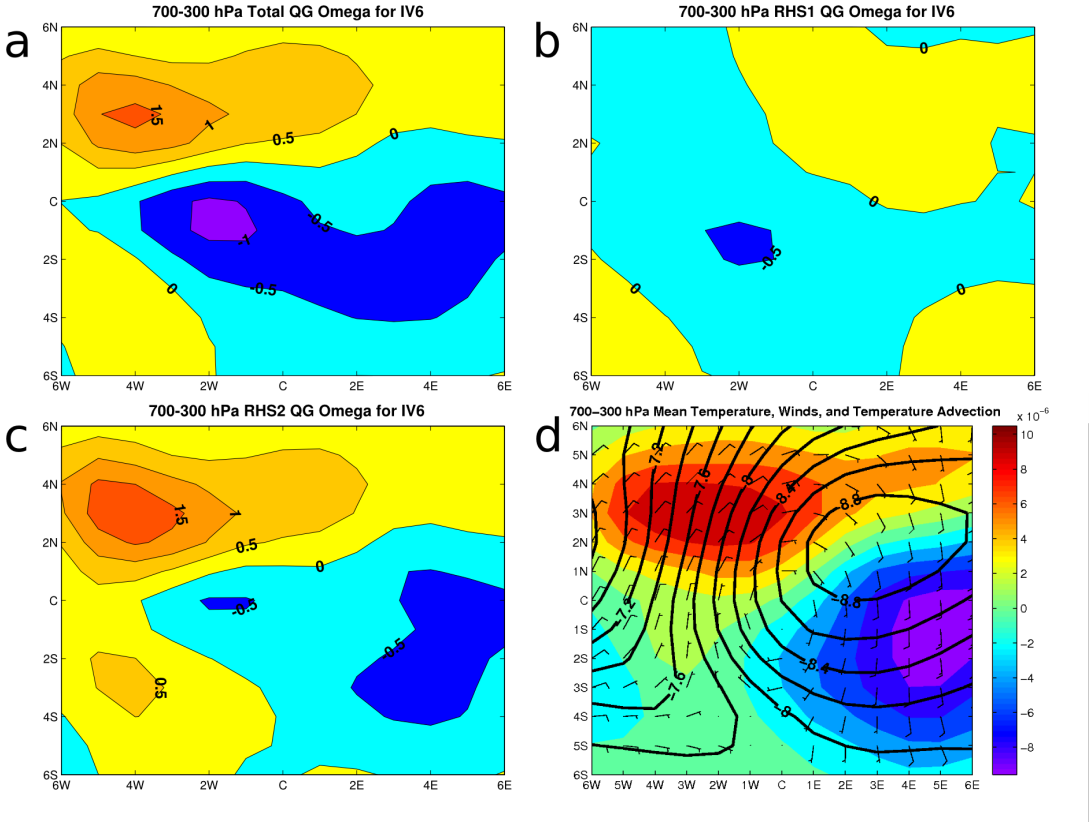

Figure 32: Same as Fig. 31, except over five synoptic times for IV6

6.3 Summary

While the absolute magnitudes of the total QG omega values for IV4 and IV6 are quite weak, a general spatial pattern in omega emerges from analysis of the two lows. In general, there is weak subsidence (rising motion) to the west (east) of the inverted trough. Since the spatial pattern in temperature advection mirrors total QG omega, the temperature

advection forcing function is dictating the total QG omega signal (in agreement with Erickson 1971). The temperature advection pattern, with CAA (WAA) on the forward (trailing) flank of the low, causes this spatial pattern in omega. This general spatial pattern in temperature advection (CAA on the forward flank and WAA on the trailing flank) is a common feature of upper-level troughs. Hence, the spatial pattern in total QG omega may well hold for other inverted troughs not considered in this study.

The general spatial pattern in total QG omega is in agreement with previous studies over non-NAM regions (Erickson 1971, Kelley and Mock 1982, Whitfield and Lyons 1992) that showed subsidence (rising motion) to the west (east) of the TUTT low. Yet, it seemingly does not support more recent NAM-related studies (Pytlak et al. 2005, Douglas and Englehart 2007) that indicate an increase in convective organization and rainfall along the SMO foothills when the inverted trough is located to the east. Moreover, the total QG omega spatial pattern for both IV4 and IV6 does not help to explain the increase in MCS activity over the SMO foothills and GOC coastal plain as the two inverted troughs approached from the east. From a dynamics standpoint, the total QG omega fields induce an unfavorable condition (subsidence) for increased convection to the west of the inverted trough. One has to conclude that the inverted trough modifies the convective environment in some other way that supports increased convective organization to the west of the low center. An environment more supportive for convection to the west of the inverted trough could overwhelm the weak QG omega signal that is hostile to convection on the forward flank of the low.

Midlevel CAA (Figs. 31d and 32d) has been proposed to improve the prospects of convection to the west of the low by steepening the midlevel lapse rates (Pytlak et al.

2005). However, plots of 24-h changes in the 700-300 hPa temperature do not indicate significant cooling, with magnitudes smaller than 1ºC (not shown). Weak midlevel temperature gradients for IV4 and IV6 promote weak midlevel cooling to the west of the low center. Moreover, plots at individual synoptic times indicate that areas of midlevel cooling are not consistently located in regions of significant convective development and organization (not shown). While the slight midlevel cooling on the western flank of the low may improve the prospects for convective initiation along the SMO, it does not appear to affect convective organization. The effects of midlevel cooling associated with the inverted trough are not considered further in this paper. The inverted trough can also modify the midlevel steering flow and shear profile in a way that promotes increased convective organization to the west of the low center. The next chapter considers changes in the midlevel flow and vertical wind shear associated with the two inverted troughs that could contribute to enhanced convective activity to the west of these systems.

CHAPTER 7

MECHANISMS FOR THE PROPAGATION AND ORGANIZATION OF DEEP CONVECTION IN ADVANCE OF INVERTED TROUGHS

This chapter presents an analysis of the midlevel winds and vertical wind shear associated with the two inverted troughs. Midlevel (700-400 hPa) flow and vertical wind shear was computed according to the methods described in Sections 3.8.1 and 3.8.2 respectively. The chapter is broken into two sections. The first section considers the composite midlevel flow and composite anomalous midlevel flow of the two inverted troughs. Anomalous midlevel flow is calculated by subtracting the average midlevel flow over the period 1 July – 15 August 2004 from the midlevel flow at the particular synoptic time. The second section presents plots of midlevel flow and vertical wind shear at individual synoptic times during the lifetimes of IV4 and IV6. Anomalous wind shear vectors are overlaid on IR images to suggest a relationship between locations of wind shear and convective organization.

7.1 Composite and Anomalous Midlevel Flow

7.1.1 IV4

Figure 33a illustrates the composite midlevel flow for IV4. The cyclonic circulation is immediately apparent from the plot. Midlevel winds are strong southeasterly (6.25 m s^{-1}) on the east side of the 200-hPa low center. The winds are weaker and turn more easterly near the center of the low. On the west (leading) flank of the inverted trough, midlevel winds are primarily from the east-northeast or northeast. In Ch. 5 it was shown that the vorticity (circulation) of IV4 was maximized near 200 hPa. Although vorticity is maximized in the upper levels, Fig. 33a demonstrates that there is an associated cyclonic circulation at midlevels. This is in agreement with Hoskins et al. (1985), which showed that a cyclonic upper-level PV anomaly induces a cyclonic circulation below.

In order to highlight how the passing inverted trough modifies the midlevel flow from the average monsoon conditions, Fig. 33b shows the composite anomalous midlevel winds. Average NAME midlevel flow over the latitudinal belt where the inverted trough passes is easterly to southeasterly. The anomalous midlevel cyclonic circulation induced by the passing inverted trough is more apparent in Fig. 33b. Hence, on the trailing flank of the inverted trough there is a dramatic increase (6.25 m s^{-1}) in the southerly component of the midlevel flow. There is a slight increase (2.5 m s^{-1}) in the northerly and easterly component of the midlevel wind on the leading flank of the low center. Figure 33b also illustrates the horizontal scale of midlevel flow modification. IV4 modifies the midlevel flow extending eight degrees east-west and north-south of the low center. It should be emphasized that IV4 does not act alone in determining the midlevel flow pattern. Rather, it is the interaction of the inverted trough and subtropical ridge to the north that ultimately determines the midlevel flow in the vicinity of IV4. This modification of the midlevel flow pattern can affect the convective environment near the SMO (see Section 7.2).

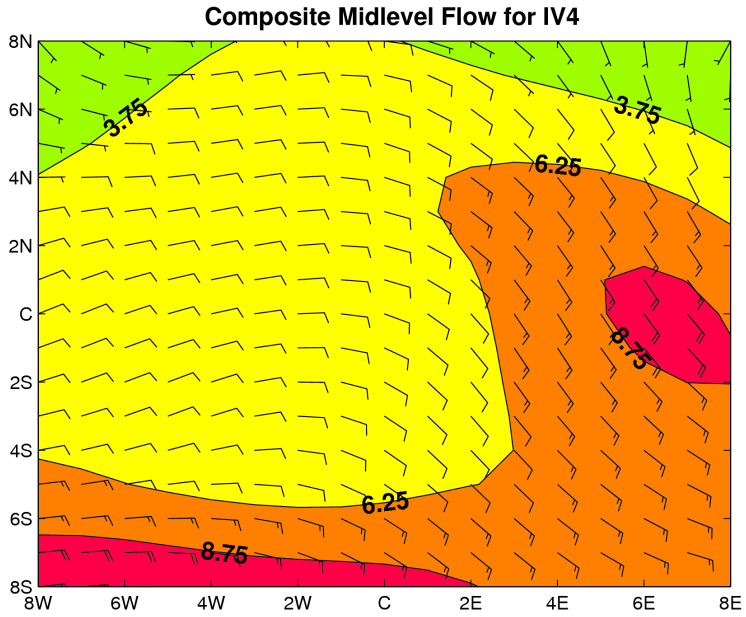

Figure 33: Composite midlevel winds for IV4 averaged over the 700-400 hPa layer. Wind speed is shaded in m s^{-1} and wind vectors are plotted. A full barb is 5 m s^{-1} and a half barb is 2.5 m s^{-1}.

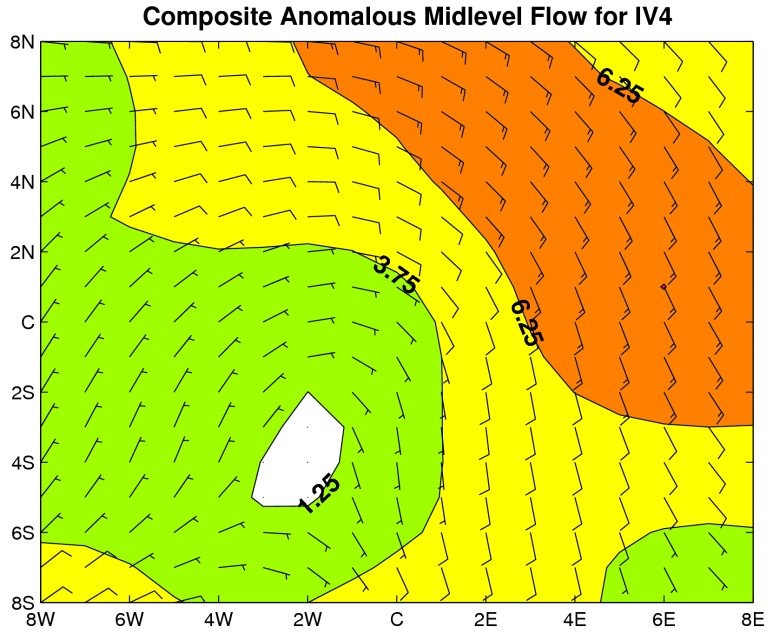

Figure 34: Composite anomalous midlevel winds for IV4 averaged over the 700-400 hPa layer. Units are the same as in Fig. 33.

7.1.2 IV6

The composite midlevel flow for IV6 is shown in Fig. 35. Compared to IV4, the midlevel cyclonic circulation associated with IV6 is even more pronounced. It has already been shown in Ch. 4 and 5 that the midlevel vorticity for IV6 is greater than IV4. On the southwestern flank of IV6, the composite midlevel winds are light (less than 1.25 m s^{-1}). The northwestern quadrant of the low is characterized by northeasterlies while the eastern flank experiences strong southerlies. The wind speeds to the east of IV6 are of comparable magnitude to IV4, however the wind direction is more southerly on the east side of the low in the case of IV6. Although the vorticity for IV6 is maximized in the upper levels (around 200 hPa), there is an associated cyclonic circulation in the midlevels that is even more pronounced than IV4.

Figure 36 illustrates the anomalous midlevel flow for IV6. There is not much difference between Figs. 36 and 35, except that the anomalous cyclonic circulation becomes more apparent in Fig. 36. Note the impressive 8.75 m s^{-1} anomalous southerly flow approximately five degrees east of the low center. The interaction between IV6 and the subtropical ridge located to the northwest of the upper low determines the midlevel flow pattern in the vicinity of IV6. The strengthened northeasterly midlevel winds in the northwest quadrant of IV6 are a direct result of increased height gradient between the upper low and the subtropical anticyclone to its northwest (Figs. 20 and 21). From the analysis presented so far, it can be concluded that both IV4 and IV6 induce an anomalous midlevel cyclonic circulation on the prevailing monsoonal flow.

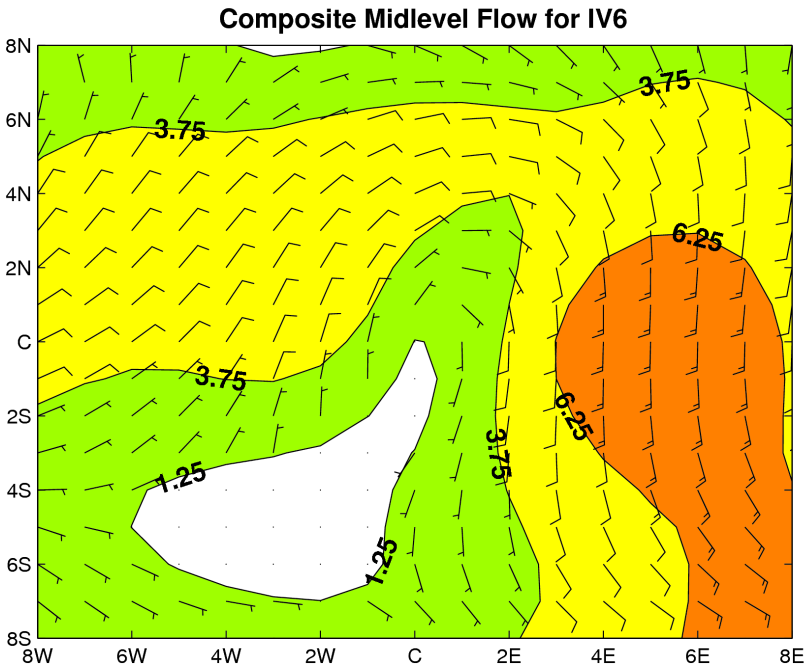

Figure 35: Same as Fig. 33, except for IV6.

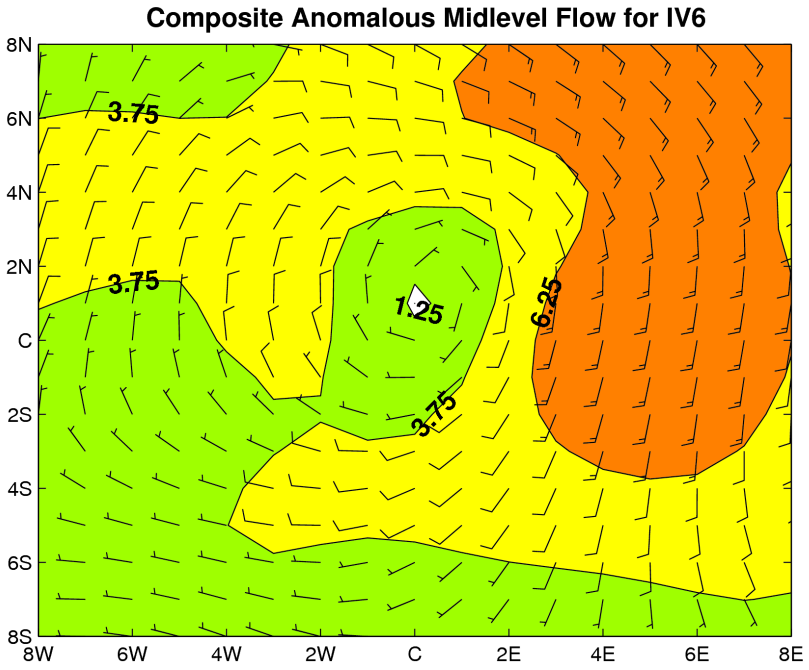

Figure 36: Same as Fig. 34, except for IV6.

7.1.3 Convective Environment

This section considers the effect that an inverted trough, through its associated midlevel cyclonic circulation, can have on kinematic parameters that are important for convective evolution around the SMO. It can be seen from Fig. 1 in Section 2.1 that the SMO peaks are oriented northwest-southeast along western Mexico. Convective cells initiate along the SMO axis almost every afternoon during the summer NAM (Lang et al. 2007). However, not all convective cells propagate off the high terrain (Lang et al. 2007). Midlevel winds are important for steering individual, ordinary convective cells (Brooks 1946), in addition to influencing vertical wind shear. Just based on steering flow, individual storms that initiate along the SMO axis are more likely to propagate toward the coastal plain on the leading flank of the inverted trough. The western flank of the low is characterized by northeasterly midlevel flow (Figs. 33 and 35) that is normal to the SMO topographic gradient. On the other hand, the eastern flank of the low is characterized by strong southeasterly midlevel flow. These midlevel winds blow parallel to the SMO topographic gradient, making it more difficult for convective cells to propagate off the high terrain.

The midlevel flow not only influences individual convective cell movement, but also convective system organization through vertical wind shear (Rotunno et al. 1988, Weisman and Rotunno 2004, Jirak and Cotton 2007). Previous studies have demonstrated an increase in convective organization with increasing magnitudes of shear. The orientation of the shear vector is also important for convective system evolution (Keenan and Carbone 1992). The two components of vertical wind shear are surface winds and

midlevel flow in the 3-6 km AGL layer. The diurnal cycle of surface flows during 2004 NAME indicate a southwesterly upslope wind during the afternoon and evening along the western slopes of the SMO (Ciesielski and Johnson 2008).

Consider changes in vertical wind shear dictated by the midlevel flow associated with the inverted trough. The normal monsoonal conditions during 2004 NAME include east-southeasterly to southeasterly midlevel winds over western Mexico (see Fig. 37a or the Douglas et al. 1993 paper). On the western flank of the inverted trough, northeasterly midlevel wind vectors are opposite from southwesterly surface wind vectors in the afternoon. Hence, shear magnitude increases during the afternoon just by changing the direction of the midlevel flow to northeasterly. Shear vectors also become more perpendicular to the SMO axis compared to average monsoonal conditions. To the east of the inverted trough, strong southeasterly midlevel winds will increase the magnitude of the shear vector, but also turn the vector more parallel to the SMO axis.

Rainfall associated with MCS activity is an important contributor to summer rainfall along the western slopes of the SMO (Douglas et al. 1993). Moreover, initiation of gulf surges along the GOC could be tied to MCSs that propagate toward the coastal plain (Hales 1972, Rogers and Johnson 2007). Thus, MCS activity along the western slopes of the SMO is an important component of the NAM. It is hypothesized that inverted troughs can influence vertical wind shear through their modification of the midlevel flow and thereby affect convective organization. The next section will examine the changes in vertical wind shear that accompany IV4 and IV6. The link between steering flow, shear, and convective development is also analyzed.

7.2 Midlevel Flow and Shear Impact on Convection

The following section will examine the midlevel (700-400 hPa) steering flow, vertical wind shear, and convective development over the core NAM region at particular synoptic times associated with the inverted trough passage. The first plot at each synoptic time shows the long-term, summer average steering flow and the steering flow at that particular synoptic time. Surface pressure contours are overlaid and serve as a proxy for elevation. Hence, one can understand how the steering flow is oriented with respect to the topographic gradient. The second plot at each synoptic time illustrates the average vertical wind shear and the vertical wind shear at that particular synoptic time. Surface pressure contours are also overlaid. By plotting the average midlevel flow and average shear vectors, deviations from the average monsoonal conditions are readily apparent. The third plot at each synoptic time overlays the anomalous shear vector on an GOES-10 IR image. While the anomalous shear vectors are valid at 0000 UTC, the IR image was chosen to represent the time (around 0000 UTC) that represents maximum convective development. The analysis will focus on the western slopes of the SMO since that is where convective organization takes place during the NAM.

7.2.1 IV4

Analysis at 0000 UTC 10 July

Figure 37a shows the average (1 July – August 15 2004) steering flow and the steering flow on 0000 UTC 10 July. The average steering flow is east-southeasterly to

southeasterly over the western slopes of the SMO. At 0000 UTC 10 July, IV4 is located well east of the core NAM region (23°N,94°W). The midlevel flow is dominated by the subtropical ridge located over west Texas (Fig. 37a). This flow regime produces strong southerly midlevel winds over Sonora. Since there are many references to Sonora and Sinaloa over the rest of the chapter, refer back to Fig. 1 in Section 2.1 and note the location of these two Mexican states. Southerly and southeasterly midlevel flow is not conducive for steering storms, which initiate along the SMO peaks, off the higher terrain in Sonora. Figure 37b shows the average shear vectors and the shear vectors on 0000 UTC 10 July. Due to the southerly midlevel flow, the shear vectors on 0000 UTC 10 July along the Sonoran foothills are largely parallel to the topographic gradient. The IR image from 0200 UTC 10 July (Fig. 37c) is consistent with the southerly midlevel flow. Thunderstorms initiate along the SMO peaks in Sonora, but the anomalous southwesterly steering flow and shear vectors in Sonora prevent significant propagation of the storms off the higher terrain.

Analysis at 0000 UTC 11 July

The midlevel flow regime has changed considerably by 0000 UTC 11 July compared to the previous day. IV4 has moved closer to the core NAM region, now located at 24°N,98°W (indicated by the red "L"). Figure 37d demonstrates the increase in northeasterly midlevel flow over Sinaloa. The northeasterly steering flow is caused by the midlevel flow on the western flank of IV4 (Fig. 33). Over Sonora, the midlevel flow is very light and not deviating from the average monsoonal conditions. In accordance with the stronger northeasterly midlevel flow over Sinaloa, the shear vector increases in magnitude and becomes oriented more normal to the topographic gradient in that locale

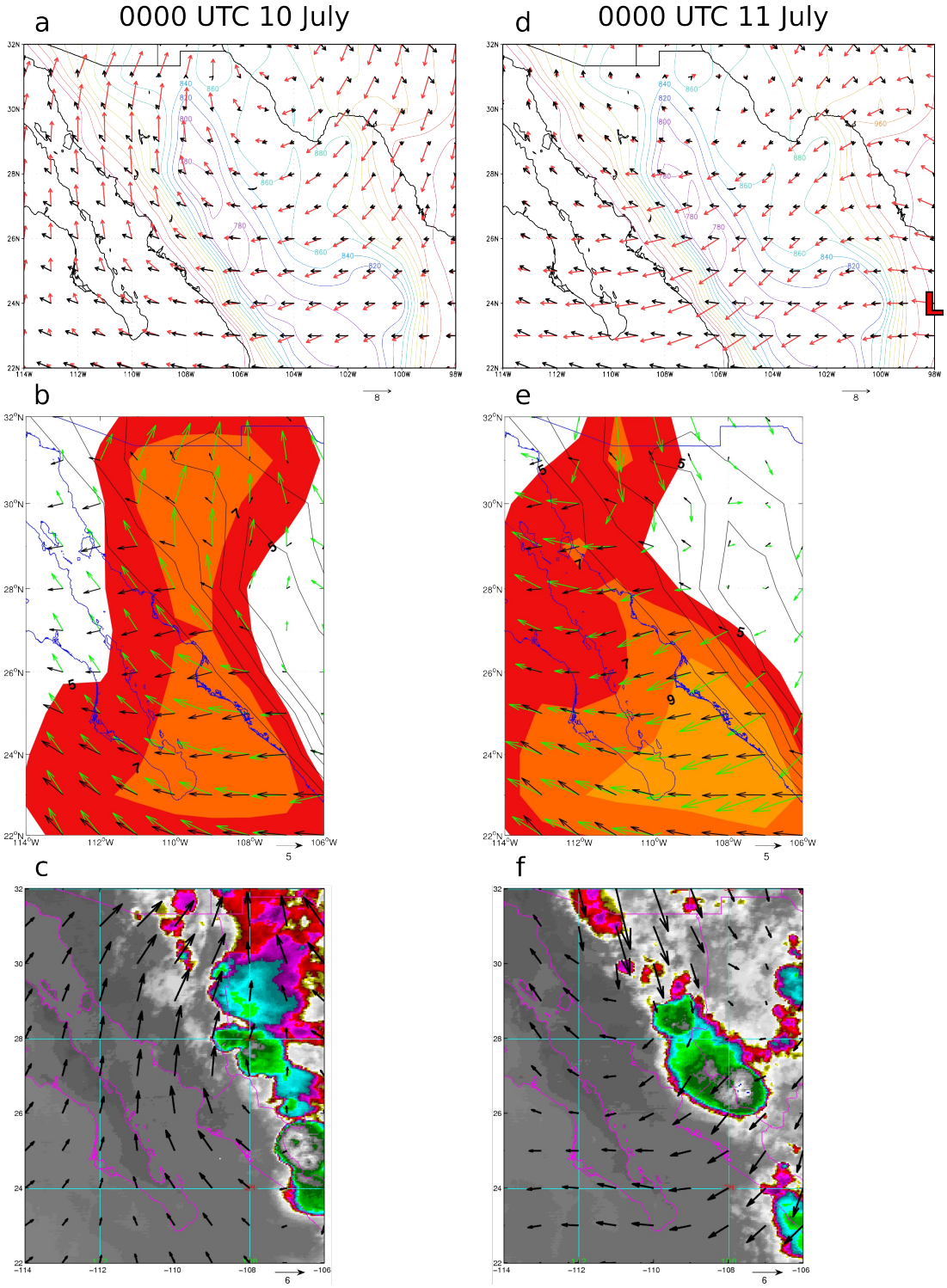

Figure 37: For (a) 0000 UTC 10 July and (d) 0000 UTC 11 July, the average midlevel flow (black vectors) and actual midlevel flow (orange vectors) in m s^{-1}. The 200-hPa inverted trough center is denoted by "L". Surface pressure is contoured. For (b) 0000 UTC 10 July and (e) 0000 UTC 11 July, the average shear (black vectors) and actual shear (green vectors) in m s^{-1}. The actual shear magnitude is shaded and surface pressure is contoured in black. For (c) 0200 UTC 10 July and (f) 0300 UTC 11 July, GOES-10 infrared image with anomalous shear (black vectors) in m s^{-1}.

(Fig. 37e). An MCS develops along the SMO foothills south of 28°N by 0300 UTC 11 July (Fig. 37f). Due to the anomalous northeasterly steering flow and shear, the convection propagates farther southwest toward the GOC coastal plain compared to the previous day (compare Fig. 37f to 37c). The convection fails to organize over the SMO foothills of Sonora north of 28°N, in the area of substantially weaker midlevel flow.

Analysis at 0000 UTC 12 July

IV4 has moved closer to the SMO foothills by 0000 UTC 12 July and is located at 25°N,103°W. Note the cyclonic turning in the midlevel wind field in Fig. 38a that is associated with the midlevel manifestation of IV4. Similar to the previous day, the strong midlevel northeasterly flow is confined to the SMO foothills south of 28°N. Over Sinaloa, the steering flow is perhaps oriented more perpendicular to the SMO axis compared to 0000 UTC 11 July, however differences are small. The shear vectors to the south of 28°N are approximately the same magnitude as the previous day and oriented normal to the SMO axis. With anomalous northeasterly steering flow and wind shear south of 28°N, we would expect convective organization to occur in the same region. Indeed, a quite large MCS develops along the SMO foothills and GOC coastal plain by 0245 UTC 12 July (Fig. 38c). In the region of anomalous northeasterly shear, the MCS organizes and propagates southwestward all the way to the GOC coastline. There is a lack of significant convective organization north of 28°N where the anomalous shear is weaker.

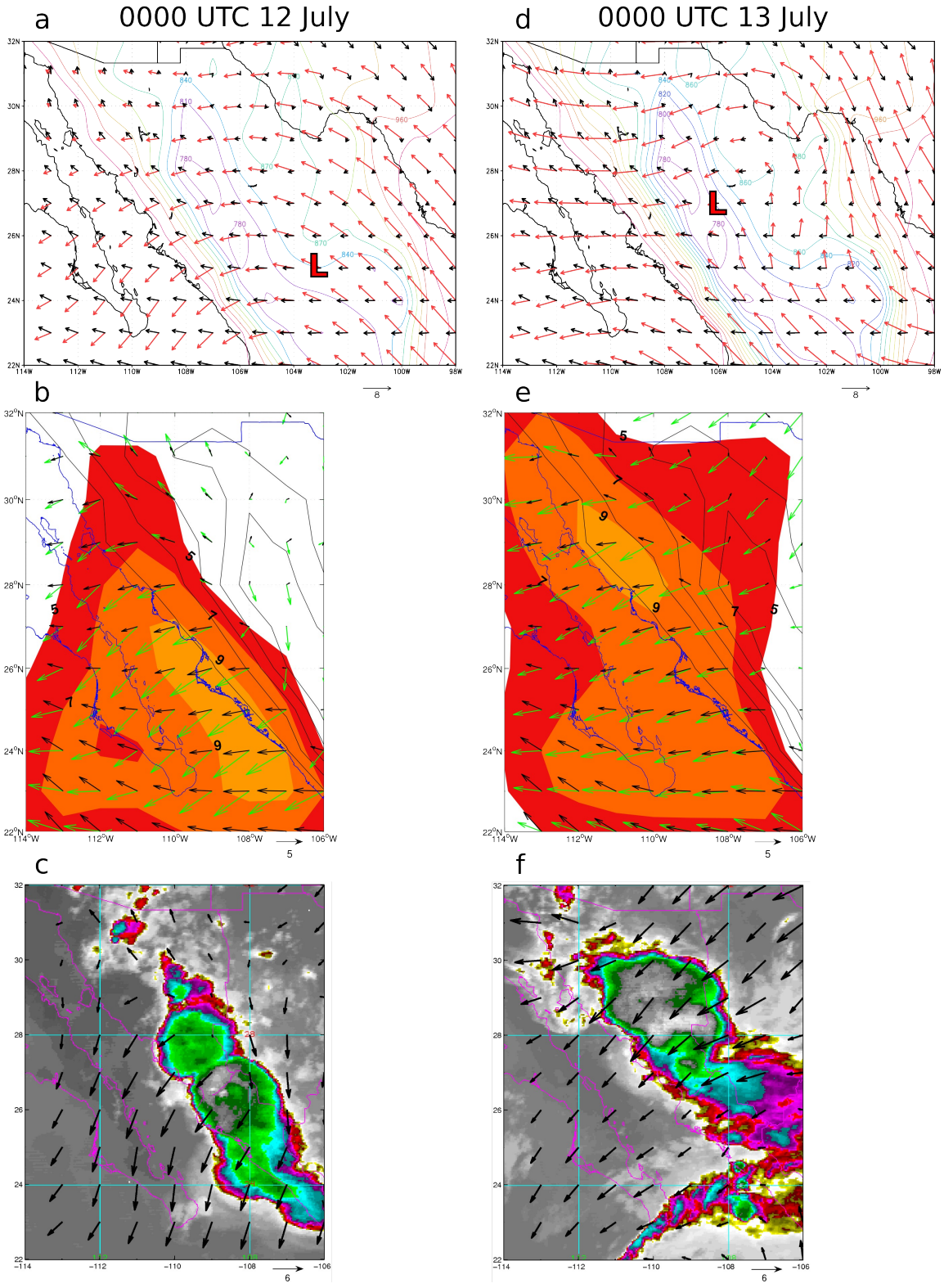

Figure 38: Same as Fig. 37, except for 0000 UTC 12 July and 0000 UTC 13 July. The GOES-10 IR image in (c) is at 0245 UTC 12 July and in (d) is at 0645 UTC 13 July.

Analysis at 0000 UTC 13 July

The midlevel wind environment over the SMO foothills north of 28°N undergoes a significant change by 0000 UTC 13 July. IV4 has moved northwestward to 27°N,106°W. Strong east-northeasterly midlevel flow is now located over Sonora (Fig. 38d). The midlevel wind speeds over Sonora are approximately 9 m s^{-1} stronger than the previous day, which represents a substantial increase. The strong midlevel flow, located over Sinaloa on 0000 UTC 12 July, has since shifted to the northwest in connection with the low's northwestward propagation. There is a 2-4 m s^{-1} increase in shear over the Sonoran coastal plain (Fig. 38e). Also, note the corresponding 2 m s^{-1} decrease in shear over the Sinaloan coastal plain. With the anomalous northeasterly shear now located over Sonora, we might expect a northerly shift in MCS development over the previous day. By 0645 UTC 13 July, a significant MCS has organized over the Sonoran foothills in the region of anomalous northeasterly shear (Fig. 38f). South of 27°N, the convective cloud tops are much warmer, and convective organization is not as pronounced. This agrees with the observed weaker wind shear over the Sinaloan foothills. The synoptic time of 0000 UTC 13 July represents the first time that significant MCS activity occurred over the Sonoran foothills over the four day period.

7.2.2 IV6

Analysis at 0000 UTC 20 July

The steering flow on 0000 UTC 20 July is shown in Fig. 39a. The midlevel flow is strong east-northeasterly over the Sinaloan foothills, but much weaker to the north of 28°N. The strong midlevel winds over Sinaloa are not associated with IV6, as IV6 has not even

formed yet. Rather, the strong flow is due to the significant midlevel anticyclone over northwestern Mexico. Despite the enhanced vertical wind shear over Sinaloa (Fig. 39b), there is minimal convective organization over the same area (Fig. 39c). Figure 39c shows considerable deep convection over the Sonoran foothills at 0245 UTC 20 July. However, the lack of significant vertical wind shear in Sonora (Fig. 39b) appears to prevent any further upscale develop. The thunderstorms over Sonora quickly die after the time indicated in the IR image.

Analysis at 0000 UTC 21 July

The midlevel flow regime on 0000 UTC 21 July is very similar to the previous day (Fig. 39d). The anticyclone is still centered over northwestern Mexico and the recently developed IV6 is located to the east of the core NAM region at 26°N,96°W. Notice that the stronger midlevel northeasterly flow on the western flank of IV6 is still east of the SMO axis. Along the SMO foothills south of 28°N, the vertical wind shear observations do not show a noteworthy increase in magnitude over the average monsoonal conditions (Fig. 39e). However, the shear vector does become oriented from the northeast, more perpendicular to the topographical gradient. By 0130 UTC 21 July a very large MCS has developed over much of the SMO foothills (Fig. 39f). This is surprising considering the weak shear magnitudes over the SMO foothills from 26-30°N. However, this could be an event where the orientation of the shear vector, and not necessarily the absolute magnitude, is important for convective system organization. The MCS does not extend into areas where the shear vectors are more southeasterly (over northern Sonora). Other mesoscale processes, such as mountain-valley circulations, convective outflows, and/or convective

instability may be equally important in this convective event (Howard and Maddox 1988c).

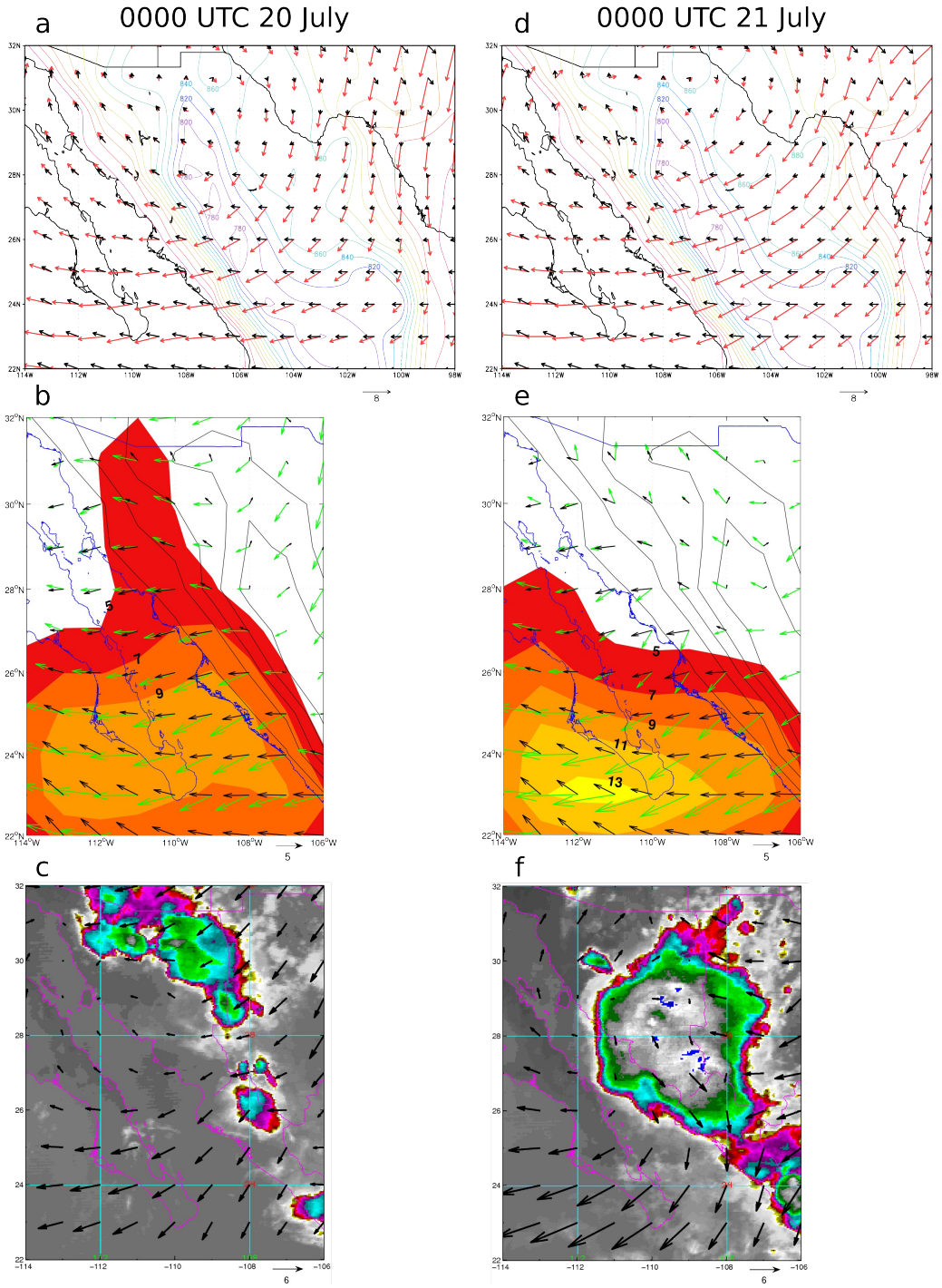

Figure 39: Same as Fig. 37, except for 0000 UTC 20 July and 0000 UTC 21 July. The GOES-10 IR image in (c) is at 0245 UTC 20 July and in (f) is at 0130 UTC 21 July.

Analysis at 0000 UTC 22 July

The midlevel flow regime on 0000 UTC 22 July is not significantly different from the previous day (Fig. 40a). This is largely because the two main synoptic influences, the midlevel ridge and IV6, do not move much. IV6 is located to the east of the SMO axis at 26°N,100°W. The steering flow has become more northerly over the SMO foothills south of 29°N. The locations of the subtropical ridge and IV6 contribute to the north-northeasterly midlevel flow. In the northern Sonoran foothills (north of 29°N), the midlevel winds are much weaker. The convective evolution at 0630 UTC 22 July is very similar to the previous day (Fig. 40c). A very large MCS develops over the SMO foothills, primarily confined between 26°N and 30°N. Both the MCS on 21 July and 22 July moved slowly southwest toward the GOC coastal plain. Similar to the previous day, the large MCS developed in a region where the shear vectors were northeasterly as opposed to southeasterly (Fig. 40b).

Analysis at 0000 UTC 23 July

There is a substantial change in the midlevel wind environment over the northern part of the core NAM region on 0000 UTC 23 July (Fig. 40d). The subtropical high that was previously situated over northwestern Mexico has moved northwest to southern California (can't be seen in this figure). This could be in response to the westward movement of IV6, which is located at 27°N,101°W by 0000 UTC 23 July, or by other large-scale synoptic features. The interaction between the high and low pressure centers produces strong midlevel northeasterly winds over the Sonoran foothills north of 28°N. There is a corresponding decrease in midlevel flow over the Sinaloan foothills south of

26°N. Owing to the strong northeasterly winds aloft, the shear vectors increase substantially (approximately 6-8 m s^{-1}) over extreme northern Sonora and become oriented from the east-northeast. The northward displacement of the large MCS on 0545 UTC 23 July compared to the previous two days is consistent with the increase in northeasterly midlevel flow over northern Sonora (Fig. 40f). The MCS is confined along the Sonoran foothills between 28°N and the International Border. Note the lack of MCS development south of 28°N where the midlevel flow and shear is weaker than farther north.

Analysis at 0000 UTC 24 July

The midlevel flow field is very similar on 0000 UTC 24 July to the previous day (Fig. 41a). IV6 has moved west to 27°N,104°W. Continued strong east-northeasterly midlevel winds are observed over northern Sonora with weaker winds along the SMO foothills south of 27°N. The midlevel wind pattern is consistent with the stronger and weaker midlevel winds in the northwest and southwest quadrants of IV6 respectively (Fig. 35). There is anomalous northeasterly shear over northern Sonora, although not quite as strong as the previous day (Fig. 41b). Shear is weaker south of 26°N than farther north. Figure 41c shows that another MCS develops along the Sonoran foothills north of 28°N, though not quite as large (in areal extent) as previous days. The MCS is embedded within the anomalously strong northeasterly midlevel flow and shear over northern Sonora. Again, significant convective organization is absent south of 26°N where the midlevel flow and shear is weaker.

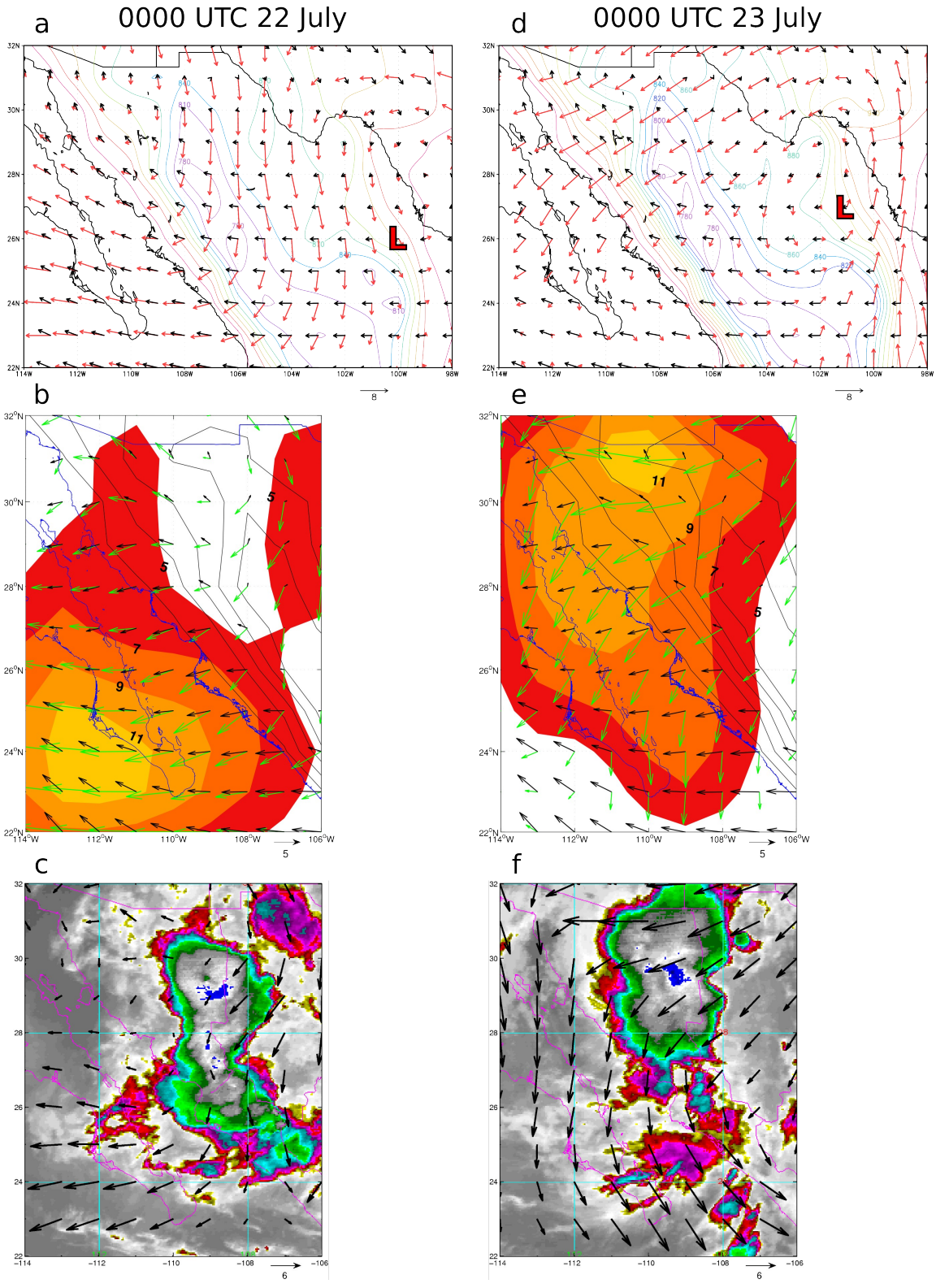

Figure 40: Same as Fig. 37, except for 0000 UTC 22 July and 0000 UTC 23 July. The GOES-10 IR image in (c) is at 0630 UTC 22 July and in (f) is at 0545 UTC 23 July.

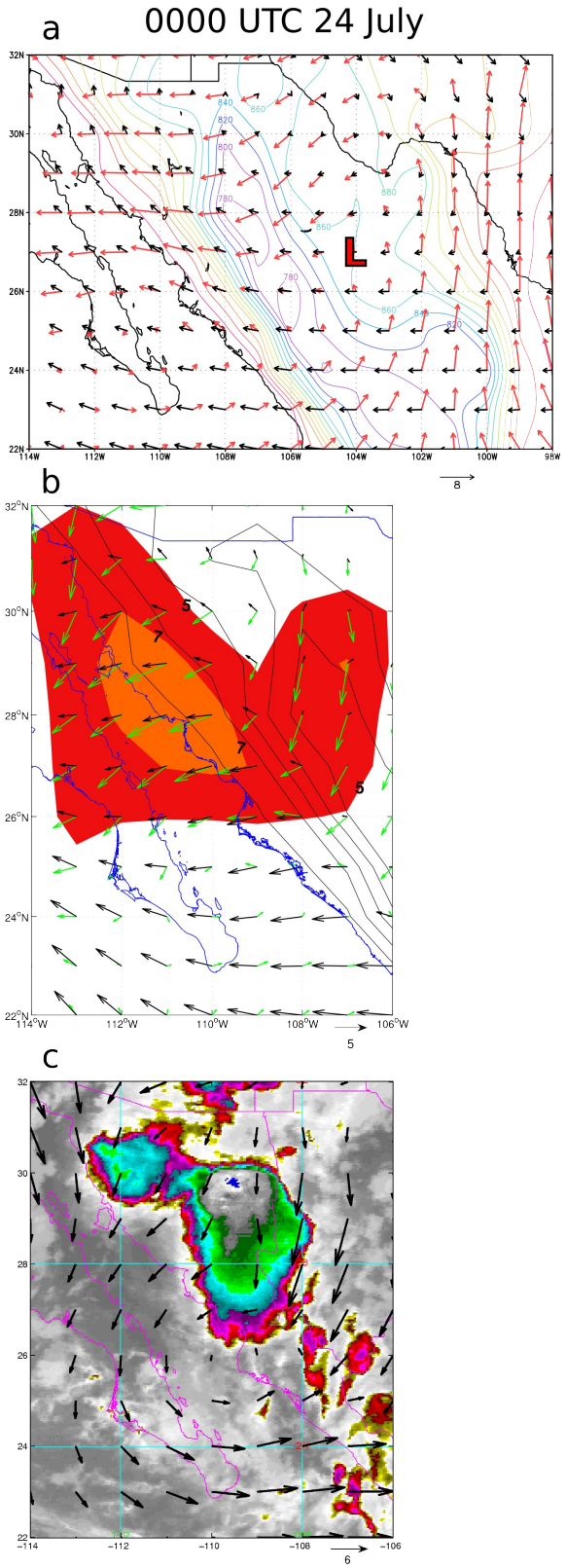

Figure 41: Same as Fig. 37, except for 0000 UTC 24 July. The GOES-10 IR image in (c) is at 0300 UTC 24 July.

7.3 Summary

The increase in convective development on the western flank of both inverted troughs is in agreement with previous NAM studies (Pytlak et al. 2005, Douglas and Englehart 2007). Moreover, the substantial convective activity over the lower elevations on 12-13 July and 21-24 July agrees with Bieda et al. (2009), who showed an enhancement of lightning counts over the low deserts on inverted trough days. Unfortunately, neither IV4 nor IV6 moved west of the SMO foothills. Thus, effects of the southeasterly midlevel flow on convective development over the eastern flank of the low can not be analyzed. The present study does not attempt to explain all factors influencing convective development and evolution. Nevertheless, the connection between anomalous steering flow/shear and subsequent convective organization is readily apparent from the two periods considered. In general, areas of enhanced northeasterly midlevel flow and anomalous northeasterly shear correspond to regions to enhanced MCS development along the SMO foothills and GOC coastal plain. Although not valid for every synoptic time considered above, this general relationship is true for the majority of the synoptic times. Significant 24-hour changes in the midlevel wind field and shear vectors (most notably from 12 to 13 July, and from 22 to 23 July) are accompanied by significant shifts in the location of MCS activity.

The total anomalous shear vector is composed of two components: the contribution from the anomalous midlevel flow and the contribution from the anomalous surface flow. Figure 42 illustrates the total anomalous shear and the contribution from the anomalous midlevel wind at two synoptic times for IV4 and IV6. If the two vectors resemble each other, then the anomalous midlevel wind (as opposed to the anomalous surface flow) is

largely determining the anomalous shear. In general, the anomalous midlevel flow tends to control the total anomalous shear signal over the GOC coastal plain and SMO foothills. The general relationship also holds for other synoptic times not shown here. This is in agreement with Periera (2008), who showed that the temporal variability in the midlevel wind resembled that of the total wind shear in the Sinaloa region. The surface wind, on the other hand, was far less variable. The present study has shown that it is fluctuations in the midlevel wind, caused by the inverted trough interacting with the subtropical ridge, that modulate shear and subsequent convective organization over the SMO foothills.

The positive relationship between shear and MCS activity over the NAM region has been documented before. In Smith and Gall (1989), the three squall lines in southern Arizona and northwestern Mexico all propagated into an environment of strong low-level wind shear. Farfán and Zehnder (1994) indicated that moving MCS days were characterized by stronger than average easterlies at the 700- and 500-hPa levels over northwest Mexico. Lang et al. (2007) showed that disturbed regimes of enhanced convective organization corresponded to periods of increased environmental wind shear. Furthermore, Periera (2008) demonstrated that there is relatively good correlation between 0-6 km wind shear and MCS rainfall. MCSs were more likely to occur when the 0-6 km wind shear was stronger in the NAME region. The Periera study revealed that the wind shear peaks were associated with episodes of stronger midlevel easterly winds.

Based on previous studies, the relationship between MCS activity and environmental wind shear has been well documented. However, the present study highlights how a transient inverted trough can affect the environmental wind shear. The interaction between the upper-level inverted trough and subtropical ridge, along with the

induction of a trough at midlevels by an upper-level PV anomaly (Hoskins et al. 1985), creates anomalous northeasterly midlevel flow on the western flank of IV4 and IV6. This means that the steering flow vector and shear vector become oriented more normal to the SMO axis on the western flank. Thus, it is proposed that the inverted trough creates an environment (on its leading flank) that is favorable for convective storms to grow upscale as they move off the high terrain of the SMO.

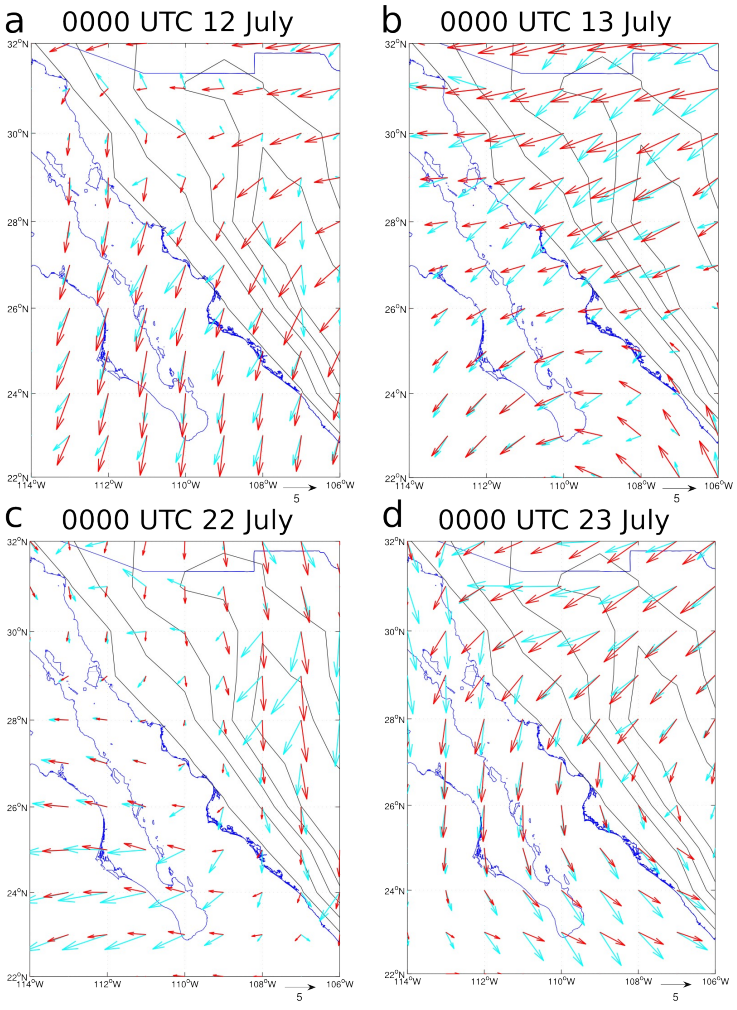

Figure 42: The total anomalous shear vector (blue) and anomalous midlevel flow vector (red) at (a) 0000 UTC 12 July, (b) 0000 UTC 13 July, (c) 0000 UTC 22 July, and (d) 0000 UTC 23 July. Surface pressure is contoured in black.

CHAPTER 8

SUMMARY AND CONCLUSIONS

8.1 Summary

This study has presented a detailed observational analysis of two inverted troughs during the 2004 North American Monsoon Experiment (NAME). Past detailed studies of upper-level inverted troughs have been confined to data-sparse areas outside the North American Monsoon (NAM) region (Erickson 1971, Kelley and Mock 1982, Whitfield and Lyons 1992). The upper-level inverted trough is an important component of the NAM system and has been shown to modulate rainfall and convective activity in the core NAM region (Pytlak et al. 2005, Douglas and Englehart 2007, Bieda et al. 2009). The spatial and temporal resolution of the 2004 NAME observational network is sufficient to explore several aspects of the transient inverted trough. Using the Colorado State University gridded dataset from NAME, the present study is unprecedented in documenting the structure of two inverted troughs in the NAM region. The two inverted troughs, IV4 and IV6, propagated over the dense observational sounding network in northwestern Mexico. For each inverted trough, the following fields are analyzed: temperature, vorticity, quasi-geostrophic (QG) omega, midlevel flow, and vertical wind shear.

8.1.1 Temperature and Vorticity Structure

In an average sense, the maximum warm anomaly for IV4 occurred near 100 hPa. The cold anomaly for IV4 extended through a deep layer of the atmosphere, from 150 hPa to the surface. The time evolution plots of temperature indicate that the cold anomaly for IV4 was strongest at the beginning of its lifetime, but weakened steadily as the low moved across northwestern Mexico. Vertical cross sections of relative vorticity for IV4 show that the strongest relative vorticity was located over the low center at 200 hPa. The circulation of IV4 decreased rapidly into the midlevels. The upper-level and midlevel circulation of IV4 weakened considerably during the last day (13 July) of its lifetime. This decrease in intensity of IV4 coincides with the system reaching the Sierra Madre Occidental (SMO) axis, where it then began to move northwestward. The evolution of relative vorticity and temperature anomaly are consistent with each other, indicating that IV4 was a steadily weakening system as it propagated across the core NAM region.

The temperature structure of IV6 had many similarities to IV4, however there were also subtle differences. The maximum warm anomaly was centered near 125 hPa while the cold anomaly extended from 250 hPa to the surface. The time evolution of temperature anomaly was more static than IV4. At upper levels, the cold anomaly showed a slight weakening with time, but not as pronounced as IV4. Maximum relative vorticity for IV6 was situated over the low center at 250 hPa. The main difference in circulation between the two inverted troughs resided in the midlevels. At 600 hPa over the low center, relative vorticity values for IV6 were three times larger than for IV4. IV6 maintained its circulation strength for the majority of its lifetime as it propagated westward across

Mexico. However, by 0000 UTC 24 July the system crossed the SMO axis and weakened substantially thereafter.

8.1.2 QG Omega

For the 700-300 hPa layer, the composite total QG omega was calculated for both inverted troughs. The general pattern of total QG omega for IV4 indicates weak subsidence to the west of the low center and weak rising motion to the east. The omega root-mean-square (rms) amplitude associated with the Laplacian of thermal advection term (RHS2) was three to four times larger than differential vorticity advection term (RHS1). Thus, the temperature advection pattern, with cold (warm) air advection to the west (east) of IV4, dictated the total QG omega signal for IV4. The general spatial pattern of total QG omega for IV6 indicated general weak subsidence to the northwest of the inverted trough and weak rising motion to the southeast. Similar to IV4, the omega rms amplitude from the RHS2 was two to three times greater than from RHS1 throughout the 700-300 hPa layer. Hence, the region of strongest subsidence to the northwest of the inverted trough was caused by the maximum in the cold air advection pattern in the same location. Warm air advection occurred southeast of the low center and induced a region of weak rising motion. Because RHS2 overwhelmed the RHS1 signal over most of the domain for both cases, understanding the temperature advection pattern is crucial to determining the total QG omega pattern in the vicinity of the inverted trough.

8.1.3 Midlevel Winds and Vertical Wind Shear

An analysis of how the midlevel circulation of the inverted troughs modifies the midlevel flow and associated convective development along the SMO foothills was performed. A composite analysis of IV4 showed that midlevel winds were east-northeasterly (southeasterly) on the west (east) side of the low. The composite midlevel flow for IV6 indicated that the midlevel winds were light in the southwestern quadrant of IV6. The northwestern quadrant of IV6 was dominated midlevel northeasterlies while the eastern flank experienced strong midlevel southerlies. The effect of IV4 and IV6 on the midlevel winds is to impose an anomalous midlevel cyclonic circulation on the prevailing monsoonal flow.

The midlevel flow, vertical wind shear, and convective development was investigated in Sonora and Sinaloa (Fig. 1) over the lifetime of IV4 (10-13 July). On the first day (0000 UTC 10 July), IV4 was located too far east to have much impact on the midlevel flow and shear pattern over the SMO foothills. However, by 0000 UTC 11 and 12 July, the anomalous northeasterly flow on the leading flank of IV4 was entrenched across the Sinaloan foothills. There was a noticeable increase in mesoscale convective system (MCS) development and westward propagation off the high terrain in Sinaloa. Further north, the midlevel winds were much weaker and convective organization was lacking. The northwestward movement of IV4 from 12 July to 13 July produced a dramatic change in the midlevel flow pattern over Sonora by 0000 UTC 13 July. Midlevel flow became strong easterly and there was an associated substantial increase in northeasterly shear in Sonora. A very large MCS developed over the Sonoran foothills on 0000 UTC 13 July in

the zone of strongest easterly steering winds.

Similar to IV4, the midlevel flow, shear, and convective development pattern was analyzed on 20-24 July when IV6 propagated across the core NAM region. While anomalous northeasterly midlevel flow occurred over Sinaloa on 0000 UTC 20 July, there was a lack of significant convective development and organization at that time. On 0000 UTC 21 and 22 July, the shear vectors became more northeasterly along the southern SMO foothills. The shear vector, becoming oriented more normal to the topographic gradient, could have enhanced convective organization on these two days. Both 21 and 22 July were characterized by large, strong MCS that developed along the SMO foothills between 26°N and 30°N. The MCS did not reach areas in northern Sonora where the midlevel flow was weaker and the shear vector was less perpendicular to the topographic gradient. There was a substantial change in the midlevel wind pattern over northern Sonora on 0000 UTC 23 July. Due to the westward movement of IV6 and the subtropical anticyclone, a band of strong northeasterly winds became established over northern Sonora by 0000 UTC 23 July. A large MCS organized along the Sonoran foothills where the wind shear was significantly higher than the previous day. The MCS placement on 0000 UTC 23 July is noticeably farther north than on 0000 UTC 21 and 22 July. Strong midlevel easterlies remain over Sonora on 0000 UTC 24 July. Embedded in anomalous northeasterly shear, an MCS developed over the Sonoran foothills on 0000 UTC 24 July.

8.2 Conclusions

The results in Ch. 4-7 provide insight into the thermodynamic and kinematic

structure of two inverted troughs during 2004 NAME. It is important to remember that the two inverted troughs represent a small sample of the inverted troughs that moved across the T2A domain during NAME. However, there are sufficient similarities in the characteristics of the two cases to make general conclusions about these important systems.

- Both inverted troughs developed at the base of thinning midlatitude troughs over the south Texas region in a manner proposed by Thorncroft et al. (1993). The inverted troughs moved westward on the southern flank of the subtropical monsoon high.
- The vertical temperature structure of the inverted troughs, with a warm anomaly around 100 hPa and a cold anomaly that extends from 200 hPa to the surface, is in agreement with previous TUTT low studies (Kelley and Mock 1982, Whitfield and Lyons 1992). The cold anomaly associated with the low is not just a feature of the upper levels, as it extends into the midlevels as well.
- The strongest circulation of the system is in the upper levels around 200 hPa. This agrees with previous TUTT low studies (Erickson 1971, Kelley and Mock 1982, Whitfield and Lyons 1992). However, the upper-level PV anomaly induces a midlevel cyclonic circulation (Hoskins et al. 1985), that is weaker than the upper-level circulation.
- Both inverted troughs show a pronounced weakening trend when the inverted trough center reaches the SMO axis. Topographic effects appear to be important in weakening the system, an idea that was suggested by Bieda et al. (2009).
- The general spatial pattern of QG omega with weak subsidence (weak rising

motion) to the west (east) of the low center is in agreement with previous studies of TUTT lows over non-NAM regions (Kelley and Mock 1982, Whitfield and Lyons 1992). The QG-forced vertical motion in these inverted troughs is weaker than midlatitude baroclinic systems owing to weak temperature gradients.

- The Laplacian of thermal advection overwhelms the vorticity advection forcing term in the QG omega equation in the vicinity of the inverted trough (in agreement with Erickson 1971). It is cold (warm) air advection to the west (east) of the low center that largely produces the subsidence (rising motion).
- In regions where topography is not important for convective initiation and evolution, the QG omega signal favors an *decreased* likelihood of precipitation on the western flank of the inverted trough. However, the weak QG signal does not agree with satellite observations during NAME that indicate a distinctive increase in MCS activity on the western flank of both IV4 and IV6. Moreover, the spatial pattern of QG omega does not agree with inferences from previous studies (Pytlak et al. 2005, Douglas and Englehart 2007) that suggest an increased likelihood for convective development on the forward flank of the inverted trough.
- Northeasterly (southeasterly) midlevel flow to the west (east) of the inverted trough is associated with the midlevel cyclonic circulation of the inverted trough. Just based on steering flow considerations, individual convective storms would tend to move southwestward *off* the high terrain to the west of the low and *along* the high terrain to the east of the low.
- Over most of the synoptic times for IV4 and IV6, significant MCS activity along the SMO foothills was collocated with regions of anomalous northeasterly midlevel

flow and increased northeasterly shear. This is in agreement with Lang et al. (2007) who showed that precipitating features in Sinaloa organized during periods of enhanced 700-hPa winds and low-level shear. The plots indicated that the inverted trough, in its interaction with the subtropical ridge, controls the location of anomalous northeasterly midlevel winds on its western flank.

- The strengthened northeasterlies induced by the inverted trough seem to be a favorable environmental condition that overwhelms the weak-QG forced subsidence to the west of the low.

The results from this study provided an unprecedented analysis of inverted troughs in the core NAM region. Inverted troughs in the NAM region interact with complex topography, much different from the subtropical upper-level lows previously studied over areas where topography is not a factor. If gulf surge initiation is indeed tied to the presence of large convective systems that reach the GOC coastline, then inverted troughs could play an indirect role in surge initiation by creating a more favorable environment for such propagating convective systems on their western flank. Significant gulf surges did occur during the lifetimes of IV4 and IV6, after significant MCS activity, and when the upper-level lows were located to the east of the SMO foothills. Perhaps future research, through modeling efforts, will focus on the role of wind shear magnitude and orientation in affecting subsequent upscale growth of convection over the complex topography of the SMO. Future studies should help to clarify the effects that these systems have on the variability of the NAM system.

REFERENCES

Adams, D. K., and A. C. Comrie, 1997: The North American Monsoon. *Bull. Amer. Meteor. Soc.*, **78**, 2197-2213.

Bieda, S. W. III, C. L. Castro, S. L. Mullen, A. C. Comrie, and E. Pytlak, 2009: The relationship of transient upper-level troughs to variability of the North American Monsoon system. *J. Climate*, **22**, 4213-4227.

Bluestein, H. B., 1992: *Synoptic-Dynamic Meteorology in Midlatitudes: Principles of Kinematics and Dynamics, Vol. 1*. Oxford University Press, New York. 431 pp.

Brooks, H. B., 1946: A summary of some radar thunderstorm observations. *Bull. Amer. Meteor. Soc.*, **27**, 557-563.

Bryson, R. A., and W. P. Lowry, 1955: Synoptic climatology of the Arizona summer precipitation singularity. *Bull. Amer. Meteor. Soc.*, **36**, 329-339.

Ciesielski, P. E., and R. H. Johnson, 2008: Diurnal cycle of surface flows during 2004 NAME and comparison to model reanalysis. *J. Climate*, **21**, 3890-3913.

Douglas, A. V., and P. J. Englehart, 2007: A climatological perspective of transient synoptic features during NAME 2004. *J. Climate*, **20**, 1947-1954.

Douglas, M. W., 1995: The summertime low-level jet over the Gulf of California. *Mon. Wea. Rev.*, **123**, 2334-2347.

Douglas, M. W., R. A. Maddox, K. Howard, and S. Reyes, 1993: The Mexican monsoon. *J. Climate*, **6**, 1665-1677.

Erickson, C. O., 1971: Diagnostic Study of a Tropical Disturbance. *Mon. Wea. Rev.*, **99**, 67-78.

Farfán, L. M., and J. A. Zehnder, 1994: Moving and stationary mesoscale convective systems over northwest Mexico during the Southwest Area Monsoon Project. *Wea. Forecasting*, **9**, 630-639.

Fuller, R. D., and D. J. Stensrud, 2000: The relationship between tropical easterly waves

and surges over the Gulf of California during the North American Monsoon. *Mon. Wea. Rev.*, **128**, 2983-2989.

Hales, J. E. Jr., 1972: Surges of maritime tropical air northward over the Gulf of California, *Mon. Wea. Rev.*, **100**, 298-306.

Higgins, R. W., and Coauthors, 2006: The North American Monsoon Experiment (NAME) 2004 field campaign and modeling strategy. *Bull. Amer. Meteor. Soc.*, **87**, 79-94.

Hoskins, B. J., M. E. McIntyre, and A. W. Robertson, 1985: On the use and significance of isentropic potential vorticity maps. *Quart. J. Roy. Meteor. Soc.,* **111**, 877-946.

Howard, K. W., and R. A. Maddox, 1988c: Mexican mesoscale convective systems-large-scale environmental conditions. Preprints, III *InterAmerican and Mexican Congress of Meteorology*, Mexico City, Mexico, 395-399.

Jirak, I. K., and W. R. Cotton, 2007: Observational analysis of the predictability of mesoscale convective systems. *Wea. Forecasting*, **22**, 813-838.

Johnson, R. H., P. E. Ciesielski, B. D. McNoldy, P. J. Rogers, and R. K. Taft, 2007: Multiscale variability of the flow during the North American Monsoon Experiment. *J. Climate*, **20**, 1628-1648.

Kalnay, E., and Coauthors, 1996: The NCEP/NCAR 40-Year Reanalysis Project. *Bull. Amer. Meteor. Soc.*, **77**, 437–471.

Keenan, T.D., and R. E. Carbone, 1992: A preliminary morphology of precipitation systems in tropical northern Australia. *Q. J. R. Meteorol. SOC.,* **118**, 283-326.

Kelley Jr., W. E., and D. R. Mock, 1982: A diagnostic study of upper tropospheric cold lows over the western North Pacific. *Mon. Wea. Rev.*, **110**, 471-480.

Lang, T. J, D. A. Ahijevych, S. W. Nesbitt, R. E. Carbone, S. A. Rutledge, and R. C. Cifelli, 2007: Radar-observed characteristics of precipitating systems during NAME 2004. *J. Climate*, **20**, 1713-1733.

Loehrer, S. M., T. A. Edmands, and J. A. Moore, 1996: TOGA COARE upper-air sounding data archive: Development and quality control procedures. *Bull. Amer. Meteor. Soc.*, **77**, 2651–2671.

Nuss, W. A., and D. W. Titley, 1994: Use of multiquadric interpolation for meteorological objective analysis. *Mon. Wea. Rev.*, **122**, 1611-1631.

Pauley, P. M., and S. J. Nieman, 1992: A comparison of quasigeostrophic and nonquasigeostrophic vertical motions for a model-simulated rapidly intensifying marine extratropical cyclone. *Mon. Wea. Rev.*, **120**, 1108-1134.

Periera, L. G. P., 2008: Characteristics and organization of precipitating features during NAME 2004 and their relationship to environmental conditions, dissertation (Ph.D.), Colorado State University.

Pytlak, E., M. Goering, and A. Bennett, 2005: Upper tropospheric troughs and their interaction with the North American Monsoon. *Preprints, 19th Conf. On Hydrology, 85th Annual Amer. Meteor. Soc. Meeting*, San Diego, CA, Amer. Meteor. Soc., CD-ROM, JP2.3.

Rasmusson, E. M., 1967: Atmospheric water vapor transport and water balance of North America: Part 1. Characteristics of the water vapor flux field. *Mon. Wea. Rev.*, **95**, 403-427.

Rogers, P. J., 2005: An observational analysis of two gulf surge events during the 2004 North American Monsoon Experiment, thesis (M.S.), Colorado State University.

Rogers, P. J., and R. H. Johnson, 2007: Analysis of the 13-14 July Gulf Surge Event during the 2004 North American Monsoon Experiment. *Mon. Wea. Rev*., **135**, 3098-3117.

Rotunno, R., J. B. Klemp, and M. L. Weisman, 1988: A theory for strong, long-lived squall lines. *J. Atmos. Sci.*, **45**, 463-485.

Sadler, J. C., 1967: The tropical upper tropospheric trough as a secondary source of typhoons and a primary source of tradewind disturbances. Hawaii Institute of Geophysics Rep. 67-12, 103 pp.

Sadler, J. C., 1975: The upper tropospheric circulation over the global tropics. Dept. of Meteorology, University of Hawaii, Rep. No. UHMET-75-05, 35 pp.

Smith, W. P., and R. L. Gall, 1989: Tropical squall lines of the Arizona monsoon. *Mon. Wea. Rev.*, **117**, 1553-1569.

Thorncroft, C. D., B. J. Hoskins, and M. E. McIntyre, 1993: Two paradigms of baroclinic-wave life-cycle behaviour. *Quart. J. Roy. Meteor. Soc.*, **119**, 17-55.

Weisman, M. L., and R. Rotunno, 2004: "A theory for strong long-lived squall lines" revisited. *J. Atmos. Sci.*, **61**, 361-382.

Whitfield, M. B., and S. W. Lyons, 1992: An upper-tropospheric low over Texas during summer. *Wea. Forecasting*, **7**, 89-106.